AMERICAN UNIVERSITY OF BEIRUT

Modeling and Analyzing the Co-existence of LTE with Wi-Fi and Other LTE Networks in the Unlicensed Band Using Stochastic Geometry

by
ABDEL KARIM SAMIH AJAMI

A dissertation
submitted in partial fulfillment of the requirements
for the degree of Doctor of Philosophy
to the Department of Electrical and Computer Engineering
of the Maroun Semaan Faculty of Engineering and Architecture
at the American University of Beirut

Beirut, Lebanon
July 2018

AMERICAN UNIVERSITY OF BEIRUT

Modeling and Analyzing the Co-existence of LTE with Wi-Fi and Other LTE Networks in the Unlicensed Band Using Stochastic Geometry

by

Abdel Karim Samih Ajami

Approved by:

Dr. Zaher Dawy, Professor Electrical and Computer Engineering	Chair of Committee
Dr. Hassan Artail, Professor Electrical and Computer Engineering	Advisor
Dr. Ibrahim Abou Faycal, Associate Professor Electrical and Computer Engineering	Member of Committee
Dr. Christian Bettstetter, Professor University of Klagenfurt	Member of Committee
Dr. Mohammad Asaad, Professor Centrale Supelec	Member of Committee

Date of dissertation defense: July 9, 2018

AMERICAN UNIVERSITY OF BEIRUT

THESIS, DISSERTATION, PROJECT RELEASE FORM

Student Name: AJAMI ABDEL KARIM SAMIH
Last First Middle

○ Master's Thesis ○ Master's Project ● Doctoral Dissertation

☐ I authorize the American University of Beirut to: (a) reproduce hard or electronic copies of my thesis, dissertation, or project; (b) include such copies in the archives and digital repositories of the University; and (c) make freely available such copies to third parties for research or educational purposes.

☑ I authorize the American University of Beirut, to: (a) reproduce hard or electronic copies of it; (b) include such copies in the archives and digital repositories of the University; and (c) make freely available such copies to third parties for research or educational purposes after:

One ___ year from the date of submission of my thesis , dissertation or project.
Two ___ years from the date of submission of my thesis , dissertation or project.
Three ✓ years from the date of submission of my thesis , dissertation or project.

Signature 06/09/2018
Date

This form is signed when submitting the thesis, dissertation, or project to the University Libraries

Acknowledgements

I would like to thank all those who helped me in completing this Thesis especially my advisor, Professor Hassan Artail, who encouraged me with ideas, advice, and helpful comments. I would like to thank the committee members for their help and suggestions. I would also like to thank my wife for her patience and massive support through all these academic years. Part of this work occurred on weekends, nights, while on vacation, and other times inconvenient to my family. For my parents, my father and mother in law, my wife, my brothers and sisters, my brothers and sisters in law, and my children, I would like to say: "I would have never done any of this without you".

An Abstract of the Dissertation of

Abdel Karim Ajami for Doctor of Philosophy
Major: Electrical and Computer Engineering

Title: Modeling and Analyzing the Co-existence of LTE with Wi-Fi and Other LTE Networks in the Unlicensed Band Using Stochastic Geometry

The users demand for high speed broadband connectivity is increasing regardless of location and time. In particular, inside an aircraft, the in-flight connectivity is one of the last venues with no high-speed Internet access. This makes it an important research area to address for both industry and academia. By using the seamless gate-to-gate connectivity concept, passengers can stay connected in all phases of the flight by using 5G technologies. Given that the backhaul capacity will be provided via direct air-to-ground communications (DA2GC) links, passengers will be able to use both LTE and Wi-Fi access technologies on-board. In order to avoid interference with licensed ground LTE network, in-cabin LTE users will be served in the unlicensed spectrum via license assisted access (LAA) technology when the aircraft is close to the ground. However, in these bands other widely used incumbent technologies already exist, and consequently, this triggered research efforts from academia, industry, and standardization bodies to analyze the coexistence of these wireless technologies in the unlicensed band and the fair coexistence between them. This thesis targets the technical exploitation of air navigation and aeronautical data by modeling and analyzing the coexistence of wireless technologies in the unlicensed bands to address emerging challenges related to the harmonious coexistence of these networks. The thesis work is divided into three main parts. The first part analyzes the extension of the LTE technology toward the unlicensed bands. It studies the fair coexistence of LTE and Wi-Fi by considering the emerging IEEE 802.11ax Wi-Fi standard where stochastic geometry is used to model and analyze the coexistence of LTE with simultaneous uplink and downlink IEEE 802.11ax transmissions. Mainly, it considers LTE with continuous transmissions (no protocol change), LTE with

discontinuous transmissions (LTE-U), and licensed assisted access (LAA) coexistence mechanisms. LAA has been adopted by 3GPP as a global LTE technology for the unlicensed bands, where the LAA design should also allow for harmonious LAA-LAA coexistence in the unlicensed bands (i.e., between multiple LTE operators). Hence the second part studies the LAA-LAA coexistence to understand the impact on the performance of multiple coexisting LAA networks as their number scale, where devices of different networks may have different channel access priorities. The findings unveil new questions regarding practical aspects for deploying LAA networks. The last part of the thesis addresses a recent proposal from the Federal Communications Commission (FCC) to permit devices that operate in the unlicensed spectrum, e.g., IEEE 802.11 devices, to operate in the 5.9 GHz band allocated to the intelligent transportation system (ITS). Since the nature of these bands poses a challenge where the ITS Dedicated Short Range Communications (DSRC) networks use them to share safety-critical messages, the thesis looks into the impact of possible coexistence of Wi-Fi networks on the performance of DSRC through an analytical framework that is based on stochastic geometry as well. In all, the proposed analysis framework in the thesis can serve to increase the awareness among regulatory bodies of the extent to which coexistence will adversely affect the performance of incumbent wireless communication technologies.

Contents

List of Figures

List of Tables

Chapter 1

Introduction

The tremendous growth in wireless communication systems traffic has triggered a critical need for additional spectral resources for wireless networks. As we can see from Fig. 1.1, operators throughout the world are facing the challenge of the ever increasing number of users as well as the traffic demand per user that is mainly caused by the evolution of multimedia applications and services. Although cellular networks are highly efficient when operating in the licensed spectrum where it has exclusive occupancy, the licensed spectrum option faces major challenges due to its scarcity and high cost. An alternative solution is the use of unlicensed spectrum where the amount of spectrum already assigned or planned to be assigned is comparable to or exceeds the amount of the licensed spectrum as shown in Fig. 1.2.

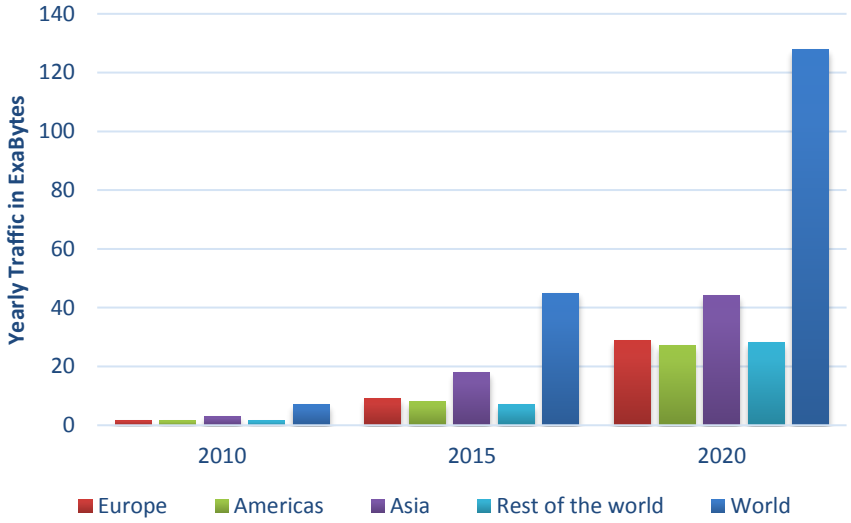

Figure 1.1: Total Mobile Traffic (ExaBytes per year) [1]

The use of the unlicensed spectrum such as the industrial, scientific and medical (ISM) bands at 2.4 GHz and the unlicensed national information infrastructure

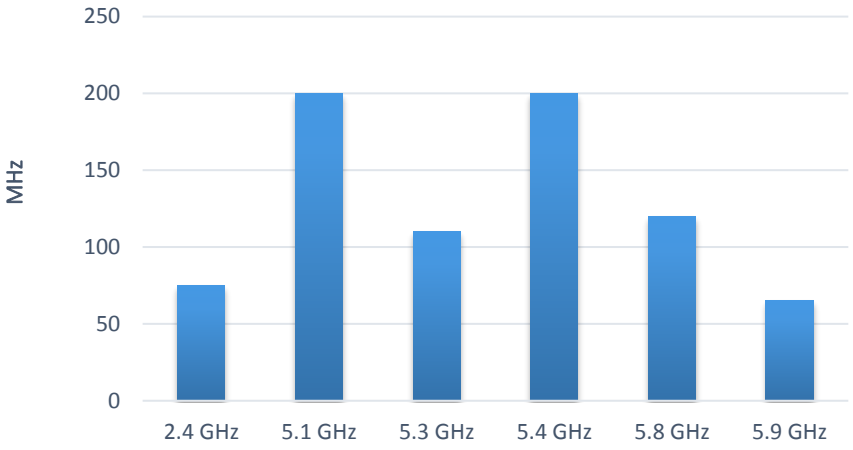

Figure 1.2: Available unlicensed spectrum [2]

(UNII) bands at 5 GHz become more interesting [3, 8]. However, the access to the unlicensed spectrum has been the key to the development of innovative wireless technologies such as Wi-Fi that face similar challenges where there is an increasing number of devices and demand for extra bandwidth to support multimedia applications and services. In fact, Cisco estimates that almost half of all the worldwide Internet traffic is carried through the unlicensed bands by utilizing the Wi-Fi technology [9]. In addition, statistics show that a sample of cable Wi-Fi networks like Comcast in US operates more than 10 million Wi-Fi hotspots [10], similarly Liberty Global operates about 6 million hotspots in Europe [11].

In a similar step to the efforts done to extend the LTE to the unlicensed spectrum and in order to respond to the increasing number of Wi-Fi devices, the FCC issued a Notice of Proposed Rulemaking (NPRM) 12-22 in 2013 that proposed to open up additional 195 MHz of unlicensed spectrum to be used by unlicensed devices in the 5 GHz bands [12]. In particular, the FCC proposal includes opening up additional spectrum in the 5.350-5.470 GHz and the 5.850-5.925 GHz bands. Clearly, this additional spectrum would overlap completely with the intelligent transportation System (ITS) band, and would create a spectrum sharing scenario between DSRC and Wi-Fi, where DSRC would be the incumbent system and Wi-Fi is the secondary one.

A key requirement for extending any wireless technology into the unlicensed band is the capability to coexist in a fair-sharing manner with other technologies in the same band. In this thesis, we model and analyze using tools from stochastic geometry the extension of LTE into the unlicensed UNII bands as well as the extension of Wi-Fi into the ITS band. In order to investigate the issue of fair coexistence between LTE and Wi-Fi and LTE-LTE in the 5 GHz UNII band as well as the DSRC-Wi-Fi coexistence in the 5.9 GHz ITS band, we consider in

our research the next generation IEEE 802.11ax Wi-Fi standard [13]. Hence, we analyze the following coexistence scenarios:

1. In Chapter 3, we present and validate a framework based on stochastic geometry to analyze the coexistence of overlaid LTE and IEEE 802.11ax Wi-Fi networks. In particular, we analyze three coexistence mechanisms (LTE, LTE-U, and LAA) in addition to the Wi-Fi baseline scenario based on the fact that LTE transmissions shall not affect the quality of service (QoS) supported by Wi-Fi networks. We consider both PHY and MAC enhancements of IEEE 802.11ax for the purpose of supporting QoS requirements for applications using Wi-Fi especially in dense environments.

2. In chapter 4, we present and validate two frameworks using stochastic geometry. The first framework is used to analyze the effect of different channel access priorities on the performance of four different coexisting LAA networks in the unlicensed band. The coexistence of LAA networks with each other is a major issue on the road toward 5G. Based on this, we adopt 3GPP release 14 specification for LAA downlink. On the other hand, the second framework is used for assessing the performance of an arbitrary number of coexisting LAA operators using load based equipment (LBE) channel access as LBT mechanism and finite user density. This framework allows to analyze individual system throughput per unit area (in Gbps/km^2) of coexisting operators as their number increases, and the trade-off between the number of operators and subscribers per operator.

3. In Chapter 5, we present and validate an analytical framework that uses stochastic geometry to assess the impact of allowing 802.11ax Wi-Fi to coexist in the unlicensed ITS band with DSRC. Throughout the analysis, we use the area system throughput (AST) as a performance metric to evaluate the impact of coexistence.

Hence, given the considered coexistence scheme, the contributions of this thesis are:

- From LTE perspective, we consider three LTE coexistence mechanisms which are (1) LTE with continuous transmission and no protocol change (conventional LTE), (2) LTE with discontinuous transmission using fixed duty cycle (LTE-U), and (3) licensed assisted access (LAA) LTE. Compared to [37], in [37] the random back off time was uniformly distributed over [0,1] or [1,2] in case of Wi-Fi APs and LAA eNBs. These intervals were chosen for tractability and are not based on 3GPP specifications. However, in this work, we generalize the interval over which the random back off time is distributed in order to capture the channel access parameters of LAA based on 3GPP release 14 [49] 3GPP, 3rd generation partnership project; Technical specification group radio access network; Physical Layer Procedures (Release 14), 3GPP TS 36.213 and analyze different traffic

types.

- On the other hand, from Wi-Fi perspective, compared to the DL only scenario in [36] [37] for legacy Wi-Fi, we consider simultaneous uplink (UL) and DL transmissions using the IEEE 802.11ax standard with different modes including single user (SU) and multi-user (MU) operation mode.

- In SU operation mode Wi-Fi uses EDCA in both UL and DL. In this case, the priority of channel access depends on the type of traffic carried by the Wi-Fi device. Hence, in order to capture this, we generalized the interval over which the random back off time is distributed. Mainly we consider in our analysis voice (VO) and best effort (BE) traffic to analyze the effect of traffic priority on the network performance.

-The derived performance metrics account for the hidden terminal problem effect on UL transmissions for dense deployments of LTE and Wi-Fi networks.

- Furthermore, in MU operation mode, the IEEE 802.11ax defines MU DL transmissions in the DL where as in the UL, MU UL transmissions are handled through two types of trigger based access schemes which are deterministic and random trigger-based access. Thus, we provide analytical expressions for the considered performance metrics for MU UL and DL.

- Also, in order to improve the network performance, IEEE 802.11ax implements a spatial re-use (SR) technique, where a certain AP may ignore the transmissions received from other overlapping APs transmissions as described later. Hence, we discuss the effect of the SR technique on the network performance and we quantify the performance gain through analytical expressions throughout the chapter.

- We also address the effect of channel access priorities on the network performance of coexisting LAA networks where the contention window size utilized in this protocol is mainly affected by the manufacturer choice and the associated data traffic type. Therefore, particular network operators may target certain traffic types, and hence use different contention window sizes which may lead to serious degradation of the performance of the corresponding networks. Thus our framework allows us to model and analyze the network throughput per unit area of several LTE-LAA networks with persistent downlink transmissions and having different contention window sizes. Our results identify coexistence issues not accounted for in the standard and provide analytical tools to help overcome them.

- Finally, we analyze the impact of the possible coexistence of the DSRC and Wi-Fi networks on each other in the ITS bands as proposed by the FCC using stochastic geometry. The proposed framework helps in increasing the awareness among regulatory bodies regarding the possible advantages and drawbacks of approving such proposal.

-For each scenario, the considered system model for the radio channel model, spatial location model, and channel access model will be described when studying each scenario. Then we will derive several performance metrics including medium

access probability (MAP), SINR coverage probability, density of successful transmissions (DST), rate coverage probability, and area system throughput (AST). Also, The accuracy of the analytical results is validated against the simulation results using SINR coverage probability, where we use a spatial discrete event simulator as in [32].

Chapter 2

Related Work

2.1 LTE-WiFi and LTE-LTE Coexistence

Simulation studies in [14]-[15] showed that the neighboring LTE nodes transmissions will block the transmission of Wi-Fi and severely degrade its throughput. This demonstrated the need for new LTE mechanisms to achieve fair coexistence with Wi-Fi when operating in the unlicensed band. Several coexistence mechanisms were proposed in the literature to solve this issue as shown in Fig. 2.1. Out of these mechanisms is the LTE MulteFire mainly for LTE beyond release 13 which is expected to operate solely in the unlicensed band and deliver LTE like performance with Wi-Fi like simplicity. Yet little information is available in the literature about how does this coexistence mechanism operate and hence will be out of the scope of our analysis. Other coexistence mechanisms use licensed assisted access where the unlicensed band is exploited only for data transmissions and remains synchronized with control channels operating in the licensed bands. In [16], one of these mechanisms that is known as LTE-U was proposed where the LTE protocol utilizes a discontinuous transmission pattern. This can be achieved by using a feature called almost-blank subframes (ABS), where the LTE transmissions are blanked for a specific fraction of the time. The ABS feature has been studied using different indoor scenarios, outdoor scenarios, and mixed indoor/outdoor scenarios in [15]-[19], where it was shown that Wi-Fi performance can be effectively increased when adopting the LTE-U mechanism. LTE-U allows for supplement downlink data channel, where the user is allocated extra bandwidth in the downlink from the unlicensed band on an opportunistic basis. On the other hand, another coexistence mechanism known as the license assisted access (LAA) LTE was proposed in 3GPP [20] that targets both uplink and downlink transmissions. The LAA mechanism is based on the listen-before-talk (LBT) feature where an LTE node only transmit, after sensing the channel and finding it idle. Based on the LBT feature, the draft in [21] proposes two different MAC protocols for LAA which are frame based equipment (FBE) and

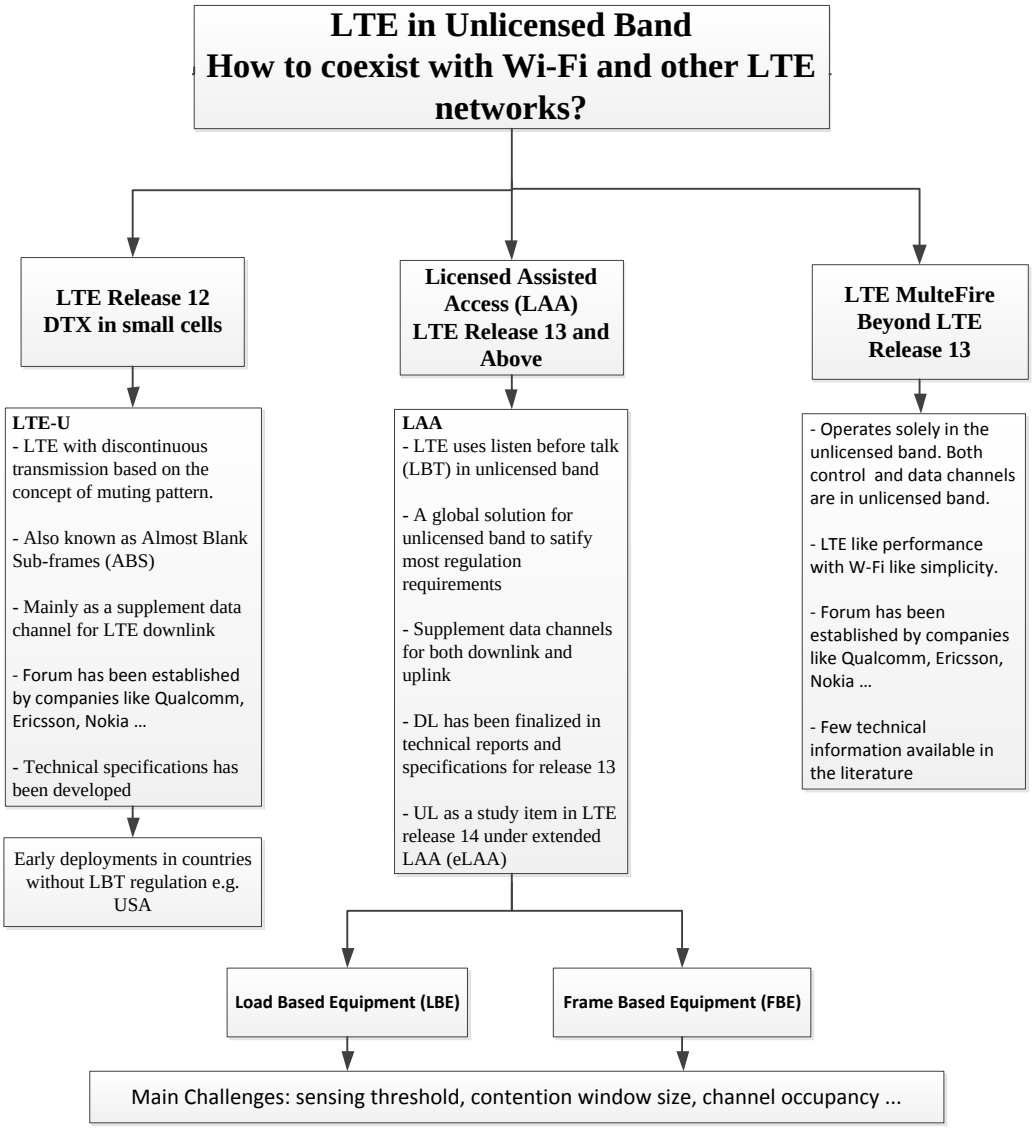

Figure 2.1: LTE coexistence mechanisms

load based equipment (LBE). The former transmit/receive using a fixed timing scheme where only at the begining of a time slot the device will contend for the channel access, whereas the latter is demand-driven; a device will contend for channel access whenever it has data traffic to send. In order to study the LBT feature, different scenarios were studied in the literature where various versions of LBT were presented and evaluated in [22]-[23]. The simulation results showed that LTE can deliver a promising throughput performance while maintaining fair coexistence with Wi-Fi. However, all the mentioned evaluations are based on system level simulations, and few analytical studies can be found in the literature on this coexistence. Thus, there is a need for fundamental theoretical analysis that allow for extra comparison between various coexistence mechanisms. This can be achieved effectively using a powerful mathematical tool known as stochastic geometry, which was lately utilized to achieve tractable models for different performance metrics in various wireless networks, including cellular networks [24]-[31], IEEE 802.11 networks [32], adhoc networks [33], and cognitive radio networks [34]. It has been also adopted for system level performance evaluation and optimization [35].
Recently, stochastic geometry was used to model the coexistence of dense LTE and Wi-Fi networks. In particular, in [36] and [37], the coverage and throughput performance of coexisting LTE and Wi-Fi networks were derived using stochastic geometry where the effect of sensing thresholds and contention window were investigated. However the authors in [36] and [37] considered only the downlink Wi-Fi transmissions of Wi-Fi APs which are assumed to operate in the distributed coordination function (DCF) and with same traffic type. Hence, given the limitations in the work of [36] and [37], we investigate further the issue of fair coexistence between LTE and Wi-Fi in the unlicensed band where we consider in this chapter the coexistence of LTE with the upcoming IEEE 802.11ax Wi-Fi standard [13]. In particular, we consider both PHY and MAC enhancements of the IEEE 802.11ax for the purpose of supporting QoS requirements for applications using Wi-Fi especially in dense environments. In addition, the LAA design should allow also harmonious LAA-LAA coexistence in the unlicensed bands (i.e., between multiple LTE operators) [60]. Hence, we study the LAA-LAA coexistence in order understand the unclear capacity limit of multiple coexisting LAA networks as their number scale. The understanding of how multiple operators coexist in unlicensed spectrum is critical to assess the benefits of this expansion option.

2.2 DSRC-WiFi Coexistence

The Federal Communications Commission (FCC) allocated in 1999 the 5.850-5.925 GHz spectrum band, known as the intelligent transportation System (ITS)

band. This 75 MHz band was allocated to the vehicular communication technolgy, referred to as Dedicated Short Range Communications (DSRC) and is based on the physical (PHY) and medium access control (MAC) layers of the IEEE 802.11p standard.

On the other hand, in order to respond to the increasing number of Wi-Fi devices, the FCC issued a Notice of Proposed Rulemaking (NPRM) 12-22 in 2013 that proposed to open up additional 195 MHz of unlicensed spectrum to be used by unlicensed devices in the 5 GHz bands [12]. In particular, the FCC proposal includes opening up additional spectrum in the 5.350-5.470 GHz and the 5.850-5.925 GHz bands. Clearly, this additional spectrum would overlap completely with the ITS band, and would create a spectrum sharing scnerario between DSRC and Wi-Fi, where DSRC would be the incumbent system and Wi-Fi is the secondary one.

To study the coexistence of DSRC and Wi-Fi, the IEEE 802.11 Regulatory Standing Committee created a subcomiitee called the DSRC Coexistence Tiger Team in order to explore possible coexistence of DSRC and unlicensed systems, e.g. Wi-Fi, and assist in the regulatory process. Later, in March 2015, the tiger team published their final report that summarizes the issues related to the proposed band sharing ideas. But the report only provided high level discussions and stressed on the requirement for futher analysis, simulations and field testing to select a relevant coexistence approach.

The coexistence between 802.11p and Wi-Fi has not gathered much attention since then. The Wi-Fi transmitters have no support for preamble detection of the 10 MHz-wide signals of 802.11p, while 802.11p cannot decode the preambles of the 20 MHz-wide signals of Wi-Fi (802.11ax also offers channels of widths of 40, 80, and 160 MHz). Thus, if 802.11p and Wi-Fi transmitters were to operate in the same spectrum, both transmitters would detect each others using Energy Detection (ED) where the ED threshold is higher by approximately 20 dB than preamble detection. Hence, the sensing range of both transmitters would be much smaller than the stand-alone scenario, resulting in increased probability of collisions in both networks.

Up to date, few research works have studied the coexistence of DSRC and WiFi, mainly 802.11ac, in the ITS band [40]-[45]. In [40], the tiger team reported on the coexistence of DSRC and Wi-Fi described two main proposals. The first proosal is to use existing DSRC channelization and the Clear Channel Assessment (CCA) method in the 10 MHz channels. However, this requires that all Wi-Fi devices, e.g. 802.11ac, to be equipped with a component to detect 802.11p preambles. This approach requires an 802.11ac device to refrain from accessing the channel in the ITS band for 10 seconds after it detects a DSRC preamble, which may result in significant degradation in the throughput of the 802.11ac users. The second proposal suggests modifying the DSRC channelization scheme so that each DSRC channel is 20 MHz wide. Going in the same direction, Lansford et. al. in [41], suggested increasing particular channel access parameters

such as the inter-frame spacing (IFS) to provide higher channel access priority to 802.11p nodes. In this regard, Park et. al. in [42] showed that increasing the arbitration IFS (AIFS) value of 802.11ac transmitters would protect the DSRC transmissions, but they did not consider the impact on 802.11ac devices. On the other hand, the authors in [43] showed using their experimental findings that not all the 802.11ac bandwidth options can be used without causing significant interference to DSRC nodes. Finally, in [44], the authors quantified the impact of 802.11ac Wi-Fi transmissions on the DSRC performance based on the influence of the IFS and sensing range.

In this thesis we contribute to the fundamental understanding of the coexistence of DSRC and Wi-Fi by considering the next generation Wi-Fi 802.11ax standard (i.e., in contrast to prior work that was limited to 802.11 protocols, up to the 802.11ac standard). This aligns with the recent efforts from the community to make the 802.11ax standard the next Wi-Fi [46]. In addition, as compared to the previous works that was mentioned above which are mostly based on experimental evaluation and system level simulations, we present here a fundamental theoretical analysis using stochastic geometry that allows for additional evaluation of the possible coexistence of the DSRC and Wi-Fi networks.

Chapter 3

Coexistence of LTE and IEEE 802.11ax Wi-Fi in the Unlicensed Bands

In this chapter, we investigate further the issue of fair coexistence between LTE and Wi-Fi in the unlicensed band and based on the fact that LTE transmissions shall not affect the quality of service (QoS) supported by Wi-Fi networks, we consider in this chapter the coexistence of LTE with the IEEE 802.11ax Wi-Fi standard.

3.1 System Model

3.1.1 Radio Channel Model

We denote by $l(d)$ the path loss between the transmitter and the receiver which are separated by a distance d. We use here a common free space path loss model with reference distance of one meter for both Wi-Fi and LTE links. Hence $l(d)$ is given by $l(d) = \left(\frac{4\pi}{\Lambda_c}\right)^2 \times d^{\alpha}$ where Λ_c represents the wavelength and α is the path-loss exponent. For simplicity we ignore the large scale shadowing effect as in [37]. Also, we assume that all channels are subject to i.i.d Rayleigh fading where each fading variable is exponentially distributed with parameter μ.

3.1.2 Spatial Location Model

We consider mainly a scenario in which two operators coexist in a single unlicensed frequency band that has a bandwidth denoted by B. We assume that operator 1 uses Wi-Fi, while operator 2 uses LTE with different coexistence mechanisms. In particular, we consider three LTE mechanisms which are LTE with continuous transmission (i.e. no protocol change), LTE with discontinuous transmission (LTE-U), and licensed assisted access (LAA). In baseline scenario, both

operators use Wi-Fi. The LTE eNBs are assumed to be low power small cell (pico-cell) eNBs as in [37, 38].

We model the location of Wi-Fi APs, Wi-Fi users, and LTE eNBs, having traffic for transmission and co-existing in the same band, as realizations of three independent homogeneous Poisson point processes (PPP) on $\mathbb{R}^2$. The Wi-Fi users process with persistent UL traffic is denoted as $\Phi_U = \{z_p\}$ and has intensity λ_U, while the Wi-Fi APs process with persistent DL traffic is denoted as $\Phi_D = \{x_j\}$ with intensity λ_D. Also, the LTE eNB process with persistent DL traffic is denoted as $\Phi_L = \{y_k\}$ with intensity λ_L. The LTE UEs process are modeled as independent homogeneous PPPs denoted as $\Phi_{UE} = \{u_m\}$. Thus based on Slivnyak′s theorem [39], we analyze the performance of a typical Wi-Fi user/LTE UE in the DL and typical AP in the UL which are assumed to be at the origin. For the UL of Wi-Fi, we focus on the case where the Wi-Fi user connects to the Internet through the closest AP and that no direct user-user communication exists. Similarly, each UE is associated with its closest eNB, which provides the strongest average received power [37]. Furthermore, index 0 is used for typical user/UE and its serving AP/eNB in the DL which will be called the tagged AP/eNB in the rest of the chapter. Also in the UL, index 0 will be used for the typical AP and its serving (tagged) user. The link between the tagged AP/eNB and the typical Wi-Fi user/LTE UE in the DL is referred to as the typical Wi-Fi DL/LTE link, while the link between the tagged user and the typical AP in the UL is referred to as the typical Wi-Fi UL. Given that Φ_D is a PPP with intensity λ_D, the probability density function (PDF) of the distance from the tagged AP to the typical user in the DL is $f_{\|x_0\|}(r) = 2\pi r\lambda_D e^{-\lambda_D \pi r^2}$. Similarly, given that the users that are associated to an AP should be those users inside the Voronoi cell of this AP, the distribution of $\|z_0\|$ can be approximated by that of $\|x_0\|$ where UL and DL links are assumed to be reciprocal. Hence the PDF of the distance from the the tagged Wi-Fi user to the typical AP in the UL is $f_{\|z_0\|}(r) = 2\pi r\lambda_D e^{-\lambda_D \pi r^2}$. Also, the PDF of the distance from the tagged eNB to the typical UE is $f_{\|y_0\|}(r) = 2\pi r\lambda_L e^{-\lambda_L \pi r^2}$.

$$
\begin{aligned}
SINR_0^U &= \frac{P_U G_{0,0}^{UD}/l(\|z_0\|)}{\sum\limits_{z_p\in\Phi_U\setminus\{z_0\}} P_U G_{p,0}^{UD} e_p^U/l(\|z_p\|) + \sum\limits_{x_j\in\Phi_D} P_D G_{j,0}^{D} e_j^D/l(\|x_j\|) + \sum\limits_{y_m\in\Phi_L} P_L G_{m,0}^{LD} e_m^L/l(\|y_m\|) + \sigma_N^2} \\
SINR_0^D &= \frac{P_U G_{0,0}^{DU}/l(\|x_0\|)}{\sum\limits_{x_j\in\Phi_D\setminus\{x_0\}} P_D G_{j,0}^{DU} e_j^D/l(\|x_j\|) + \sum\limits_{z_p\in\Phi_U} P_U G_{p,0}^{U} e_p^U/l(\|z_p\|) + \sum\limits_{y_m\in\Phi_L} P_L G_{m,0}^{LU} e_m^L/l(\|y_m\|) + \sigma_N^2} \\
SINR_0^L &= \frac{P_L G_{0,0}^{L}/l(\|y_0\|)}{\sum\limits_{y_m\in\Phi_L\setminus\{y_0\}} P_L G_{m,0}^{L} e_m^L/l(\|y_m\|) + \sum\limits_{z_p\in\Phi_U} P_U G_{p,0}^{UL} e_p^U/l(\|z_p\|) + \sum\limits_{x_j\in\Phi_D} P_D G_{j,0}^{DL} e_j^D/l(\|x_j\|) + \sigma_N^2}
\end{aligned}
\tag{3.1}
$$

3.1.3 Modelling Channel Access for LTE and IEEE 802.11 ax Wi-Fi

The 802.11ax standard brings several enhancements for high efficiency WLANs where it defines two modes of operation which are the single-user (SU) mode and the multi-user (MU) mode [47, 48, 13]. In the SU mode, Wi-Fi users/APs send and receive data one at a time once they secure access to the medium using the CSMA/CA protocol as defined in the legacy IEEE 802.11 standard. On the other hand, the MU mode defines simultaneous operation of multiple WiFi users. The MU mode is further divided into DL and UL MU modes.

The MU mode is enabled by the OFDMA technology that builds on existing OFDM digital modulation scheme where the 802.11ax standard further assigns specific set of subcarriers to individual users. Hence, it divides the existing 802.11 channels with 20, 40, 80 and 160 MHz wide into smaller sub-channels called resource units (RUs) with a predefined number of subcarriers. In this context, the AP decides how to allocate the channel based on MU traffic needs where it may allocate the whole channel e.g. 20 MHz to one user at a time (as in the case of 802.11ac) or it may partition it to serve multiple users simultaneously. For example, in case of 20 MHz channel, the AP may partition the channel into N_{RU} = 2, 4 or 9 RUs.

In the DL MU mode, the AP serves multiple data transmissions associated to WiFi users at the same time. On the other hand, in the UL MU mode we have simultaneous UL transmissions of data from multiple users to the AP. Hence, in the MU mode, the AP acts as a central coordinator for scheduling transmissions and hence users will not transmit in this case unless the AP assigns it RUs. In the case of simultaneous DL transmissions, after successful access to the channel, the AP will send DL data to several users simultaneously on different RUs. Whereas in case of simultaneous UL transmissions the AP will transmit a trigger frame (TF) after accessing the channel. Hence, in both cases the AP will initially contend using EDCA parameters for channel access as in case of SU mode and it is clear that the access of the user depends on the probability of the AP to access the channel.

In order to schedule UL transmissions, the AP polls the users with a TF. After receiving the trigger frame, two channel access mechanisms may be used by the user which are the trigger-based deterministic access (DA) and the trigger-based random access (RA). In the trigger-based DA mechanism, the user will send a data frame on the scheduled RUs that were indicated in the trigger frame. Whereas in the trigger-based RA, users that receive the trigger frame will contend for channel access on the specified RUs using the CSMA/CA protocol. Then, users that win access to the medium on randomly selected RU from a set of specified RUs, will send their data frames to the AP. In both UL and DL OFDMA transmissions, the AP will have to contend for channel access. In this case, the AP may choose any access category (AC) where the chosen AC may give the AP

higher priority in accessing the channel compared to its associated users. The different ACs are defined based on the parametrized arbitration inter-frame spacing (AIFS[AC]) and the contention window size to differentiate between traffic types (voice, video, best effort, and background traffic) inside each user/AP.

Also, to improve network performance, the 802.11ax implements a SR technique, where a certain AP may ignore the transmissions received from other overlapping APs transmissions. This can be realized through color codes which is a bit defined in the MAC header and can be used to differ between transmissions of different basic service sets (BSS). In this case, the AP will consider the medium busy if it detects a MAC header with the same color bit where APs that belong to different BSS will have different color codes.

In the CSMA/CA protocol, a Wi-Fi AP/user performs clear channel assessment (CCA) process to detect the presence of active transmitters for which the received signal power exceeds a certain detection threshold. Using the CCA process, a channel is determined busy if the intending transmitter detects another Wi-Fi signal above the carrier sense (CS) threshold Γ_{cs}, or if any other signal that is not decodable, such as an LTE signal that is detected above the energy detection (ED) threshold Γ_{ed}. If the channel is found idle, the CSMA/CA device will then follow a random back-off period before transmission that is selected randomly from a contention window, which is a set of possible values with a predefined maximum and minimum that determines the priority for a CSMA/CA device to access the medium.

In case of conventional LTE or LTE-U, eNBs will transmit without sensing the channel. In particular, in the case of LTE-U mechanism, LTE adopts a discontinuous transmission pattern where LTE transmits for a fraction τ of time (duty cycle) and is muted for the other $1-\tau$ of time where $0 \leq \tau \leq 1$. Hence it is clear that conventional LTE with continuous transmission is a special case of LTE-U where $\tau = 1$. Usually τ shall be chosen to ensure fairness between Wi-Fi and LTE in the unlicensed band. In other words, when selecting τ, interference from LTE shall not affect Wi-Fi performance more than any other Wi-Fi network that may coexist with the initial one. However, in case of LAA, LTE uses the LBT mechanism with random back off, where the eNB first performs a CCA process similar to the one used by Wi-Fi. However, LAA uses energy detection to detect the presence of any interferer by using energy detection threshold Γ_L. In addition, LAA defines different channel ACs for different traffic types. Each AC has its own defer period and contention window size to differentiate between traffic types such as voice, video, best effort, and background traffic inside each LAA eNB. We define the contender of a Wi-Fi AP x_i as the other Wi-Fi APs, Wi-Fi user and LTE eNBs from which the received power at x_i exceeds thresholds Γ_{cs}, Γ_{cs}, and Γ_{ed} respectively. Similarly, we define the contenders of a Wi-Fi user z_n as the other Wi-Fi users, Wi-Fi APs and LTE eNBs from which the received power at z_n exceeds thresholds Γ_{cs}, Γ_{cs}, and Γ_{ed} respectively. On the other hand, in case of LAA, we define the contenders of eNB y_m, as the other Wi-Fi users,

Wi-Fi APs and LAA eNBs from which the received power at y_m exceeds threshold Γ_L.

Each Wi-Fi AP x_i has an independent mark t_i^D that represents the random back-off period, which is uniformly distributed in the interval $[\Delta_D, CW_D + \Delta_D]$. Also, each Wi-Fi user z_n has an independent mark t_n^U that is uniformly distributed in the interval $[\Delta_U, CW_U + \Delta_U]$. Furthermore, each LAA eNB y_m has an independent mark t_m^L that is uniformly distributed in the interval $[\Delta_L, CW_L + \Delta_L]$. Note that Δ was introduced to capture the difference between different inter frame spaces of different traffic types and CW is the contention window size. Mainly, we consider coexistence of voice and best effort traffic. In addition, based on [49] where channel access parameters of LAA were designed similar to those in Wi-Fi for different traffic types. Thus, we consider t_{VO} and t_{BE} to be uniformly distributed in the intervals [0, 3] and [2,17], respectively. Each Wi-Fi user/AP/LAA eNB is retained when contending for channel access if it has a smaller timer (or back-off period) than all its contenders. A medium access indicator e_n^U is assigned to each Wi-Fi user (e_i^D to each AP and e_k^L to each LTE eNB) which is equal to one if the Wi-Fi user, AP or eNB are allowed to transmit by the corresponding MAC layer protocol and zero otherwise.

In the considered model for Wi-Fi channel access, two Wi-Fi users that operate using EDCA and are associated with the same AP may get access to the channel simultaneously given that they are not in the contention domain of each other. The interference resulting from the transmission of one user on the useful transmission of the other user is captured later in the derivation of the SINR coverage probability at the AP in the UL. This problem is well known in the literature as the hidden terminal problem. Although the request-to-send (RTS) - clear-to-send (CTS) approach was proposed to solve this problem, however it is rarely used in practice since it introduce latency and reduce the network throughput [50]. Hence we assume that users do not use the RTS-CTS mechanism in the UL. Note that we denote by medium access probability (MAP), the Palm probability [39] that the medium access indicator of a Wi-Fi user/AP/LTE eNB is equal to 1. This channel access model, which may have some limitations with its fixed contention window size (that does not capture the exponential backoff and the dynamics of the timer history), has shown its ability as a conservative model of the CSMA/CA in IEEE 802.11 standard as demonstrated in simulation results of [51].

3.1.4 Performance Metrics

In this section, we define the performance metrics that are used in our analysis. In addition to the MAP that will be derived for each coexistence mechanism in the following sections, we also base our analysis on the SINR coverage probability for the typical (receiver) user. Thus, in general, given the fact that the tagged (transmitter) node transmits, by applying Slivnyak′s theorem, the received SINR

Table 3.1: Used Symbols and Simulation Values

Symbol	Definition	Simulation Value
P_D, P_U, P_L	Wi-Fi AP, Wi-Fi user, LTE eNB transmit power	23 dBm, 18 dBm, 23 dBm
f_c, B	Carrier frequency and bandwidth of the unlicensed band	5 GHz, 20 MHz
α	Path loss exponent	4
μ	Parameter for Rayleigh fading channel	1
σ_N^2	Noise power	0
Γ_{cs},Γ_{ed},Γ_L	Carrier Sensing and energy detection thresholds	-82 dBm, -62 dBm, -72 dBm
Φ_U,Φ_D,Φ_L	Wi-Fi users PPP, Wi-Fi APs PPP, co-exisitng LTE eNBs (or Wi-Fi APs) PPP	
λ_U,λ_D,λ_L	Wi-Fi users, Wi-Fi APs, and coexisting LTE eNBs (or Wi-Fi APs) density	
e_n^U, e_k^L, e_i^D	Medium access indicator for user z_n, co-exisitng eNB (or AP) y_k, AP x_i	
$B(x,r)$, $B^o(x,r)$	Closed (open) ball with center x and radius r	
$G_{i,j}^U$, ($G_{i,j}^{UD}$,$G_{i,j}^{UL}$)	Fading of the channel from user i to user j (from user i to AP j, from user i to eNB (co-existing AP or UE) j respectively)	Exponentially distributed with parameter μ
$G_{i,j}^D$, ($G_{i,j}^{DL}$,$G_{i,j}^{DU}$)	Fading of the channel from AP i to AP j (from AP i to eNB (co-existing AP or UE) j, from AP i to user j respectively)	Exponentially distributed with parameter μ
$G_{i,j}^L$, ($G_{i,j}^{LD}$, $G_{i,j}^{LU}$)	Fading of the channel from eNB i to eNB (co-existing AP or UE) j (from eNB i to AP j, from eNB i to user j respectively)	Exponentially distributed with parameter μ
R_{cs}	Carrier sensing range	

at the typical node located at the origin in Wi-Fi UL, Wi-Fi DL, and LTE DL is given by (3.1). Hence for a typical node, the SINR coverage probability with a SINR threshold T is defined as $\mathbb{P}(SINR_0^X > T | e_0^X = 1)$ where X in general denotes the type of the link and may be replaced by the letters U, D, or L. This corresponds to the instantaneous SINR performance of the typical link. Now, based on the SINR coverage probability and the MAP we define the following

$$d_{suc}^X(\lambda_D,\lambda_U,\lambda_L,T) = \lambda_X\, \hat{p}_{MAP}^X(\lambda_U,\lambda_D,\lambda_L)\, \mathbb{P}(SINR_0^X > T | e_0^U = 1) \tag{3.2}$$

$$P_{throughput}^X(\lambda_D,\lambda_U,\lambda_L,\rho) = \mathbb{P}\left(B\log\left(1+SINR_0^X\right)\hat{p}_{MAP}^X(\lambda_U,\lambda_D,\lambda_L) > \rho | e_0^U = 1\right) \tag{3.3}$$

$$\begin{aligned}
e_{lte-u}^{n,U} &= \prod_{z_p\in\Phi_U\setminus\{z_n\}} \left(\mathbb{1}_{t_p^U\geq t_n^U} + \mathbb{1}_{t_p^U<t_n^U}\mathbb{1}_{G_{pn}^U/l(\|z_p-z_n\|)\leq\Gamma_{cs}/P_U}\right) \prod_{x_j\in\Phi_D} \left(\mathbb{1}_{t_j^D\geq t_n^U} + \mathbb{1}_{t_j^D<t_n^U}\mathbb{1}_{G_{jn}^{DU}/l(\|x_j-z_n\|)\leq\Gamma_{cs}/P_D}\right) \prod_{y_m\in\Phi_L} \left(\mathbb{1}_{G_{mn}^{LU}/l(\|y_m-z_n\|)\leq\Gamma_{ed}/P_L}\right) \\
e_{laa}^{n,U} &= \prod_{x_j\in\Phi_D} \left(\mathbb{1}_{t_j^D\geq t_n^U} + \mathbb{1}_{t_j^D<t_n^U}\mathbb{1}_{G_{jn}^{DU}/l(\|x_j-z_n\|)\leq\Gamma_{cs}/P_D}\right) \prod_{y_m\in\Phi_L} \left(\mathbb{1}_{t_m^L\geq t_n^U} + \mathbb{1}_{t_m^L<t_n^U}\mathbb{1}_{G_{mn}^{LU}/l(\|y_m-z_n\|)\leq\Gamma_{ed}/P_L}\right) \prod_{z_p\in\Phi_U\setminus\{z_n\}} \left(\mathbb{1}_{t_p^U\geq t_n^U} + \mathbb{1}_{t_p^U<t_n^U}\mathbb{1}_{G_{pn}^U/l(\|z_p-z_n\|)\leq\Gamma_{cs}/P_U}\right)
\end{aligned} \tag{3.4}$$

$$\begin{aligned}
\tilde{e}_{lte-u}^{i,D} &= \prod_{y_m\in\Phi_L} \left(\mathbb{1}_{G_{mi}^{LD}/l(\|y_m-x_i\|)\leq\Gamma_{ed}/P_L}\right) \prod_{z_p\in\Phi_U} \left(\mathbb{1}_{t_p^U\geq t_i^D} + \mathbb{1}_{t_p^U<t_i^D}\mathbb{1}_{G_{pi}^{UD}/l(\|z_p-x_i\|)\leq\Gamma_{cs}/P_U}\right) \\
\tilde{e}_{laa}^{i,D} &= \prod_{y_m\in\Phi_L} \left(\mathbb{1}_{t_m^L\geq t_i^D} + \mathbb{1}_{t_m^L<t_i^D}\mathbb{1}_{G_{mi}^{LD}/l(\|y_m-x_i\|)\leq\Gamma_{ed}/P_L}\right) \prod_{z_p\in\Phi_U} \left(\mathbb{1}_{t_p^U\geq t_i^D} + \mathbb{1}_{t_p^U<t_i^D}\mathbb{1}_{G_{pi}^{UD}/l(\|z_p-x_i\|)\leq\Gamma_{cs}/P_U}\right)
\end{aligned} \tag{3.5}$$

$$\begin{aligned}
e_{lte-u}^{i,D} &= \prod_{x_j\in\Phi_D\setminus\{x_i\}} \left(\mathbb{1}_{t_j^D\geq t_i^D} + \mathbb{1}_{t_j^D<t_i^D}\mathbb{1}_{G_{ji}^D/l(\|x_j-x_i\|)\leq\Gamma_{cs}/P_D}\right) \prod_{y_m\in\Phi_L} \left(\mathbb{1}_{G_{mi}^{LD}/l(\|y_m-x_i\|)\leq\Gamma_{ed}/P_L}\right) \prod_{z_p\in\Phi_U} \left(\mathbb{1}_{t_p^U\geq t_i^D} + \mathbb{1}_{t_p^U<t_i^D}\mathbb{1}_{G_{pi}^{UD}/l(\|z_p-x_i\|)\leq\Gamma_{cs}/P_U}\right) \\
e_{laa}^{i,D} &= \prod_{x_j\in\Phi_D\setminus\{x_i\}} \left(\mathbb{1}_{t_j^D\geq t_i^D} + \mathbb{1}_{t_j^D<t_i^D}\mathbb{1}_{G_{ji}^D/l(\|x_j-x_i\|)\leq\Gamma_{cs}/P_D}\right) \prod_{y_m\in\Phi_L} \left(\mathbb{1}_{t_m^L\geq t_i^D} + \mathbb{1}_{t_m^L<t_i^D}\mathbb{1}_{G_{mi}^{LD}/l(\|y_m-x_i\|)\leq\Gamma_{ed}/P_L}\right) \prod_{z_p\in\Phi_U} \left(\mathbb{1}_{t_p^U\geq t_i^D} + \mathbb{1}_{t_p^U<t_i^D}\mathbb{1}_{G_{pi}^{UD}/l(\|z_p-x_i\|)\leq\Gamma_{cs}/P_U}\right)
\end{aligned} \tag{3.6}$$

two performance metrics that are used to analyze the coexistence mechanisms. Note that the Wi-Fi UL/Wi-Fi DL/LTE DL are only activated when the tagged Wi-Fi user/AP/eNB access the channel, hence we have the following definitions:
1) Density of Successful Transmissions (DST): given the decoding SINR requirement T, DST is defined in (3.2) as the mean number of transmission links per unit area.
2) Shannon Throughput Probability: given the rate threshold ρ, the Shannon throughput probability is defined in (3.3) as the probability for the typical Wi-Fi UL/Wi-Fi DL/LTE DL to support at least an average throughput of ρ. Note that $\hat{p}^{X}_{MAP}(\lambda_U, \lambda_D, \lambda_L)$ in (3.3) account for the fact that the tagged Wi-Fi user/AP/eNB has a channel access for $\hat{p}^{U}_{MAP}(\lambda_U, \lambda_D, \lambda_L)/\ \hat{p}^{D}_{MAP}(\lambda_U, \lambda_D, \lambda_L)$ $/\hat{p}^{L}_{MAP}(\lambda_U, \lambda_D, \lambda_L)$ fraction of time on average which signifies that the Shannon throughput probability with threshold ρ provides the fraction of links that can support an average throughput of ρ. For the rest of the chapter, since Φ_U, Φ_D and Φ_L are stationary and isotropic, thus the above performance metrics of the typical Wi-Fi AP/Wi-Fi user/LTE UE are invariant with respect to the angle of the tagged Wi-Fi user/Wi-Fi AP/LTE eNB. Also, we assume in our case that the polar coordinates of the tagged user z_0, tagged AP x_0 and tagged eNB y_0 are $(r_0, 0)$.

Finally we define the following functions to be used throughout the chapter where $N_U(z, r, \Gamma)$ $/N_D(z, r, \Gamma)$ $/N_L(z, r, \Gamma)$ represent the expected number of users, APs and eNBs respectively in $_{\mathbb{R}^2\setminus B(0,r)}$ whose signal power received at $z \in \mathbb{R}^2$ exceeds threshold Γ.
Furthermore, $C_U(z_1, \Gamma_1, z_2, \Gamma_2, r)$, $C_D(z_1, \Gamma_1, z_2, \Gamma_2, r)$, and $C_L(z_1, \Gamma_1, z_2, \Gamma_2, r)$ represent the expected number of users, APs and eNBs respectively in $\mathbb{R}^2\setminus B(0, r)$ whose signal power received at $z_1 \in \mathbb{R}^2$ and $z_2 \in \mathbb{R}^2$ exceeds thresholds Γ_1 and Γ_2 respectively. Note that the functions $H_N(.)$ and $H_D(.)$ are used to simplify the equations of conditional MAP in the coming sections.

3.2 Analysis of LTE-U and LAA With IEEE 802.11ax Wi-Fi DL And UL For SU Operation Mode

In this section, we analyze both LTE co-existence mechanisms which are the LTE-U and LAA mechanisms. Initially, for the sake of the analysis, we consider the case of LTE-U with $\tau = 1$ or LAA while Wi-Fi IEEE 802.11ax UL and DL transmissions co-exist. Then based on that, we derive the DST and throughput for coexisiting LTE in case of LTE-U with a generic duty cycle (τ) or LAA when co-existing with IEEE 802.11ax WiFi networks.

Table 3.2: Notations and Definitions of Used Functions

Notation	Definition
$N_U(z,r,\Gamma)$	$\lambda_U \int_{\mathbb{R}^2\setminus B(0,r)} \exp\big(-\mu\frac{\Gamma}{P_U} l(\|x-z\|)\big)\mathrm{d}x$
$N_D(z,r,\Gamma)$	$\lambda_D \int_{\mathbb{R}^2\setminus B(0,r)} \exp\big(-\mu\frac{\Gamma}{P_D} l(\|x-z\|)\big)\mathrm{d}x$
$N_L(z,r,\Gamma)$	$\lambda_L \int_{\mathbb{R}^2\setminus B(0,r)} \exp\big(-\mu\frac{\Gamma}{P_L} l(\|x-z\|)\big)\mathrm{d}x$
$C_U(z_1,\Gamma_1,z_2,\Gamma_2,r)$	$\lambda_U \int_{\mathbb{R}^2\setminus B(0,r)} \exp\big(-\mu\frac{\Gamma_1}{P_U} l(\|x-z_1\|)-\mu\frac{\Gamma_2}{P_U} l(\|x-z_1\|)\big)\mathrm{d}x$
$C_D(z_1,\Gamma_1,z_2,\Gamma_2,r)$	$\lambda_D \int_{\mathbb{R}^2\setminus B(0,r)} \exp\big(-\mu\frac{\Gamma_1}{P_D} l(\|x-z_1\|)-\mu\frac{\Gamma_2}{P_D} l(\|x-z_1\|)\big)\mathrm{d}x$
$C_L(z_1,\Gamma_1,z_2,\Gamma_2,r)$	$\lambda_L \int_{\mathbb{R}^2\setminus B(0,r)} \exp\big(-\mu\frac{\Gamma_1}{P_L} l(\|x-z_1\|)-\mu\frac{\Gamma_2}{P_L} l(\|x-z_1\|)\big)\mathrm{d}x$
$N_U(z,\Gamma), N_D(z,\Gamma), N_L(z,\Gamma)$	$N_U(z,\|z\|,\Gamma), N_D(z,\|z\|,\Gamma), N_L(z,\|z\|,\Gamma)$
$C_U(z_1,z_2), C_D(z_1,z_2), C_L(z_1,z_2)$	$C_U(z_1,\Gamma_{cs},z_2,\Gamma_{cs},R_{cs}), C_D(z_1,\Gamma_{cs},z_2,\Gamma_{cs},\|z_2\|)$, $C_L(z_1,\Gamma_{ed},z_2,\Gamma_{ed},\|z_2\|)$
$N_U(\Gamma), N_D(\Gamma), N_L(\Gamma)$	$N_U(o,\Gamma), N_D(o,\Gamma), N_L(o,\Gamma)$
$N_U(z), N_D(z), N_L(z)$	$N_U(z,\Gamma_{cs}), N_D(z,\Gamma_{cs}), N_L(z,\Gamma_{ed})$
$C_U(z), C_D(z), C_L(z)$	$C_U(z,o), C_D(z,o), C_L(z,o)$
N_U, N_D, N_L	$N_U(\Gamma_{cs}), N_D(\Gamma_{cs}), N_L(\Gamma_{ed})$
$H_N\Big(x_1,x_2,y,\Delta_1,CW_1,\Delta_2,CW_2,N_1(t),N_2(t')\Big)$	$\frac{1-\exp(-\mu y l(\|x_1-x_2\|))}{CW_1 CW_2}\int_{\Delta_2}^{CW_2+\Delta_2}\int_{\Delta_1}^{CW_1+\Delta_1}\exp\Big[-N_1(t)-N_2(t')\Big]\mathrm{d}t\mathrm{d}t'$
$H_D\Big(x,y,\Delta,CW,N_1(t),N_2(t)\Big)$	$=\frac{1}{CW}\int_{\Delta}^{CW+\Delta}\Big(1-N_1(t)\exp[-\mu y l(\|x\|)]\Big)\exp[-N_2(t)]\mathrm{d}t$
$H_{MAP}\Big(\Delta,CW,N_1(t)\Big)$	$=\frac{1}{CW}\int_{\Delta}^{CW+\Delta}\exp[-N_1(t)]\mathrm{d}t$

3.2.1 Medium Access Probability

The duty cycle $0 \leq \tau \leq 1$ corresponds to the medium access probability of LTE-U. In case of LTE with continuous transmission, the medium access probability of LTE is equal to one ($\tau = 1$). Hence, when LTE transmits continuously, either Wi-Fi users in the UL or Wi-Fi APs in the DL will not transmit each time it has any LTE eNB as its contender since they will both sense the channel busy all the time in such scenario. Whereas in the case of LAA, Wi-Fi users and APs will contend with each other and with LAA eNBs to access the channel. Based on that, we derive the MAP of IEEE 802.11ax Wi-Fi UL and DL for the SU operation mode initially. In addition, we consider both cases in the presence/absence of the SR technique utilized by the APs for the purpose of increasing network capacity.

MAP For IEEE 802.11ax UL and DL Under SU Mode Operation

In the SU operation mode, each Wi-Fi user and AP will contend for channel access using EDCA. Hence, in the presence/absence of the SR technique that is utilized by APs, a Wi-Fi user z_n will have the medium access indicator $e^{n,U}_{lte-u}/e^{n,U}_{laa}$ in case of coexistence with LTE-U/LAA that is derived as in (3.4). Note that $\mathbb{1}_A$ is the indicator function of the event A, $\mathbb{1}_A$ is equal to one if A exists and zero otherwise. On the other hand, when WiFi APs utilize SR technique, each Wi-Fi AP x_i will have a medium access indicator $\tilde{e}^{i,D}_{lte-u}/\tilde{e}^{i,D}_{laa}$ as in (3.5). Whereas, in the absence of the SR technique, each Wi-Fi AP x_i will have a medium access indicator $e^{i,D}_{lte-u}/e^{i,D}_{laa}$ provided in (3.6). Note that the energy detection is implemented

based on the strongest interferer which is a reasonable model that is used instead of total interference (based on IEEE 802.11 specifications) as shown in [37]. The medium access probability (MAP) of a tagged Wi-Fi user is the palm probability that its medium access indicator is equal to one given that its timer is equal to t and it is located at $z_0 = (0, r_0)$. The MAP for the tagged Wi-Fi user z_n is defined as $\hat{p}^U_{SU,MAP}(\lambda_U, \lambda_D, \lambda_L) = \mathbb{P}[e^U_n = 1 | t^U_n = t, z_0 = (0, r_0)]$ where $e^U_n = e^{n,U}_{lte-u}$ or $e^{n,U}_{laa}$. The MAPs of user z_n in case of SU operation are derived in Lemma 1.

Lemma 1. Given that a WiFi AP x_j has a timer $t^D_j \in [\Delta_D, CW_D + \Delta_D]$ with cumulative distribution function (CDF) $F_D(t)$, a Wi-Fi user z_n has a timer $t^U_n \in [\Delta_U, CW_U + \Delta_U]$ with $F_U(t)$, and LAA eNB y_m has a timer $t^L_m \in [\Delta_L, CW_L + \Delta_L]$ with $F_L(t)$. The MAP in IEEE 802.11ax SU operation mode for a tagged Wi-Fi user of SR technique is given by (3.7).

$$\hat{p}^L_{SU,MAP}(\lambda_D, \lambda_U, \lambda_L) = \int_0^\infty H_{MAP}\big(\Delta_L, CW_L, -F_L(t)N_L(y_0, \Gamma_L) - F_D(t)N_D(\Gamma_L) f_{\|y_0\|}(r_0)\mathrm{d}r_0 \tag{3.10}$$

$$\hat{p}^U_{SINR,SU}(T, \lambda_D, \lambda_U, \lambda_L) \approx \int_0^\infty \exp\Big(-\mu T l(r_0)\frac{\sigma^2_N}{P_U}\Big) \exp\Big(-\int_{\mathbb{R}^2} \frac{Tl(r_0)\lambda_L p^{y/z_0}_{1,MAP}}{\frac{P_U}{P_L} l(\|x\|) + Tl(r_0)}\mathrm{d}x\Big) \exp\Big(-\int_{\mathbb{R}^2} \frac{Tl(r_0)\lambda_D p^{x/z_0}_{1,MAP}}{\frac{P_U}{P_D} l(\|x\|) + Tl(r_0)}\mathrm{d}x\Big) \exp\Big(-\int_{\mathbb{R}^2 \setminus B(z_0, R_{cs})} \frac{Tl(r_0)\lambda_U p^{z/z_0}_{1,MAP}}{l(\|x\|) + Tl(r_0)}\mathrm{d}x\Big) f_{\|z_0\|}(r_0)\mathrm{d}r_0 \tag{3.11}$$

Proof In the SU mode, the MAP of a tagged Wi-Fi user z_n in case of LTE-U is given by (3.8) where (a) follows from the fact that Φ_D, Φ_U and Φ_L are independent. (b) follows from slivnyak′s theorem, the probability generating functional (P.G.FL) of the PPP, and by de-conditioning on $t \sim U(\Delta_U, CW_U + \Delta_U)$ and using the definition of N_D, N_U and N_L in Table 4.2 gives the desired result.

$$\begin{aligned}
&\text{LTE} - \text{U}: \quad \hat{p}^U_{SU,MAP}(\lambda_D, \lambda_U, \lambda_L) = \int_0^\infty H_{MAP}\big(\Delta_U, CW_U, -N_L - F_D(t)N_D - F_U(t)N_U(z_0, \Gamma_{cs}, R_{cs})\big) \times f_{\|z_0\|}(r_0)\mathrm{d}r_0 \\
&\text{LAA}: \quad \hat{p}^U_{SU,MAP}(\lambda_D, \lambda_U, \lambda_L) = \int_0^\infty H_{MAP}\big(\Delta_U, CW_U, -F_L(t)N_L - F_D(t)N_D - F_U(t)N_U(z_0, \Gamma_{cs}, R_{cs})\big) \times f_{\|z_0\|}(r_0)\mathrm{d}r_0
\end{aligned} \tag{3.7}$$

$$\begin{aligned}
&\hat{p}^U_{SU,MAP}(\lambda_D, \lambda_U, \lambda_L) = \mathbb{P}[e^{n,U}_{lte-u} = 1 | t^U_n = t, z_0 = (0, r_0)] = \mathbb{E}^{z_n}_{\Phi_U}(e^{n,U}_{lte-u}) \\
&= \mathbb{E}^{z_n}_{\Phi_U}\Big[\prod_{x_j \in \Phi_D} \Big(\mathbb{1}_{t^D_j \geq t^U_n} + \mathbb{1}_{t^D_j < t^U_n} \mathbb{1}_{G^{DU}_{jn}/l(\|x_j - z_n\|) \leq \Gamma_{cs}/P_D}\Big) \prod_{y_m \in \Phi_L} \big(\mathbb{1}_{G^{LU}_{mn}/l(\|y_m - z_n\|) \leq \Gamma_{ed}/P_L}\big) \prod_{z_p \in \Phi_U \cap B^c(z_0, R_{cs}) \setminus \{z_n\}} \Big(\mathbb{1}_{t^U_p \geq t^U_n} + \mathbb{1}_{t^U_p < t^U_n} \mathbb{1}_{G^{UU}_{pn}/l(\|z_p - z_n\|) \leq \Gamma_{cs}/P_U}\Big)\Big] \\
&\overset{(a)}{=} \mathbb{E}\left[\prod_{x_j \in \Phi_D} \Big(1 - F_D(t)\exp\Big(-\mu \frac{\Gamma_{cs}}{P_D} l(\|x_j - z_n\|)\Big)\Big)\right] \times \mathbb{E}\left[\prod_{y_m \in \Phi_L} \Big(1 - \exp\Big(-\mu \frac{\Gamma_{ed}}{P_L} l(\|y_m - z_n\|)\Big)\Big)\right] \times \mathbb{E}^{!z_n}_{\Phi_U}\left[\prod_{z_p \in \Phi_U \cap B^c(z_0, R_{cs})} \Big(1 - F_U(t)\exp\Big(-\mu \frac{\Gamma_{cs}}{P_U} l(\|z_p - z_n\|)\Big)\Big)\right] \\
&\overset{(b)}{=} \frac{1}{CW_U} \int_{\Delta_U}^{CW_U + \Delta_U} \exp(-N_L - F_D(t)N_D - F_U(t)N_U(z_0, \Gamma_{cs}, R_{cs}))\mathrm{d}t
\end{aligned} \tag{3.8}$$

$$\begin{aligned}
&\text{LTE} - \text{U with SR}: \quad \hat{p}^D_{SU,MAP}(\lambda_D, \lambda_U, \lambda_L) = \int_0^\infty H_{MAP}\big(\Delta_D, CW_D, -N_L - F_U(t)N_U\big) f_{\|x_0\|}(r_0)\mathrm{d}r_0 \\
&\text{LTE} - \text{U}: \quad \hat{p}^D_{SU,MAP}(\lambda_D, \lambda_U, \lambda_L) = \int_0^\infty H_{MAP}\big(\Delta_D, CW_D, -N_L - F_D(t)N_D(r_0) - F_U(t)N_U\big) f_{\|x_0\|}(r_0)\mathrm{d}r_0 \\
&\text{LAA} \quad \text{with} \quad \text{SR}: \quad \hat{p}^D_{SU,MAP}(\lambda_D, \lambda_U, \lambda_L) = \int_0^\infty H_{MAP}\big(\Delta_D, CW_D, -F_L(t)N_L - F_U(t)N_U\big) f_{\|x_0\|}(r_0)\mathrm{d}r_0 \\
&\text{LAA}: \quad \hat{p}^D_{SU,MAP}(\lambda_D, \lambda_U, \lambda_L) = \int_0^\infty H_{MAP}\big(\Delta_D, CW_D, -F_L(t)N_L - F_D(t)N_D(r_0) - F_U(t)N_U\big) f_{\|x_0\|}(r_0)\mathrm{d}r_0
\end{aligned} \tag{3.9}$$

Table 3.3: Parameters of $p_{1,MAP}^{z/z_0}$

LTE-U	LAA
$N_{11}(t) = F_U(t)\big(-N_U(z_0,\Gamma_{cs},R_{cs}) + C_U(z,z_0)\big)$ $+F_D(t)\big(-N_D + C_D(z-z_0)\big) - N_L + C_L(z-z_0)$	$N_{11}(t) = F_U(t)\big(-N_U(z_0,\Gamma_{cs},R_{cs}) + C_U(z,z_0)\big)$ $+F_D(t)\big(-N_D + C_D(z-z_0)\big) + F_L(t)C_L(z-z_0)$
$N_{12}(t') = -F_D(t')N_D - F_U(t')N_U(z,\Gamma_{cs},R_{cs})$	$N_{12}(t') = -F_D(t')N_D - F_U(t')N_U(z,\Gamma_{cs},R_{cs}) - F_L(t')N_L$
$N_{13}(t) = -F_D(t)N_D - F_U(t)N_U(z_0,\Gamma_{cs},R_{cs})$	

Table 3.4: Timers Distributions For VO and BE Traffic

Voice (VO) Traffic	Best Effort (BE) Traffic
$F_{t_{VO}}(t_{VO}) = \frac{t_{VO}}{3} \quad \forall \quad 0 \le t_{VO} \le 3$	$F_{t_{BE}}(t_{BE}) = \frac{t_{BE}-2}{15} \quad \forall \quad 2 \le t_{BE} \le 17$
$F_{t_{VO}}(t_{BE}) = \begin{cases} \frac{t_{BE}}{3} & \forall \quad 2 \le t_{BE} \le 3 \\ 1 & \forall \quad 3 \le t_{BE} \le 17 \end{cases}$	$F_{t_{BE}}(t_{VO}) = \frac{t_{VO}-2}{15} \quad \forall \quad 2 \le t_{VO} \le 3$

Then by de-conditioning over r_0 we get the expression in Lemma 1. Note that the MAP in case of LAA can be proved in a similar manner. R_{cs} can be obtained by setting $N_U = \pi R_{cs}^2$ [32].■

Remark. The expression of $F_D(t)$ and $F_U(t)$ depend on the relation between t and each of t_j^D and t_p^U. It depends on the type of traffic transmitted by the Wi-Fi users and the APs. Given two types of traffic which are voice (VO) and best effort (BE) traffic with related channel access parameters as described earlier in section 3.1.3. The expressions of $F_D(t)$ and $F_U(t)$ can be computed using Table 3.4 for all combinations of considered traffic in the UL and the DL.

Similarly, for Wi-Fi DL, the MAPs of the tagged AP in of presence/absence of SR technique can be derived as in (3.9). Furthermore, in the case of LAA, the MAP of the tagged eNB is shown in (3.10). Based on the system parameters in Table 4.21, we show in Fig. 3.1 the MAP of various types of traffic versus the variation of the density of Wi-Fi APs, Wi-Fi users and LTE eNBs. The density of Wi-Fi users is considered to be equal to that of APs. By inspecting Fig. 3.1 (a), (b), and (c), we can see that the highest MAP is achieved when WiFi users

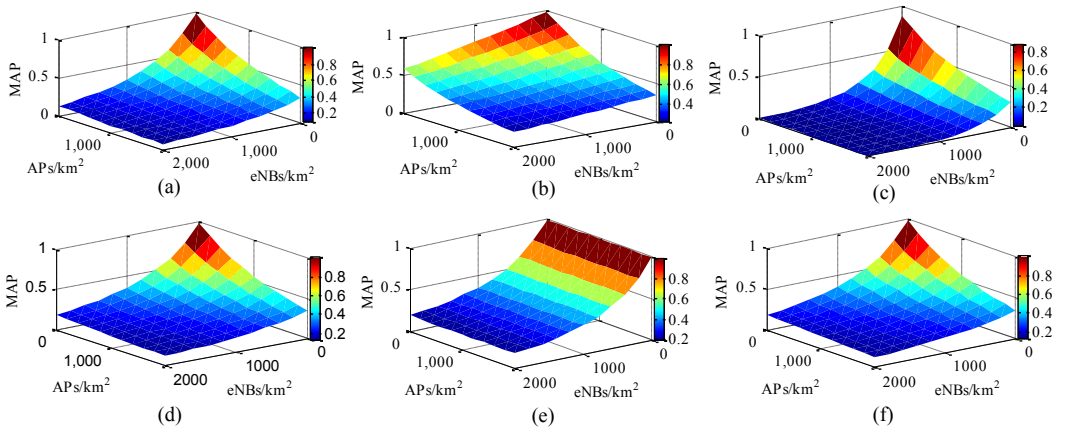

Figure 3.1: MAP for Wi-Fi user with LTE-U (τ=1) in case of (a) VO/VO Traffic (b) VO/BE Traffic (c) BE/VO Traffic, Wi-Fi user (d) with LAA in case of VO/VO Traffic, Wi-Fi AP (VO/VO Traffic) with LAA (e) using spatial reuse technique (f) without spatial reuse technique.

carry VO traffic where as APs carry BE traffic. On the other hand, the worst performance is achieved when Wi-Fi users carry BE traffic while APs carry VO traffic. Also, by inspecting Fig. 3.1 (a) and (d), we can see that LAA allows for better performance than LTE-U with τ=1. Finally, by analyzing Fig. 3.1 (e) and (f), we realize that the SR technique leads to a remarkable improvement in the MAP of a Wi-Fi AP when coexisting with other Wi-Fi APs, Wi-Fi users, and LAA.

3.2.2 SINR Coverage Probability

SINR Coverage Probability of Typical Wi-Fi AP in the UL

The medium access indicator for each LTE eNB is equal to one because LTE eNBs transmit continuously.

Corollary 1. *Conditioned on the fact that the tagged Wi-Fi user $z_0 = (r_0, 0)$ is retained by the CSMA/CA scheme when operating in EDCA mode, the probability for another Wi-Fi user $z \in \Phi_U \cap B^c(z_0, r_0)$ operating in EDCA mode to transmit:*

$$p_{1,MAP}^{z/z_0} = \frac{H_N\big(z, z_0, \Gamma_{cs}/P_U, \Delta_U, CW_U, \Delta_U, CW_U, N_{11}(t), N_{12}(t')\big)}{H_D\big(z - z_0, \Gamma_{cs}/P_U, \Delta_U, CW_U, F_U(t), N_{13}(t)\big)} \tag{3.12}$$

Where $N_{11}(t), N_{12}(t), N_{13}(t)$ in case of LTE-U and LAA are provided in Table 3.3. Note that Corollary 1 is also the same in case of presence/absence of spatial reuse technique.

Proof For every UL Wi-Fi user $z_n \in \Phi_U \cap B^c(z_0, R_{cs})$, given that the tagged user located at $z_0 = (r_0, 0)$ and associated to AP w_0, the conditional MAP is derived as in 3.35

$$\mathbb{P}\big[e_n^U = 1 \big| e_0^U = 1, z_0 = (r_0, 0), z_n \in \Phi_U\big] \overset{(a)}{=} \frac{\mathbb{P}_{\Phi_U}^{z_n, z_0}\big[\hat{e}_n^U = 1, \hat{e}_0^U = 1\big]}{\mathbb{P}_{\Phi_U}^{z_n, z_0}\big[\hat{e}_0^U = 1\big]} \overset{(b)}{=} \frac{\mathbb{E}_{\Phi_U}^{z_n}\big[\hat{e}_n^U \hat{e}_0^U\big]}{\mathbb{E}_{\Phi_U}^{z_n}\big[\hat{e}_0^U\big]} \tag{3.13}$$

where (a) follows from re-writing $z_0 = (r_0, 0)$ as $z_0 \in \Phi_U, \Phi_U(B^o(z_0, R_{cs})) = 0$. Then by using Bayes rule and de-conditioning on $\Phi_U(B^o(z_0, R_{cs})) = 0$. Step (b) follows from slivnyak′s theorem. The modified access indicators for z_0 and z_n are shown in (3.14). Therefore, the denominator $E_{\Phi_U}^{z_n}[\hat{e}_0^U]$ in (4.26) is given by (3.15) where (a) follows from slivnyak′s theorem and from setting $t_0^U = t$. Then by deconditioning on t and using the P.G.FL of PPP. Next, the numerator $\mathbb{E}_{\Phi_U}^{z_n}(\hat{e}_n^U \hat{e}_0^U)$ can be calculated using (3.16). ■

$$\hat{e}_n^U = \prod_{x_j \in \Phi_D} \Big(\mathbb{1}_{t_j^D \geq t_n^U} + \mathbb{1}_{t_j^D < t_n^U} \mathbb{1}_{G_{jn}^{DU}/l(\|x_j - z_n\|) \leq \Gamma_{cs}/P_D}\Big) \prod_{y_m \in \Phi_L} \big(\mathbb{1}_{G_{mn}^{LU}/l(\|y_m - z_n\|) \leq \Gamma_{ed}/P_L}\big) \prod_{z_p \in (\Phi_U \cap B^c(z_0, R_{cs}) + \delta_{z_0}) \setminus \{z_n\}} \Big(\mathbb{1}_{t_p^U \geq t_n^U} + \mathbb{1}_{t_p^U < t_n^U} \mathbb{1}_{G_{pn}^{U}/l(\|z_p - z_n\|) \leq \Gamma_{cs}/P_U}\Big)$$

$$\hat{e}_0^U = \prod_{x_j \in \Phi_D} \Big(\mathbb{1}_{t_j^D \geq t_0^U} + \mathbb{1}_{t_j^D < t_0^U} \mathbb{1}_{G_{j0}^{DU}/l(\|x_j - z_0\|) \leq \Gamma_{cs}/P_D}\Big) \prod_{y_m \in \Phi_L} \Big(\mathbb{1}_{G_{m0}^{LU}/l(\|y_m - z_0\|) \leq \Gamma_{ed}/P_L}\Big) \prod_{z_p \in \Phi_U \cap B^c(z_0, R_{cs})} \Big(\mathbb{1}_{t_p^U \geq t_0^U} + \mathbb{1}_{t_p^U < t_0^U} \mathbb{1}_{G_{p0}^{U}/l(\|z_p - z_0\|) \leq \Gamma_{cs}/P_U}\Big) \tag{3.14}$$

Table 3.5: Parameters of $p_{1,MAP}^{x/z_0}$

LTE-U (With SR)	LAA (With SR)
$N_{21}(t) = F_U(t)\big(-N_U(z_0,\Gamma_{cs},R_{cs}) + C_U(x,z_0)\big)$ $-F_D(t)N_D - N_L + C_L(x-z_0)$	$N_{21}(t) = F_U(t)\big(-N_U(z_0,\Gamma_{cs},R_{cs}) + C_U(x,z_0)\big)$ $-F_D(t)N_D + F_L(t)C_L(x-z_0)$
$N_{22}(t') = -F_U(t')N_U(x,\Gamma_{cs},R_{cs})$	$N_{22}(t') = -F_U(t')N_U(x,\Gamma_{cs},R_{cs}) - F_L(t')N_L$
$N_{23}(t) = -F_D(t)N_D - F_U(t)N_U(z_0,\Gamma_{cs},R_{cs})$	
LTE-U (Without SR)	**LAA (Without SR)**
$N_{21}(t) = F_U(t)\big(-N_U(z_0,\Gamma_{cs},R_{cs}) + C_U(x,z_0)\big)$ $+F_D(t)\big(-N_D + C_D(x-z_0)\big) - N_L + C_L(x-z_0)$	$N_{21}(t) = F_U(t)\big(-N_U(z_0,\Gamma_{cs},R_{cs}) + C_U(x,z_0)\big)$ $+F_D(t)\big(-N_D + C_D(x-z_0)\big) + F_L(t)C_L(x-z_0)$
$N_{22}(t') = -F_D(t')N_D - F_U(t')N_U(x,\Gamma_{cs},R_{cs})$	$N_{22}(t') = -F_D(t')N_D - F_U(t')N_U(x,\Gamma_{cs},R_{cs}) - F_L(t')N_L$
$N_{23}(t) = -F_D(t)N_D - F_U(t)N_U(z_0,\Gamma_{cs},R_{cs})$	

Table 3.6: Parameters of $p_{1,MAP}^{y/z_0}$

$N_{31}(t) = F_U(t)\big(-N_U(z_0,\Gamma_{cs},R_{cs}) + C_U(y,z_0)\big) + F_D(t)\big(-N_D + C_D(y-z_0)\big) + F_L(t)\big(-N_L + C_L(y-z_0)\big)$
$N_{32}(t') = -F_D(t')N_D - F_U(t')N_U(y,\Gamma_{cs},R_{cs}) - F_L(t')N_L$
$N_{33}(t) = -F_D(t)N_D - F_U(t)N_U(z_0,\Gamma_{cs},R_{cs}) - F_L(t)N_L$

$$\begin{aligned}
&\mathbb{E}_{\Phi_U}^{z_n}\Big[\prod_{x_j\in\Phi_D}\Big(\mathbb{1}_{t_j^D\geq t_0^U}+\mathbb{1}_{t_j^D<t_0^U}\mathbb{1}_{G_{j0}^{DU}/l(\|x_j-z_0\|)\leq\Gamma_{cs}/P_D}\Big)\prod_{y_m\in\Phi_L}\Big(\mathbb{1}_{G_{m0}^{LU}/l(\|y_m-z_0\|)\leq\Gamma_{cd}/P_L}\Big)\prod_{z_p\in\Phi_U\cap B^c(z_0,R_{cs})}\Big(\mathbb{1}_{t_p^U\geq t_0^U}+\mathbb{1}_{t_p^U<t_0^U}\mathbb{1}_{G_{p0}^{U}/l(\|z_p-z_0\|)\leq\Gamma_{cs}/P_U}\Big)\Big]\\
&\overset{(a)}{=}\frac{1}{CW_U}\int_{\Delta_U}^{\Delta_U+CW_U}\Big(1-F_U(t)\exp\Big(-\mu\frac{\Gamma_{cs}}{P_U}l(\|z_p-z_0\|)\Big)\Big)\exp\Big(-N_L-F_D(t)N_D-F_U(t)N_U(z_0,\Gamma_{cs},R_{cs})\Big)\mathrm{d}t
\end{aligned}\tag{3.15}$$

$$\begin{aligned}
&\mathbb{E}_{\Phi_U}^{z_n}\big[\hat{e}_n^U\hat{e}_0^U\big] = \mathbb{E}\Big[\prod_{x_j\in\Phi_D}\Big(\mathbb{1}_{t_j^D\geq t_n^U}+\mathbb{1}_{t_j^D<t_n^U}\mathbb{1}_{G_{jn}^{DU}/l(\|x_j-z_n\|)\leq\Gamma_{cs}/P_D}\Big)\Big(\mathbb{1}_{t_j^D\geq t_0^U}+\mathbb{1}_{t_j^D<t_0^U}\mathbb{1}_{G_{j0}^{DU}/l(\|x_j-z_0\|)\leq\Gamma_{cs}/P_D}\Big)\\
&\prod_{y_m\in\Phi_L}\big(\mathbb{1}_{G_{mn}^{LU}/l(\|y_m-z_n\|)\leq\Gamma_{ed}/P_L}\big)\big(\mathbb{1}_{G_{m0}^{LU}/l(\|y_m-z_0\|)\leq\Gamma_{ed}/P_L}\big)\prod_{z_p\in(\Phi_U\cap B^c(z_0,R_{cs})+\delta_{z_0})}\Big(\mathbb{1}_{t_p^U\geq t_n^U}+\mathbb{1}_{t_p^U<t_n^U}\mathbb{1}_{G_{pn}^{U}/l(\|z_p-z_n\|)\leq\Gamma_{cs}/P_U}\Big)\\
&\prod_{z_p\in(\Phi_U\cap B^c(z_0,R_{cs})+\delta_{z_n})}\Big(\mathbb{1}_{t_p^U\geq t_0^U}+\mathbb{1}_{t_p^U<t_0^U}\mathbb{1}_{G_{p0}^{U}/l(\|z_p-z_0\|)\leq\Gamma_{cs}/P_U}\Big)\Big/t_0^U=t,t_n^U=t'\Big] = \frac{1-\exp\Big(-\mu\frac{\Gamma_{cs}}{P_U}l(\|z_n-z_0\|)\Big)}{CW_U^2}\int_{\Delta_U}^{\Delta_U+CW_U}\int_{\Delta_U}^{\Delta_U+CW_U}\\
&\exp\Big(-F_D(t')N_D-F_U(t')N_U(z_n,\Gamma_{cs},R_{cs})+F_U(t)\big(-N_U(z_0,\Gamma_{cs},R_{cs})+C_U(z_n,z_0)\big)+F_D(t)\big(-N_D+C_D(z_n-z_0)\big)-2N_L+C_L(z_n-z_0)\Big)\mathrm{d}t\mathrm{d}t'
\end{aligned}\tag{3.16}$$

Similarly, conditioned on the fact that the tagged Wi-Fi user $z_0 = (r_0, 0)$ is retained by the CSMA/CA scheme, the probability $p_{1,MAP}^{x/z_0}$ for a Wi-Fi AP

$$\begin{aligned}
&\mathbb{P}[SINR_0^U > T | z_0 = (r_0,0), e_0^U = 1]\\
&= \mathbb{P}\Big[\frac{P_U G_{0,0}^{UD}/l(\|z_0\|)}{\sum_{z_p\in\Phi_U\setminus\{z_0\}}P_U G_{p,0}^{UD}e_p^U/l(\|z_p\|)+\sum_{x_j\in\Phi_D}P_D G_{j,0}^{D}e_j^D/l(\|x_j\|)+\sum_{y_m\in\Phi_L}P_L G_{m,0}^{LD}e_m^L/l(\|y_m\|)+\sigma_N^2} > T\Big| z_0=(r_0,0), e_0^U=1\Big]\\
&\overset{(a)}{=}\mathbb{P}\Big[\frac{P_U G_{0,0}^{UD}/l(\|z_0\|)}{\sum_{z_p\in\Phi_U\setminus\{z_0\}}P_U G_{p,0}^{UD}e_p^U/l(\|z_p\|)+\sum_{x_j\in\Phi_D}P_D G_{j,0}^{D}e_j^D/l(\|x_j\|)+\sum_{y_m\in\Phi_L}P_L G_{m,0}^{LD}e_m^L/l(\|y_m\|)+\sigma_N^2} > T | z_0\in\Phi_U, \Phi_U(B^o(z_0,R_{cs}))=0, e_0^U=1\Big]\\
&\overset{(b)}{=}\mathbb{P}\Big[\frac{P_U G_{0,0}^{UD}/l(\|z_0\|)}{\sum_{z_p\in\Phi_U\cap B^c(z_0,R_{cs})}P_U G_{p,0}^{UD}\hat{e}_p^U/l(\|z_p\|)+\sum_{x_j\in\Phi_D}P_D G_{j,0}^{D}\hat{e}_j^D/l(\|x_j\|)+\sum_{y_m\in\Phi_L}P_L G_{m,0}^{LD}\hat{e}_m^L/l(\|y_m\|)+\sigma_N^2} > T\Big|\hat{e}_0^U=1\Big]\\
&\overset{(c)}{\approx}\mathbb{E}\Big[\exp\Big(-\mu T l(\|r_0\|)\sum_{x_j\in\Phi_D}\frac{P_D}{P_U}G_{j,0}^{D}\hat{e}_j^D/l(\|x_j\|)\Big)\Big|\hat{e}_0^U=1\Big]\times\mathbb{E}\Big[\exp\Big(-\mu T l(\|r_0\|)\frac{\sigma_N^2}{P_U}\Big)\Big]\\
&\quad\times\mathbb{E}\Big[\exp\Big(-\mu T l(\|r_0\|)\sum_{z_p\in\Phi_U\cap B^c(z_0,R_{cs})}G_{p,0}^{UD}\hat{e}_p^U/l(\|z_p\|)\Big)\Big|\hat{e}_0^U=1\Big]\times\mathbb{E}\Big[\exp\Big(-\mu T l(\|r_0\|)\sum_{y_m\in\Phi_L}\frac{P_L}{P_U}G_{m,0}^{LD}/l(\|y_m\|)\Big)\Big|\hat{e}_0^U=1\Big]
\end{aligned}\tag{3.17}$$

$x \in \Phi_D$ and $p_{1,MAP}^{y/z_0}$ for a LAA eNB $y \in \Phi_L$ to transmit are derived as follows:

$$p_{1,MAP}^{x/z_0} = \frac{H_N\big(x, z_0, \Gamma_{cs}/P_D, \Delta_D, CW_D, \Delta_U, CW_U, N_{21}(t), N_{22}(t')\big)}{H_D\big(x - z_0, \Gamma_{cs}/P_D, \Delta_U, CW_U, F_D(t), N_{23}(t)\big)}$$
$$p_{1,MAP}^{y/z_0} = \frac{H_N\big(y, z_0, \Gamma_{ed}/P_L, \Delta_L, CW_L, \Delta_U, CW_U, N_{31}(t), N_{32}(t')\big)}{H_D\big(y - z_0, \Gamma_{ed}/P_L, \Delta_U, CW_U, F_L(t), N_{33}(t)\big)} \tag{3.18}$$

Where $N_{21}(t), N_{22}(t), N_{23}(t)$ in case of LTE-U and LAA with/without spatial reuse (SR) technique are provided in Table 3.5. Similarly those of $N_{31}(t), N_{32}(t)$, and $N_{33}(t)$ are provided in Table 3.6. Note that in case of LTE-U, $p_{1,MAP}^{y/z_0}$ is equal to τ and that $p_{1,MAP}^{x/z_0}$ and $p_{1,MAP}^{y/z_0}$ (in case of LAA) can be proved in a similar manner to Corollary 1. Based on the above, the SINR coverage of the typical Wi-Fi user $\hat{p}_{SINR,SU}^{U}(T, \lambda_D, \lambda_U, \lambda_L)$ is obtained in Lemma 2.

Lemma 2. *Given the tagged Wi-Fi user is located at $z_0 = (r_0, 0)$, during SU operation mode, the SINR coverage probability of the typical Wi-Fi AP with SINR threshold T in the UL is approximated as in (3.11).*

Proof The conditional SINR coverage of the typical Wi-Fi AP is derived as in (3.17) where (a) follows from Bayes rule by re-writing $z_0 = (r_0, 0)$ as $z_0 \in \Phi_U, \Phi_U(B^o(z_0, R_{cs})) = 0$. Step (b) follows from slivnyak's theorem and de-conditioning on $\Phi_U(B^o(z_0, R_{cs})) = 0$. The conditional probabilities that Wi-Fi

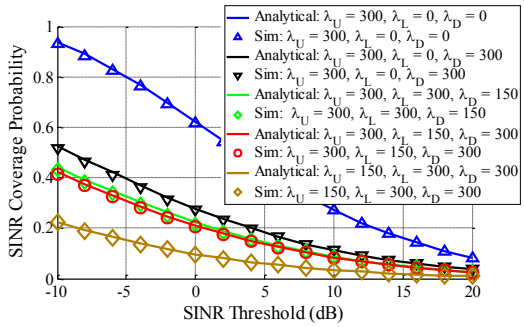

Figure 3.2: SINR coverage for typical Wi-Fi AP when coexisting with LAA in case of voice traffic.

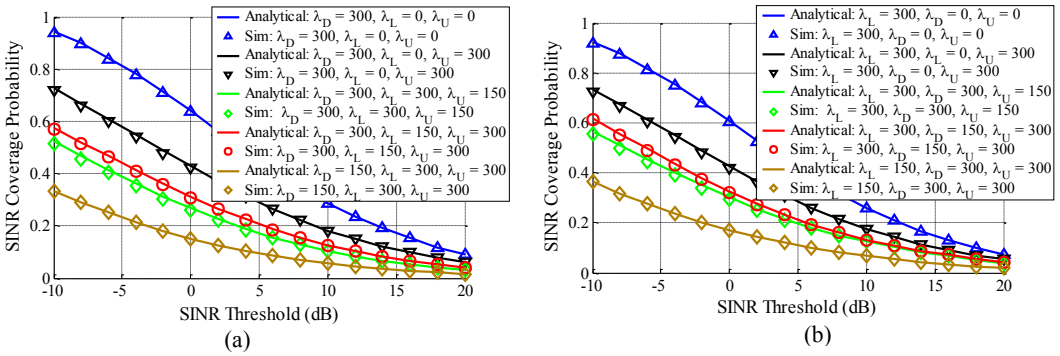

Figure 3.3: SINR coverage for (a) typical WiFi user when coexisting with LTE, (b) typical LTE LAA UE in case of voice traffic

Table 3.7: Parameters of $p^{z/x_0}_{1,MAP}$

LTE-U (With SR)	LAA (With SR)
$N_{41}(t) = F_U(t)\big(-N_U + C_U(z-x_0)\big) - N_L + C_L(z-x_0)\big)$	$N_{41}(t) = F_U(t)\big(-N_U + C_U(z-x_0)\big) + F_L(t)C_L(z-x_0)$
$N_{42}(t') = -F_U(t')N_U - F_D(t')N_D(r_0)$	$N_{42}(t') = -F_U(t')N_U - F_D(t')N_D(r_0) - F_L(t')N_L$
$N_{43}(t) = -F_U(t)N_U$	
LTE-U (Without SR)	**LAA (Without SR)**
$N_{41}(t) = F_U(t)\big(-N_U + C_U(z-x_0)\big)\big)$ $+F_D(t)\big(-N_D(r_0) + C_D(z,x_0)\big) - N_L + C_L(z-x_0)$	$N_{41}(t) = F_U(t)\big(-N_U + C_U(z-x_0)\big)$ $+F_D(t)\big(-N_D(r_0) + C_D(z,x_0)\big) + F_L(t)C_L(z-x_0)$
$N_{42}(t') = -F_U(t')N_U - F_D(t')N_D(r_0)$	$N_{42}(t') = -F_U(t')N_U - F_D(t')N_D(r_0) - F_L(t')N_L$
$N_{43}(t) = -F_D(t)N_D(x_0) - F_U(t)N_U$	

user $z_n \in \Phi_U \cap B^c(z_0, R_{cs})$, Wi-Fi AP $x_j \in \Phi_D$, and LAA eNB $y_m \in \Phi_L$ transmit were derived in 3.12, and 3.18 respectively. Step (c) follows from the fact that channels are Rayleigh fading channels and from the assumption that interference from LTE and Wi-Fi is independent. Finally (3.11) can be derived by approximating the law of interfering APs/users/eNBs as a non-homogeneous PPP with intensity $\lambda_D p^{x/z_0}_{1,MAP}/\lambda_U p^{z/z_0}_{1,MAP}/\lambda_L p^{y/z_0}_{1,MAP}$ (in case of LAA) and by deconditioning on r_0.■

Note that the first, second, and third terms in (3.11) result from noise, LTE and

Table 3.8: Parameters of $p^{x/x_0}_{1,MAP}$

LTE-U (With SR)	LAA (With SR)
$N_{51}(t) = F_U(t)\big(-N_U + C_U(x-x_0)\big) - N_L + C_L(x-x_0)\big)$	$N_{51}(t) = F_U(t)\big(-N_U + C_U(x-x_0)\big) + F_L(t)C_L(x-x_0)$
$N_{52}(t') = -F_U(t')N_U$	$N_{52}(t') = -F_U(t')N_U - F_L(t')N_L$
$N_{53}(t) = -F_U(t)N_U$	
LTE-U (Without SR)	**LAA (Without SR)**
$N_{51}(t) = F_U(t)\big(-N_U + C_U(x-x_0)\big)$ $+F_D(t)\big(-N_D(r_0) + C_D(x,x_0)\big) - N_L + C_L(x-x_0)$	$N_{51}(t) = F_U(t)\big(-N_U + C_U(x-x_0)\big)$ $+F_D(t)\big(-N_D(r_0) + C_D(x,x_0)\big) + F_L(t)C_L(x-x_0)$
$N_{52}(t') = -F_U(t')N_U - F_D(t')N_D(r_0)$	$N_{52}(t') = -F_U(t')N_U - F_D(t')N_D(r_0) - F_L(t')N_L$
$N_{53}(t) = -F_D(t)N_D(x_0) - F_U(t)N_U$	

Wi-Fi APs interference respectively where as the fourth term results from other interfering Wi-Fi users. Based on the parameters in Table 4.21, we show in Fig. 3.2 the SINR coverage probability of the typical Wi-Fi AP in the UL under different LTE eNB, Wi-Fi user and Wi-Fi AP densities. In the last section (section 4.2.2), we consider a detailed analysis of various scenarios, however, for validation purposes only, we consider in this case that LTE uses LAA mechanism and that Wi-Fi AP, users, and LTE eNBs carry VO traffic. The simulation results are obtained from the definition of SINR in (3.1). It can be observed from Fig. 3.2 that the approximation in Lemma 2 gives an accurate estimation of the actual SINR coverage. In addition, we can see that without the coexistence of LAA

Table 3.9: Parameters of $p^{y/x_0}_{1,MAP}$

With SR	Without SR
$N_{61}(t) = F_U(t)\big(-N_U + C_U(y-x_0) + F_L(t)\big(-N_L\big)$ $+C_L(y-x_0)\big)$	$N_{61}(t) = F_U(t)\big(-N_U + C_U(y-x_0)\big) + F_D(t)\big(-N_D(r_0)$ $+C_D(y,x_0)\big) + F_L(t)\big(-N_L + C_L(y-x_0)\big)$
$N_{62}(t') = -F_U(t')N_U - F_L(t')N_L$	$N_{62}(t') = -F_U(t')N_U - F_D(t')N_D(r_0) - F_L(t')N_L$
$N_{63}(t) = -F_U(t)N_U - F_L(t)N_L$	$N_{63}(t) = -F_D(t)N_D(r_0) - F_U(t)N_U - F_L(t)N_L$

eNBs ($\lambda_L = 0$), the SINR performance of Wi-Fi APs due to UL transmissions by users operating in SU mode is affected by the coexisting DL AP transmissions especially in the low SINR threshold regime (less than 0 dB).

SINR Coverage Probability of Typical Wi-Fi user in the DL Under SU Mode

Conditioned on the fact that the tagged Wi-Fi AP $x_0 = (r_0, 0)$ is retained by the CSMA/CA scheme, the probabilities $p_{1,MAP}^{z/x_0}$ for a Wi-Fi user $z \in \Phi_U$, $p_{1,MAP}^{x/x_0}$ for a Wi-Fi AP $_{x \in \Phi_D \cap B^c(r_0,0)}$, and $p_{1,MAP}^{y/x_0}$ for a LAA eNB $y \in \Phi_L$ to transmit are derived as follows:

$$\begin{aligned}
p_{1,MAP}^{z/x_0} &= \frac{H_N\big(z, x_0, \Gamma_{cs}/P_U, \Delta_U, CW_U, \Delta_D, CW_D, N_{41}(t), N_{42}(t')\big)}{H_D\big(z - x_0, \Gamma_{cs}/P_U, \Delta_D, CW_D, F_U(t), N_{43}(t)\big)} \\
p_{1,MAP}^{x/x_0} &= \frac{H_N\big(x, x_0, \Gamma_{cs}/P_D, \Delta_D, CW_D, \Delta_D, CW_D, N_{51}(t), N_{52}(t')\big)}{H_D\big(x - x_0, \Gamma_{cs}/P_D, \Delta_D, CW_D, F_D(t), N_{53}(t)\big)} \\
p_{1,MAP}^{y/x_0} &= \frac{H_N\big(y, x_0, \Gamma_{ed}/P_L, \Delta_L, CW_L, \Delta_D, CW_D, N_{61}(t), N_{62}(t')\big)}{H_D\big(y - x_0, \Gamma_{ed}/P_L, \Delta_D, CW_D, F_L(t), N_{63}(t)\big)}
\end{aligned} \tag{3.20}$$

Where $N_{41}(t), N_{42}(t), N_{43}(t), N_{51}(t), N_{52}(t)$, and $N_{53}(t)$ in case of LTE-U and LAA with/without SR technique are provided in Tables 3.7 and 3.8. Similarly those of $N_{61}(t), N_{62}(t)$, and $N_{63}(t)$ with/without SR technique are provided in Table 3.9. The proofs can be derived in a similar way to corollary 1, thus we omit the detailed proofs. Hence, given the tagged Wi-Fi AP is located at $x_0 = (r_0, 0)$, the SINR coverage probability of the typical Wi-Fi user with SINR threshold T under SU mode is approximated as in (3.19). Note that (3.19) can be derived by approximating the law of interfering Wi-Fi user/AP processes as non-homogenous PPP with intensity $\lambda_U p_{1,MAP}^{z/x_0}/\lambda_D p_{1,MAP}^{x/x_0}/\lambda_L p_{1,MAP}^{y/x_0}$. The SINR performance of the typical Wi-Fi user in the DL is shown in Fig. 3.3 where it is evaluated using both simulation and analytical results from (3.19). From Fig. 3.3 we can see that the accuracy of (3.19) is validated. First, we can see in Fig. 3.3 (a) that, during the DL, in the absence of co-existing LTE network, the SINR performance of the typical Wi-Fi user is affected by UL transmissions especially in the low SINR threshold regime. However, when LTE eNBs coexist with Wi-Fi, the SINR performance of the typical Wi-Fi user is severely degraded.

$$\hat{p}_{SINR,SU}^{D}(T, \lambda_D, \lambda_U, \lambda_L) \approx \int_0^\infty \exp\Big(-\mu T l(r_0)\frac{\sigma_N^2}{P_D}\Big) \exp\Big(-\int_{\mathbb{R}^2} \frac{T l(r_0)\lambda_L p_{1,MAP}^{y/x_0}}{\frac{P_D}{P_L} l(\|x\|) + T l(r_0)} \mathrm{d}x\Big) \exp\Big(-\int_{\mathbb{R}^2 \setminus B(0,r_0)} \frac{T l(r_0)\lambda_D p_{1,MAP}^{x/x_0}}{l(\|x\|) + T l(r_0)} \mathrm{d}x\Big) \exp\Big(-\int_{\mathbb{R}^2} \frac{T l(r_0)\lambda_U p_{1,MAP}^{z/x_0}}{\frac{P_D}{P_U} l(\|x\|) + T l(r_0)} \mathrm{d}x\Big) f_{\|x_0\|}(r_0) \mathrm{d}r_0 \tag{3.19}$$

Table 3.10: Parameters of $p_{1,MAP}^{x/y_0}$

With SR	Without SR
$N_{91}(t) = F_U(t)\big(-N_U + C_U(x-y_0)\big) + F_L(t)\big(-N_L(y_0) + C_L(x,y_0)\big) - F_D(t)N_D\big)$	$N_{91}(t) = F_U(t)\big(-N_U + C_U(x-y_0)\big) + F_L(t)\big(-N_L(y_0) + C_L(x,y_0)\big) + F_D(t)\big(-N_D + C_D(x-y_0)\big)$
$N_{92}(t') = -F_U(t')N_U - F_L(t')N_L(y_0)$	$N_{92}(t') = -F_U(t')N_U - F_L(t')N_L(y_0) - F_D(t')N_D$
$N_{93}(t) = -F_U(t)N_U - F_L(t)N_L$	$N_{93}(t) = -F_L(t)N_L(y_0) - F_U(t)N_U - F_D(t)N_D$

SINR Coverage Probability of Typical UE

In case of LTE-U, given that the tagged eNB $y_0 = (r_0, 0)$ transmits, we treat the medium access indicators of each Wi-Fi user/AP as independent retain indicator. Hence, the modified MAP of the typical Wi-Fi user z and typical Wi-Fi AP x in SU mode operation are given by:

$$\begin{aligned} p_{1,MAP}^{z/y_0} &= \frac{1}{CW_U}\int_{\Delta_U}^{CW_U+\Delta_U} \exp\big(-N_L(z,r_0) - F_D(t)N_D - F_U(t)N_U\big)\mathrm{d}t \\ p_{1,MAP}^{x/y_0} &= \frac{1}{CW_D}\int_{\Delta_D}^{CW_D+\Delta_D} \exp\big(-N_L(x,r_0) - F_D(t)N_D - F_U(t)N_U\big)\mathrm{d}t \end{aligned} \tag{3.22}$$

On the other hand, in case of LAA, we derive in the following corollaries, the conditional MAP of each Wi-Fi user/AP/eNB given that the tagged eNB $y_0 = (r_0, 0)$ transmits. Conditioned on the fact that the tagged Wi-Fi AP $y_0 = (r_0, 0)$ is retained by the CSMA/CA scheme, the probabilities $p_{1,MAP}^{z/y_0}$ for a Wi-Fi user $z \in \Phi_U$, $p_{1,MAP}^{x/y_0}$ for a Wi-Fi AP $x \in \Phi_D$, and $p_{1,MAP}^{y/y_0}$ for a LAA eNB $y \in \Phi_L \cap B^c(r_0, 0)$ to transmit are derived as:

$$\begin{aligned} p_{1,MAP}^{z/y_0} &= \frac{H_N\big(z, y_0, \Gamma_L/P_U, \Delta_U, CW_U, \Delta_L, CW_L, N_{71}(t), N_{72}(t')\big)}{H_D\big(z - y_0, \Gamma_L/P_U, \Delta_L, CW_L, F_U(t), N_{73}(t)\big)} \\ p_{1,MAP}^{y/y_0} &= \frac{H_N\big(y, y_0, \Gamma_L/P_L, \Delta_L, CW_L, \Delta_L, CW_L, N_{81}(t), N_{82}(t')\big)}{H_D\big(y - y_0, \Gamma_L/P_L, \Delta_L, CW_L, F_L(t), N_{83}(t)\big)} \\ p_{1,MAP}^{x/y_0} &= \frac{H_N\big(x, y_0, \Gamma_L/P_D, \Delta_D, CW_D, \Delta_L, CW_L, N_{91}(t), N_{92}(t')\big)}{H_D\big(x - y_0, \Gamma_L/P_D, \Delta_L, CW_L, F_D(t), N_{93}(t)\big)} \end{aligned} \tag{3.23}$$

Where $N_{71}(t)$, $N_{72}(t)$, $N_{73}(t)$, $N_{81}(t)$, $N_{82}(t)$, and $N_{83}(t)$ are provided in Tables 3.11. Similarly those of $N_{91}(t), N_{92}(t)$, and $N_{93}(t)$ with/without SR technique are provided in Table 3.10. The proofs can be derived in a similar way to Corollary 1. Thus, given that the tagged eNB is located at $y_0 = (r_0, 0)$, the SINR coverage probability of the typical UE with SINR threshold T is approximated as in (3.21).

Fig. 3.3 (b) shows the SINR coverage probability of the typical LTE UE using both simulation and analytical result from (3.21) where we can see that the accuracy of (3.21) is validated. In this case, we consider LAA just for demonstration

---

$$\hat{p}_{SINR}^{L}(T, \lambda_D, \lambda_U, \lambda_L) \approx \int_0^\infty \hat{p}_1^L(r_0, T, \lambda_U, \lambda_D, \lambda_L) \times f_{\|y_0\|}(r_0)\mathrm{d}r_0 \quad \text{where} \quad \hat{p}_1^L(r_0, T, \lambda_U, \lambda_D, \lambda_L) = \exp\Big(-\mu T l(r_0)\frac{\sigma_N^2}{P_L}\Big)\exp\Big(-\int_{\mathbb{R}^2\setminus B(0,r_0)} \frac{Tl(r_0)\lambda_L p_{1,MAP}^{y/y_0}}{l(\|x\|) + Tl(r_0)}\mathrm{d}x\Big)\exp\Big(-\int_{\mathbb{R}^2} \frac{Tl(r_0)\lambda_D p_{1,MAP}^{x/y_0}}{\frac{P_D}{P_U}l(\|y\|) + Tl(r_0)}\mathrm{d}y\Big)\exp\Big(-\int_{\mathbb{R}^2} \frac{Tl(r_0)\lambda_U p_{1,MAP}^{z/y_0}}{\frac{P_L}{P_U}l(\|z\|) + Tl(r_0)}\mathrm{d}z\Big) \tag{3.21}$$

Table 3.11: Parameters of $p_{1,MAP}^{z/y_0}$ and $p_{1,MAP}^{y/y_0}$

$N_{71}(t) = F_U(t)\big(-N_U + C_U(z-y_0)\big) + F_D(t)\big(-N_D(r_0) + C_D(z-y_0)\big) + F_L(t)C_L(z,y_0)$
$N_{72}(t') = -F_U(t')N_U - F_L(t')N_L(y) - F_D(t')N_D$
$N_{73}(t) = -F_L(t)N_L(y) - F_U(t)N_U$
$N_{81}(t) = F_U(t)\big(-N_U + C_U(y-y_0)\big) + F_L(t)\big(-N_L(x) + C_L(y,y_0)\big) + F_D(t)C_D(y-y_0)$
$N_{82}(t') = -F_U(t')N_U - F_L(t')N_L(x) - F_D(t')N_D$
$N_{83}(t) = -F_L(t)N_L(x) - F_U(t)N_U$

purposes where we can observe from Fig. 3.3 (b), that the SINR performance of the typical LTE UE is better when the density of LTE eNBs increase or when the density of Wi-Fi APs (and/or Wi-Fi users) decrease where the upper bound of SINR coverage is given when $\lambda_D = 0$ and $\lambda_U = 0$.

3.3 Analysis of LTE-U and LAA With IEEE 802.11ax Wi-Fi DL and UL For MU Operation Mode

In both cases UL and DL MU operation mode, the AP will initially contend using EDCA parameters for channel access as in the case of SU mode. In this analysis we consider that we either have MU DL transmissions or MU UL transmissions for operator 1. Whereas operator 2 may be either LTE (LTE-U or LAA) or Wi-Fi SU mode as a baseline scenario. Based on that, by assuming that APs are associated with MU DL traffic or MU UL traffic, we derive the MAP of an AP in the MU mode as follows in presence/absence of SR technique:

$$\hat{p}_{MU,MAP}^{D}(\lambda_D, \lambda_L) = \hat{p}_{SU,MAP}^{D}(\lambda_D, \lambda_U = 0, \lambda_L) \tag{3.24}$$

Furthermore, given that the tagged Wi-Fi AP is located at $x_0 = (r_0, 0)$, during MU mode, the SINR coverage probability of the typical Wi-Fi user with SINR threshold T in the DL is:

$$\hat{p}_{SINR,MU}^{D}(T, \lambda_D, \lambda_L) = \hat{p}_{SINR,SU}^{D}(T, \lambda_D, \lambda_U = 0, \lambda_L) \tag{3.25}$$

Where $p_{1,MAP}^{x/x_0}$ and $p_{1,MAP}^{y/x_0}$ used to calculate $\hat{p}_{SINR,SU}^{D}(T, \lambda_D, \lambda_U = 0, \lambda_L)$ in case of presence/absence of SR technique were already derived in section 3.2.2.

On the other hand, in case of simultaneous UL transmissions in MU mode, the AP first sends a trigger frame to the users assigning them corresponding RU grants. Then, users may operate based on two different trigger-based access schemes. The first one is the trigger-based deterministic access (TR-DA) in which the user will transmit directly on the allocated RUs. Thus, in the TR-DA, the MAP of a user in the UL is:

$$\hat{p}_{MU,MAP}^{U}(\lambda_D, \lambda_U, \lambda_L) = \hat{p}_{SU,MAP}^{D}(\lambda_D, \lambda_L) \times P_{DA} \tag{3.26}$$

Where P_{DA} is the average probability that a user is selected to be scheduled on a particular RU. We assume that the AP uniformly schedules a user on a particular

RU. Thus, in case that the number of nodes $k+1$ in a certain BSS is smaller than or equal the available number of channels N_{RU}, the probability for a node to be scheduled by an AP is equal to one. On the other hand, when the number of nodes $k+1$ is larger than N_{RU}, the probability for a node to be scheduled by an AP is equal to $\frac{N_{RU}}{k+1}$. Therefore, according to [52], P_{DA} can be computed as follows:

$$P_{DA} = \frac{\exp(-N_U)}{N_U}\left[N_{RU}\big(\exp(N_U)-1\big) - \sum_{k=1}^{N_{RU}} \frac{(N_{RU}-k)(N_U)^k}{k!}\right] \tag{3.27}$$

In addition, given that the tagged Wi-Fi user is located at $z_0 = (r_0, 0)$, during MU mode, the SINR coverage probability of the typical Wi-Fi AP with SINR threshold T in the UL is:

$$\hat{p}^U_{SINR,MU}\left(T, \lambda_D, \lambda_U, \lambda_L\right) = \hat{p}^U_{SINR,SU}\left(T, \lambda_D, \lambda_U^{MU}, \lambda_L\right) \tag{3.28}$$

Where $\lambda_U^{MU} = \lambda_U \times \hat{p}^U_{MU,MAP}\left(\lambda_D, \lambda_U, \lambda_L\right)$.
Also, when computing $\hat{p}^U_{SINR,SU}\left(T, \lambda_D, \lambda_U^{MU}, \lambda_L\right)$, $p^{z/z_0}_{1,MAP}$ is equal to one in this case. In addition, $p^{y/z_0}_{1,MAP}$ is equal to one in case of LTE-U while $p^{x/z_0}_{1,MAP}$ and $p^{y/z_0}_{1,MAP}$ (in case of LAA) can be derived as follows:

$$\begin{aligned} p^{x/z_0}_{1,MAP} &= \frac{1}{CW_D}\int_{\Delta_D}^{CW_D+\Delta_D} \exp\big(-N_L - N_U - F_D(t)N_D\big)\mathrm{d}t \\ p^{y/z_0}_{1,MAP} &= \frac{1}{CW_L}\int_{\Delta_L}^{CW_L+\Delta_L} \exp\big(-F_D(t)N_D - N_U - F_L(t)N_L\big)\mathrm{d}t \end{aligned} \tag{3.29}$$

The second scheme is the trigger-based random access (TR-RA) mechanism where users will contend for channel access on the assigned set of RUs where we assume in this case that a user selects a particular RU uniformly. Hence, if the AP assigns N_{RU} to users, and after the user contends and wins access to the channel, each user will select a particular RU with probability P_{RA} in order to transmit its data to the AP. Thus, in the TR-RA, the MAP of a user in the UL is:

$$\hat{p}^U_{MU,MAP}\left(\lambda_D, \lambda_U, \lambda_L\right) = \hat{p}^D_{SU,MAP}\left(\lambda_D, \lambda_L\right) \times \hat{p}^U_{SU,MAP}\left(\lambda_D, \lambda_L\right) \times P_{RA} \tag{3.30}$$

where P_{RA} is the average probability that a user uniquely selects a particular RU that is not selected by any other user. Hence, given that the number of users is k in a certain BSS and that the assigned number of channels is N_{RU}, the probability that the first user to select a random RU is 1. Then the probability that the second node will select a different RU out of N_{RU} is $\frac{N_{RU}-1}{N_{RU}}$. Furthermore the probability for the k^{th} node to uniquely select a particular RU that is not selected by any other user is $\frac{N_{RU}-k+1}{N_{RU}}$. Therefore, by generalizing the above, P_{RA} can

be derived as follows:

$$P_{RA} = \sum_{k=1}^{N_{RU}} \frac{N_{RU}!(N_U)^k}{(N_{RU})^k(N_{RU}-k)!}\frac{\exp(-N_U)}{k!} = \frac{N_{RU}!}{\exp(N_U)}\sum_{k=1}^{N_{RU}} \frac{\left(\frac{N_U}{N_{RU}}\right)^k}{k!(N_{RU}-k)!} \tag{3.31}$$

Furthermore, given that the tagged Wi-Fi user is located at $z_0 = (r_0, 0)$, during MU operation mode, the SINR coverage probability of the typical Wi-Fi AP with SINR threshold T in the UL when using trigger-based random access, we have:

$$\hat{p}^U_{SINR,MU}\left(T, \lambda_D, \lambda_U, \lambda_L\right) = \hat{p}^U_{SINR,SU}\left(T, \lambda_D, \lambda_U^{MU}, \lambda_L\right) \tag{3.32}$$

Where $\lambda_U^{MU} = \lambda_U \times \hat{p}^U_{MU,MAP}\left(\lambda_D, \lambda_U, \lambda_L\right)$.
Also, $p^{x/z_0}_{1,MAP}$, $p^{y/z_0}_{1,MAP}$, and $p^{z/z_0}_{1,MAP}$ which were derived in section 3.2.2 can be used to compute $\hat{p}^U_{SINR,SU}(T, \eta\lambda_D, \lambda_U^{MU}, \lambda_L)$ in this case.

3.4 Throughput and DST Analysis For LTE-U With IEEE 802.11ax Wi-Fi

3.4.1 LTE-U with Synchronous Muting Pattern

When LTE adopts discontinuous transmission with synchronous muting pattern, all LTE-U eNBs will transmit and mute at the same time. Based on this, we use the definition of the DST and Shannon throughput probability in (3.2) and (3.3) to derive the time averaged DST and Shannon throughput for the Wi-Fi/LTE networks. Hence, given that LTE-U adopts a synchronous muting pattern with duty cycle τ, the time-averaged DST with SINR threshold T for Wi-Fi UL or DL and LTE-U are given by (3.33). In addition, when LTE-U adopts a synchronous muting pattern with duty cycle τ, the time-averaged throughput probability with rate threshold ρ for Wi-Fi UL and DL and LTE-U are given in

---

$$\begin{aligned}
&d^X_{suc}(\lambda_D, \lambda_U, \lambda_L, T, \tau) = \\
&\tau N_{RU}\lambda_X \hat{p}^X_{1,MAP}(\lambda_U, \lambda_D, \lambda_L)\hat{p}^X_{1,SINR}(T, \lambda_U, \lambda_D, \lambda_L) + (1-\tau)N_{RU}\lambda_U \hat{p}^X_{1,MAP}(\lambda_U, \lambda_D, \lambda_L = 0)\hat{p}^X_{1,SINR}(T, \lambda_U, \lambda_D, \lambda_L = 0) \\
&d^L_{suc}(\lambda_D, \lambda_U, \lambda_L, T, \tau) = \tau\lambda_L \hat{p}^L_{1,SINR}(T, \lambda_U, \lambda_D, \lambda_L)
\end{aligned} \tag{3.33}$$

$$\begin{aligned}
&P^X_{1,throughput}(\lambda_D, \lambda_U, \lambda_L, \rho, \tau) \approx \\
&\tau\hat{p}^X_{1,SINR}\left(2^{\frac{\rho N_{RU}}{B\hat{p}^X_{1,MAP}(\lambda_U,\lambda_D,\lambda_L)}} - 1, \lambda_U, \lambda_D, \lambda_L\right) + (1-\tau)\hat{p}^X_{1,SINR}\left(2^{\frac{\rho N_{RU}}{B\hat{p}^X_{1,MAP}(\lambda_U,\lambda_D,\lambda_L=0)}} - 1, \lambda_U, \lambda_D, \lambda_L\right) \\
&P^L_{1,throughput}(\lambda_D, \lambda_U, \lambda_L, \rho, \tau) \approx \tau\hat{p}^L_{1,SINR}\left(2^{\frac{\rho}{B\tau}} - 1, \lambda_U, \lambda_D, \lambda_L\right)
\end{aligned} \tag{3.34}$$

(3.34). Where X can be replaced by U or D to denote the UL or DL, respectively. Furthermore, during the LTE-U on/off periods: The MAPs of the tagged Wi-Fi user in the UL, tagged Wi-Fi AP in the DL, and tagged LTE-U eNB are $\hat{p}^{U}_{1,MAP}(\lambda_D, \lambda_U, \lambda_L)/\hat{p}^{U}_{1,MAP}(\lambda_D, \lambda_U, 0)$, $\hat{p}^{D}_{1,MAP}(\lambda_D, \lambda_U, \lambda_L)/\hat{p}^{D}_{1,MAP}(\lambda_D, \lambda_U, 0)$, and $\tau/(1-\tau)$ respectively. Whereas the SINR coverage probabilities with threshold T of the typical AP, typical Wi-Fi user, and typical LTE UE are $\hat{p}^{U}_{1,SINR}(T, \lambda_U, \lambda_D, \lambda_L)$ / $\hat{p}^{U}_{1,SINR}(T, \lambda_U, \lambda_D, \lambda_L = 0)$, $\hat{p}^{D}_{1,SINR}(T, \lambda_U, \lambda_D, \lambda_L)$/ $\hat{p}^{D}_{1,SINR}(T, \lambda_U, \lambda_D\ , \lambda_L = 0)$, and $\hat{p}^{L}_{1,SINR}(T, \lambda_U, \lambda_D, \lambda_L)$/ $\hat{p}^{L}_{1,SINR}(T, \lambda_U, \lambda_D, \lambda_L = 0) = 0$.

3.4.2 LTE-U with Asynchronous Muting Pattern

When LTE-U utilize discontinuous transmission with asynchronous muting pattern, each LTE-U eNB will transmit independently with probability τ at a given time. Hence the interfering eNBs to the Wi-Fi network will be a PPP with intensity $\tau\lambda_L$ which results in the following: The MAP of the tagged Wi-Fi user and the tagged Wi-Fi AP are $\hat{p}^{U}_{1,MAP}(\lambda_D, \lambda_U, \tau\lambda_L)$ and $\hat{p}^{D}_{1,MAP}(\lambda_D, \lambda_U, \tau\lambda_L)$ respectively. Whereas, the SINR coverage probability with threshold T of the typical AP and Wi-Fi user are $\hat{p}^{U}_{1,SINR}(T, \lambda_D, \lambda_U, \tau\lambda_L)$ and $\hat{p}^{D}_{1,SINR}(T, \lambda_D, \lambda_U, \tau\lambda_L)$ respectively. Based on the above, the time-averaged DST with SINR threshold T for Wi-Fi UL or DL is given by:

$$d^{X}_{2,suc}(\lambda_D, \lambda_U, \lambda_L, T, \tau) = \lambda_U N_{RU} \hat{p}^{X}_{1,MAP}(\lambda_U, \lambda_D, \tau\lambda_L)\hat{p}^{X}_{1,SINR}(T, \lambda_U, \lambda_D, \tau\lambda_L) \tag{3.35}$$

In addition, the time averaged throughput probability with threshold ρ for Wi-Fi UL or Wi-Fi DL is given by:

$$P^{X}_{2,throughput}(\lambda_D, \lambda_U, \lambda_L, \rho, \tau) = \hat{p}^{X}_{1,SINR}\left(2^{\frac{\rho N_{RU}}{B\hat{p}^{X}_{1,MAP}(\lambda_U, \lambda_D, \tau\lambda_L)}} - 1, \lambda_U, \lambda_D, \tau\lambda_L\right) \tag{3.36}$$

Where X can be replaced by U or D to denote the UL or DL, respectively. On the other hand, for the LTE network, and by Slivnyak′s theorem, when the tagged eNB transmit to the typical UE during a fraction τ of time, the interfering eNBs will be a PPP with intensity $\tau\lambda_L$. Thus the time averaged DST of the LTE network is given by:

$$d^{L}_{2,suc}(\lambda_D, \lambda_U, \lambda_L, T, \tau) = \lambda_L \tau \int_0^{\infty} \hat{p}^{L}_{1,SINR}(r_0, T, \lambda_U, \lambda_D, \tau\lambda_L) 2\pi\lambda_L r_0 \exp(-\lambda_L \pi {r_0}^2) \mathrm{d}r_0 \tag{3.37}$$

and the time averaged throughput probability is given by:

$$P^{L}_{2,throughput}(\lambda_D, \lambda_U, \lambda_L, \rho, \tau) = \int_0^{\infty} \hat{p}^{L}_{1,SINR}(r_0, 2^{\frac{\rho}{B\tau}} - 1, \lambda_U, \lambda_D, \tau\lambda_L) 2\pi\lambda_L r_0 \exp(-\lambda_L \pi {r_0}^2) \mathrm{d}r_0 \tag{3.38}$$

Where $\hat{p}^{L}_{1,SINR}(r_0, T, \lambda_U, \lambda_D, \tau\lambda_L)$ was derived in (3.21).

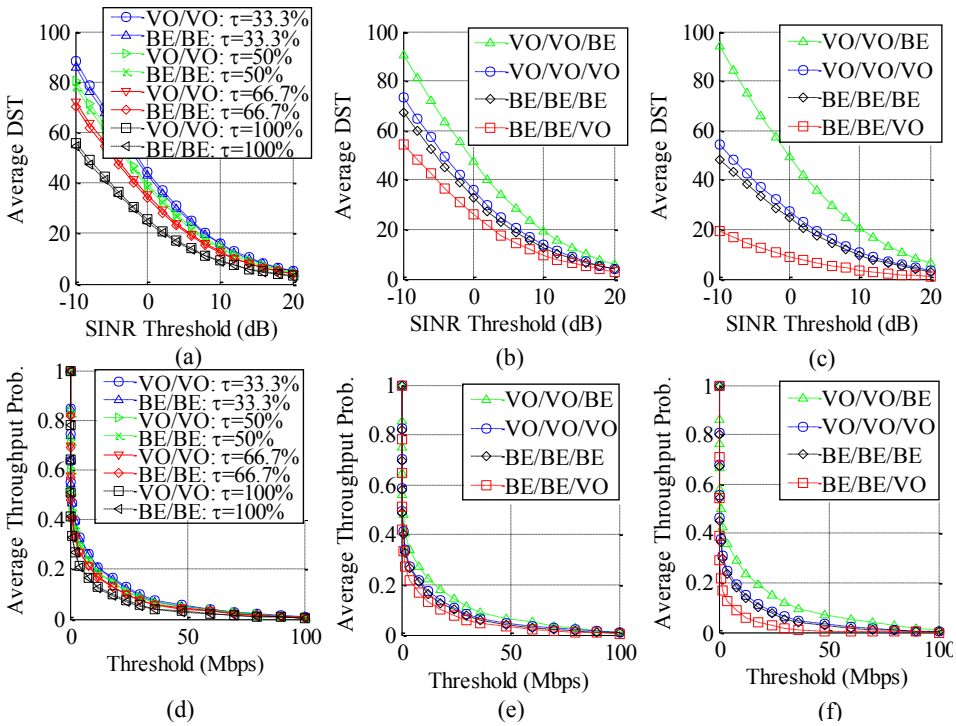

Figure 3.4: Analytical average DST and throughput probability of Wi-Fi UL when operator 2 is LTE-U in (a) and (d), LAA in (b) and (e), and baseline scenario in (c) and (f) respectively.

3.5 Performance Evaluation of Coexistence Scenarios With Simultaneous IEEE 802.11ax Wi-Fi UL and DL

In this section, we study the performance of the IEEE 802.11ax Wi-Fi with SU and MU operation modes when coexisting with LTE in the unlicensed band. Three scenarios were considered for two operators where in scenario 1 we have LTE-U (operator 1) + Wi-Fi (operator 2), scenario 2 is LAA (operator 1) + Wi-Fi (operator 2) and scenario 3 is the baseline scenario where we have Wi-Fi (operator 1) + Wi-Fi (operator 2). We focus mainly on dense network deployment. Hence, we choose $\lambda_D = 400$ APs/km^2, $\lambda_L = 400$ eNBs/km^2 and $\lambda_U = 400$ users/km^2. Based on the MAP and the SINR coverage probability, we analyze the performance of the coexistence scenarios using the DST and the throughput that were derived in the previous sections. We start first by analyzing the coexistence of the IEEE 802.11ax WiFi with LTE in the case of SU mode where we study the UL performance when WiFi users, APs, and LTE eNBs/Wi-Fi APs transmissions co-exist. In this case, Wi-Fi users and APs will use EDCA to access the channel. Fig. 3.4 shows the analytical time-averaged DST and throughput probability for IEEE 802.11ax Wi-Fi UL in case of different traffic

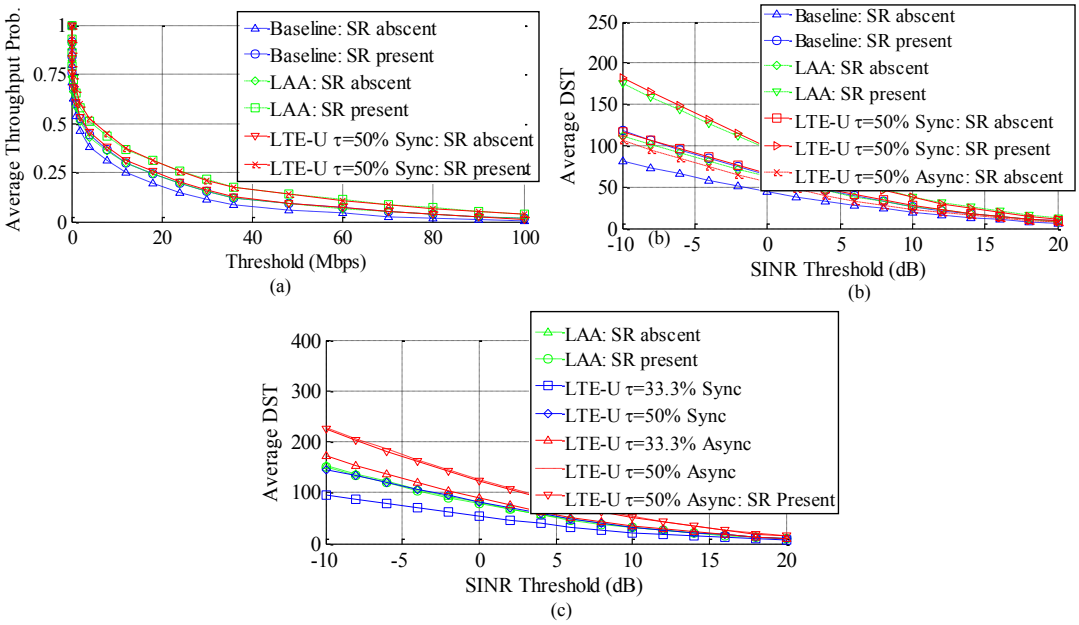

Figure 3.5: (a) Analytical average throughput probability for Wi-Fi DL and DST for (b) Wi-Fi DL, (c) LTE DL in case of presence/absence of SR technique.

types for Wi-Fi UL/Wi-Fi DL/(LTE DL or Wi-Fi DL in case of baseline scenario). From Fig. 3.4, we can see that in general both performance metrics follow the same trend for a specific traffic type. Also, by inspecting Fig. 3.4 (c) and (f), which correspond to the baseline scenario, we can see that, on average, the DST and the throughput probability in case where Wi-Fi UL carries voice (VO) traffic is better than the case of best effort (BE) traffic. Futhermore, the performance is the best in case where UL carries higher priority traffic (VO/VO/BE). Whereas, in the case where same traffic is carried (VO/VO/VO or BE/BE/BE), the performance looks similar. Finally we can see that the worst performance occurs when operator 2 carries higher priority traffic (BE/BE/VO). On the other hand, in case of LAA (Fig. 3.4 (b) and (e)), we can see that when Wi-Fi UL carries higher priority traffic than LAA (VO/VO/BE), the performance remains approximately the same. However, the DST and throughput probability start to increase when Wi-Fi UL carries same/lower priority traffic as LAA where we have an increase in the performance metrics under study by 50% in case of (VO/VO/VO)/(BE/BE/BE) and 100% in case of (BE/BE/VO). This can be explained by the fact that Wi-Fi uses a more aggressive sensing threshold when contending against other Wi-Fi transmissions compared to the case of of LAA transmissions and hence less Wi-Fi nodes will access the channel. Finally, when UL transmissions coexists with LTE-U, as shown in Fig. 3.4 (a) and (d), we can see that the performance of Wi-Fi UL increase as τ (fraction of time that LTE transmits) decrease. In particular, the best performance for UL is achieved when LTE-U uses $\tau = 33.3\%$ whereas the worst performance especially is achieved in

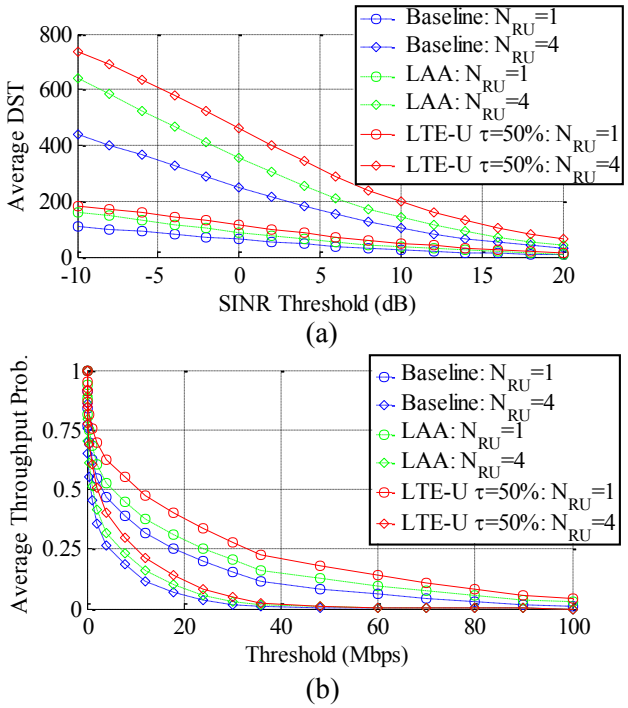

Figure 3.6: (a) Analytical average DST and (b) throughput probability of MU DL.

case where $\tau = 100\%$, which is the case of conventional LTE with continuous transmission and no protocol change. Also, compared to the baseline scenario, we can see that when LTE-U uses $\tau = 33.3\%$, this is similar to the case where operator 2 uses BE traffic (e.g. VO/VO/BE).

Next, we analyze the effect of the SR technique when used by the APs on the performance of Wi-Fi DL in SU mode when coexisting with Wi-Fi UL and LTE DL/WiFi DL (baseline scenario). We consider VO traffic carried over all links where Fig. 3.5 (a) and (b) show that when Wi-Fi APs use the SR technique, the average DST and throughput probability increase by 60% in the baseline scenario whereas there is an increase by 40% in case of LAA or LTE-U with $\tau = 50\%$. Also, we can see that the performance of Wi-Fi DL is better in case of synchronous LTE-U than that of asynchronous LTE-U. On the other hand, we can see from Fig. 3.5 (c), that the performance of LAA and LTE-U is not degraded even when APs use the SR technique. Also, the performance of LTE-U DL seems to be better in the case of asynchronous LTE-U than that of the synchronous LTE-U transmissions. On the other hand, Fig. 3.6 shows the MU Wi-Fi DL performance when operator 1 has only MU DL transmissions while coexisting with operator 2 that may have LAA DL, LTE-U DL, or SU WiFi UL (baseline scenario) transmissions. Also, we consider that all traffic is VO traffic. N_{RU} represents the number of subchannels that divides the total bandwidth B. Hence, $N_{RU} = 1$ corresponds to the SU case. By analyzing Fig. 3.6, we can see

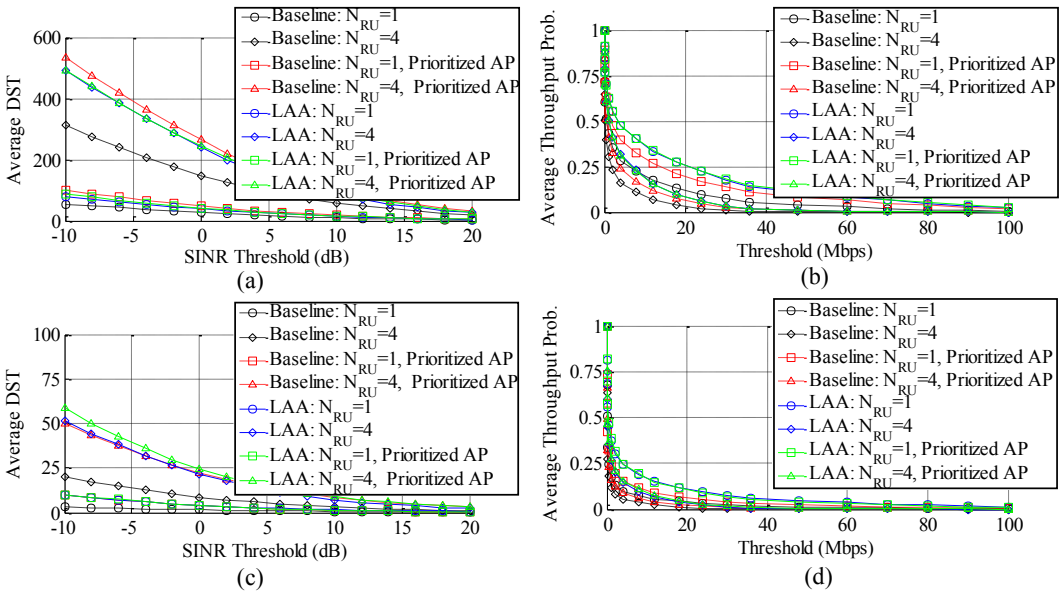

Figure 3.7: Analytical average DST and throughput probability of MU UL trigger-based deterministic access (a)-(b) and trigger-based random access (c)-(d).

that in case of Wi-Fi MU DL, the average DST in the low SINR threshold regime increases by 320% as N_{RU} increases from 1 to 4 in case of baseline scenario and 250% in case of LAA or LTE-U ($\tau = 50\%$). This is can be explained by the fact that we have N_{RU} simultaneous transmissions at each AP. However, the increase in DST is accompanied by an equivalent decrease in the average throughput of each link where the total bandwidth of the channel is divided by N_{RU}. As for the case of MU UL, we study both TR-DA and TR-RA mechanisms as shown in Fig. 3.7. In particular, we consider that operator 1 has only MU UL transmissions while coexisting with operator 2 that may have LAA DL or SU WiFi DL (baseline scenario) transmissions. By analyzing Fig. 3.7 we can see that in terms of the average DST and throughput probability, the performance of TR-DA is much better than that of TR-RA. This is due to the fact that in case of random access users will have to contend for channel access with other users. Also, we can see that when operator 2 is LAA, the performance enhancement with the increase of N_{RU} is higher than that of the baseline scenario. On the other hand, in case of prioritized AP (t_i^D uniformly distributed in the interval $[0, 1]$ and corresponding distributions can be derived in a similar manner to Table 3.4) where the IEEE 802.11ax AP that sends trigger frames will have faster access to the channel, we can see that both the average DST and throughput of MU UL are enhanced as compared to the case where the IEEE 802.11ax AP uses legacy EDCA parameters to access the channel.

3.6 Summary

In this chapter, we have presented and validated a framework based on stochastic geometry to analyze the coexistence of overlaid LTE and IEEE 802.11ax Wi-Fi networks. In particular, three coexistence mechanisms (LTE, LTE-U, and LAA) in addition to the Wi-Fi baseline scenario were evaluated analytically and numerically. Several performance metrics were utilized which are MAP, SINR coverage probability, DST and Shannon throughput. Analysis shows that the effect of the coexistence of LTE is not the same for all traffic types. In addition, in most scenarios, LTE-U and LAA appear as a good neighbor to IEEE 802.11ax when compared to the baseline scenario. Also, we showed that the SR technique provides a boost in performance of IEEE 802.11ax transmissions. Finally, we discussed the performance of different type of MU mode where we showed that the trigger based deterministic access has the best performance.

Chapter 4

Coexistence of LTE-LAA Networks in the Unlicensed Band

In this chapter, we analyze the effect of channel access priorities as well as the effect of the scaling the number of LTE operators sharing an unlicensed band on the network performance in licensed assisted access.

4.1 LTE-LAA Coexistence: Effect of Channel Access Priorities

In this section, we address the effect of channel access priorities on the network performance of coexisting LAA networks. The contention window size utilized in this protocol is mainly affected by the manufacturer choice and the associated data traffic type. Therefore, particular network operators may target certain traffic types, and hence use different contention window sizes. Given the serious impact that this has on the performance of the corresponding networks, we make use of stochastic geometry in this work to model and analyze the coexistence of three LTE-LAA networks with persistent downlink transmissions and having different contention window sizes.

4.1.1 System Model

In this section, we present the radio channel model. the propagation assumptions, and the spatial location model of LTE eNBs, and LTE user equipments (UEs). In addition, we present the channel access model for LTE and the corresponding performance metrics under study.

Radio Channel Model

We denote by $l(d)$ the path loss between the transmitter and the receiver which are separated by a distance d. We use here a common free space path loss model with reference distance of one meter for both Wi-Fi and LTE links. Hence $l(d)$ is given by $l(d) = (\frac{4\pi}{\Lambda_c})^2 d^\alpha$ where Λ_c represents the wavelength and α is the path-loss exponent that depends on the scenario considered. For simplicity we ignore the large scale shadowing effect. Also, we assume that channels are subject to i.i.d Rayleigh fading where each fading variable is exponentially distributed with parameter μ.

Spatial Location Model

We consider mainly a scenario in which we have four sets of eNBs that coexist in a single unlicensed frequency band that has a bandwidth denoted by B. We assume that each set of eNBs use LTE-LAA but with different channel access priority class where the channel access parameters for classes A, B, C, and D are shown in Table 4.21. The LTE-LAA eNBs are assumed to be low power small cell (pico-cell or femto-cell) eNBs. We model the location of eNBs having traffic for transmission and co-existing in the same band, as realizations of four independent homogeneous Poisson point processes (PPP) on $\mathbb{R}^2$. The LTE eNB process for each class is assumed to have persistent downlink traffic.

Denote by $\Phi_A = \{x_j\}, \Phi_B = \{w_k\}, \Phi_C = \{y_n\}$, and $\Phi_D = \{z_p\}$ the LTE eNB processes for LTE-LAA class A, B, C, and D with intensities λ_A, λ_B, λ_C, and λ_D respectively. The receiving LTE UEs process are modeled as independent homogeneous PPPs denoted as $\Phi_{A'}$, $\Phi_{B'}$, $\Phi_{C'}$, and $\Phi_{D'}$ with intensities $\lambda_{A'}$, $\lambda_{B'}$, $\lambda_{C'}$, and $\lambda_{D'}$ respectively.
Thus based on Slivnyak′s theorem [39], we analyze the performance of a typical UE in the downlink that is assumed to be at the origin. It is worth mentioning that the PPP assumption for eNBs is used for tractability as in [37] and that it will have similar SINR trends with a fixed SINR gap compared to other more accurate spatial models for cellular base stations (BSs) [66].
Each UE is associated with its closest eNB, which provides the strongest average received power. Furthermore, index 0 is used for typical UE and its serving eNB in the downlink which will be called the tagged eNB in the rest of the chapter. The link between the typical UE and tagged eNB in the downlink is referred to as the typical LTE link.
Given that each of Φ_A, Φ_B, Φ_C, and Φ_D is a PPP with intensities $\lambda_A, \lambda_B, \lambda_C$, and λ_D respectively, the probability density function (PDF) of the distance from the typical UE to the tagged eNB in the downlink is $f_R(r) = 2\pi r \lambda_X e^{-\lambda_X \pi r^2}$ where $\lambda_X = \lambda_A, \lambda_B, \lambda_C$, or λ_D accordingly.

Channel Access Model of LTE-LAA

3GPP in release 14 [49], presents a channel access procedure for LTE downlink that is intended to be used by eNBs when accessing the channel in the unlicensed band. This MAC protocol will prevent an LTE-LAA device using a shared unlicensed spectrum to transmit on the channel when transmissions from other devices are present.
In case of LAA downlink MAC protocol, the LAA eNB performs clear channel assessment (CCA) procedure where the channel is observed initially for a defer period to detect the presence of active transmitters for which the received signal power exceeds a certain energy detection threshold level (T_{Thresh}). It is important to note that in the 3GPP specifications [49], energy detection is implemented based on total interference where each eNB will decide that the channel is busy if the total interference exceeds the energy detection threshold. However, the authors in [37] showed that when the eNBs have PPP distribution, the strongest interferer model is a reasonable model that can be used instead of the total interference model in [49]. Thus, to facilitate the analysis, and since the eNBs form a PPP, we adopt the method of energy detection based on the strongest interferer, as in [37], where a channel is determined busy if the intending transmitter detects another LTE signal above T_{Thresh}. Once the channel is found idle the LTE eNB will then follow a random back-off period before transmission that is selected randomly from a contention window in the interval $[0; CW]$ where CW $\in [CW_{min}, CW_{max}]$.

Table 4.1: Different Channel Access Priority Classes For LAA Downlink Based on 3GPP Release 14 [49]

Channel Access Priority Class	Defer Period (Δ)	CW_{min}	CW_{max}	Allowed CW sizes
A	1	3	7	3, 7
B	1	7	15	7, 15
C	3	15	63	15, 31, 63
D	7	15	1023	15, 31, 63, 127, 255, 511, 1023

Both the defer period and the contention window size CW depends on the priority class where 3GPP defines four priority classes for LAA as shown in Table 4.21 and Fig. 4.1. The selected values of the defer period and CW determine the priority for a LTE-LAA device to access the medium. Consequently, this may have a relevant impact on the coexistence of nodes with different traffic types and corresponding priority classes, as will be shown later in our results. Although, the contention window specified in the random back-off mechanism is dynamic, we utilize the modified Matern Hardcore point process with a fixed contention window size when modeling the channel access of eNBs as described here after.

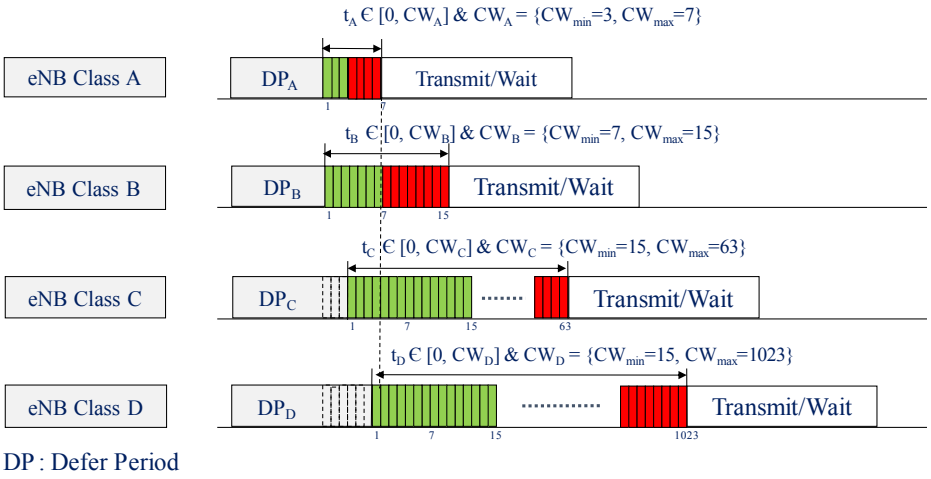

Figure 4.1: Illustration of Different Downlink Channel Access Priority Classes

This is due to the fact that the modified Matern Hardcore point process has shown an accurate estimate in the case where the back-off period is based on dynamic contention window size [32].

Throughout this study, we focus mainly on the scenario where we have an LTE-LAA network with four coexisting sets of eNBs each having a particular traffic class. We define the contender of a LTE eNB as the other LTE eNBs from which the received power at the former exceeds thresholds T_{Thresh} where T_A, T_B, T_C and T_D correspond to the energy detection threshold of the sets of eNBs for priority classes A, B, C, and D respectively. Since the defer period (Δ) varies between some classes where both classes A and B share the same defer period of one time slot where as classes C and D have defer period of 3 and 7 respectively. Thus, in order to accommodate for the variation of the defer period between different classes and based on the modified Matern Hardcore process, we define the timer for each class based on both the contention window and the defer period. Each LTE eNB $x_j \in \Phi_A$ has an independent mark t_j^A that represents the defer period and the random back-off period, which is uniformly distributed in the interval $[\Delta_A, CW_A + \Delta_A]$. Similarly, $w_k \in \Phi_B$ has an independent mark t_k^B uniformly distributed in the interval $[\Delta_B, CW_B + \Delta_B]$, $y_n \in \Phi_C$ has an independent mark t_n^C that is uniformly distributed in the interval $[\Delta_C, CW_C + \Delta_C]$ and $z_p \in \Phi_D$ has an independent mark t_p^D that is uniformly distributed over $[\Delta_D, CW_D + \Delta_D]$. Each LTE eNB is retained by the MAC protocol if it has a smaller timer than all its contenders. A medium access indicator e_j^A is assigned to each LTE eNB $x_j \in \Phi_A$ (e_k^B to each LTE eNB $w_k \in \Phi_B$, e_n^C to each LTE eNB $y_n \in \Phi_C$, and e_p^D to each LTE eNB $z_p \in \Phi_D$) which is equal to one if the eNB is allowed to transmit by the corresponding MAC layer protocol and zero otherwise.

Performance Metrics

In this section, we define the performance metrics that are used in our analysis. In addition to the MAP that will be derived in the following sections, we also base our analysis on the SINR coverage probability for each LAA priority class A, B, C and D. Thus, given the fact that the tagged eNB $x_0 \in \Phi_A$ transmits, the received SINR at the typical LTE UE located at the origin is given by:

$$SINR_0^A = \frac{P_A G_{0,0}^{AA'} / l(\|x_0\|)}{I_A + \sigma_N^2} \text{ where} \tag{4.1}$$

$$I_A = \sum_{x_j \in \Phi_A \setminus \{x_0\}} P_A G_{j,0}^{AA'} e_j^A / l(\|x_j\|) + \sum_{w_k \in \Phi_B} P_B G_{k,0}^{BA'} e_k^B / l(\|w_k\|) + \sum_{y_n \in \Phi_C} P_C G_{n,0}^{CA'} e_n^C / l(\|y_n\|) + \sum_{z_p \in \Phi_D} P_D G_{p,0}^{DA'} e_p^D / l(\|z_p\|)$$

Thus for a typical LTE UE, the SINR coverage probability with a SINR threshold T is defined as $\mathbb{P}(SINR_0^A > T | e_0^A = 1)$. This corresponds to the instantaneous SINR performance of the typical LTE-LAA downlink for priority class A. Similarly, the received SINR of the typical LTE downlink for priority class B is:

$$SINR_0^B = \frac{P_B G_{0,0}^{BB'} / l(\|w_0\|)}{I_B + \sigma_N^2} \text{ where} \tag{4.2}$$

$$I_B = \sum_{x_j \in \Phi_A} P_A G_{j,0}^{AB'} e_j^A / l(\|x_j\|) + \sum_{w_k \in \Phi_B \setminus \{w_0\}} P_B G_{k,0}^{BB'} e_k^B / l(\|w_k\|) + \sum_{y_n \in \Phi_C} P_C G_{n,0}^{CB'} e_n^C / l(\|z_y\|) + \sum_{z_p \in \Phi_D} P_D G_{p,0}^{DB'} e_p^C / l(\|z_p\|)$$

With the corresponding SINR coverage probability $\mathbb{P}(SINR_0^B > T | e_0^B = 1)$. Also, the received SINR of the typical LTE UE for priority class C, given that the tagged LTE eNB transmits is:

$$SINR_0^C = \frac{P_C G_{0,0}^{CC'} / l(\|y_0\|)}{I_C + \sigma_N^2} \text{ where} \tag{4.3}$$

$$I_C = \sum_{x_j \in \Phi_A} P_A G_{j,0}^{AC'} e_j^A / l(\|x_j\|) + \sum_{w_k \in \Phi_B} P_B G_{k,0}^{BC'} e_k^B / l(\|w_k\|) + \sum_{y_n \in \Phi_C \setminus \{y_0\}} P_C G_{n,0}^{CC'} e_n^C / l(\|y_n\|) + \sum_{z_p \in \Phi_D} P_D G_{p,0}^{DC'} e_p^D / l(\|z_p\|)$$

Hence, the SINR coverage probability is $\mathbb{P}(SINR_0^C > T | e_0^C = 1)$. Finally, the received SINR of the typical LTE UE for priority class D, given that the tagged LTE eNB transmits is:

$$SINR_0^D = \frac{P_D G_{0,0}^{DD'} / l(\|z_0\|)}{I_D + \sigma_N^2} \text{ where} \tag{4.4}$$

$$I_D = \sum_{x_j \in \Phi_A} P_A G_{j,0}^{AD'} e_j^A / l(\|x_j\|) + \sum_{w_k \in \Phi_B} P_B G_{k,0}^{BD'} e_k^B / l(\|w_k\|) + \sum_{y_n \in \Phi_C} P_C G_{n,0}^{CD'} e_n^C / l(\|y_n\|) + \sum_{z_p \in \Phi_D \setminus \{z_0\}} P_D G_{p,0}^{DD'} e_p^D / l(\|z_p\|)$$

And the SINR coverage probability is $\mathbb{P}(SINR_0^D > T | e_0^D = 1)$. Now, based on the SINR coverage probability and the MAP we define the following performance metric that is used to analyze the coexistence scenario under study:

Rate Coverage Probability: given the rate threshold ρ, the rate coverage

Table 4.2: Notations and Definitions of Used Functions ($X = A, B, C$, or D)

Notation	Definition
$N_X(z,T,r)$	$\lambda_X \int_{\mathbb{R}^2\setminus B(0,r)} \exp\big(-\mu\frac{T}{P_X} l(\|x-z\|)\big)\mathrm{d}x$
$C_X(z_1,T_1,z_2,T_2,r)$	$\lambda_X \int_{\mathbb{R}^2\setminus B(0,r)} \exp\big(-\mu\frac{T_1}{P_X} l(\|x-z_1\|) - \mu\frac{T_2}{P_X} l(\|x-z_1\|)\big)\mathrm{d}x$
$N_X(z,T)$	$N_X(z,T,\|z\|)$
$C_X(z_1,z_2)$	$C_X(z_1,T_1,z_2,T_2,r_0)$
$C_X(z_1-z_2)$	$C_X(z_1-z_2,T_1,o,T_2,r_0)$
$H_N\big(x_1,x_2,y,\Delta_1,CW_1,\Delta_2,CW_2,1,2,3,4\big)$	$\frac{1-\exp\Big(-\mu y l(\|x_1-x_2\|)\Big)}{CW_1 CW_2}\int_{\Delta_2}^{CW_2+\Delta_2}\int_{\Delta_1}^{CW_1+\Delta_1}\exp\Big[-F_{t_1}(t')N_1(x_2,T_2,r_0)-F_{t_2}(t')N_2(x_2,T_1)-F_{t_3}(t')N_3(x_2,T_2)-F_{t_4}(t')N_4(x_2,T_2)-F_{t_1}(t)N_1(x_1,T_1,r_0)-F_{t_2}(t)N_2(x_1,T_1)-F_{t_3}(t)N_3(x_1,T_1)-F_{t_4}(t)N_4(x_1,T_1)+F_{t_1}(t)Q_1(x_2,x_1)+F_{t_2}(t)Q_2(x_2-x_1)+F_{t_3}(t)Q_3(x_2-x_1)+F_{t_4}(t)Q_4(x_2-x_1)\Big]\mathrm{d}t\mathrm{d}t'$
$H_D(x,y,z,1,2,3,4,5)$	$=\frac{1}{CW_1}\int_{\Delta_1}^{CW_1+\Delta_1}\Big(1-F_{t_5}(t)\exp\Big[-\mu z l(\|y-x\|)\Big)\Big]\times \exp\Big[-F_{t_1}(t)N_1(x,T_1,r_0)-F_{t_2}(t)N_2(x,T_1)-F_{t_3}(t)N_3(x,T_1)-F_{t_4}(t)N_4(x,T_1)\Big]\mathrm{d}t$
$H_M\big(x,T_L,1,2,3,4\big)$	$\frac{1}{CW_1}\int_{\Delta_1}^{CW_1+\Delta_1}\exp\Big[-F_{t_1}(t)N_1(x,T_L,r_0)-F_{t_2}(t)N_2(x,T_L)-F_{t_3}(t)N_3(x,T_L)-F_{t_4}(t)N_4(x,T_L)\Big]dt$

probability is defined as the probability for the typical LTE downlink to support at least an average data rate of ρ. Note that, this is given by:

$$\begin{aligned}
P^A_{rate}(\lambda_A,\lambda_B,\lambda_C,\lambda_D,\rho) &= \mathbb{P}\left(B\log\left(1+SINR^A_0\right)\mathbb{E}\left[e^A_0\right] > \rho | e^A_0 = 1\right)\\
P^B_{rate}(\lambda_A,\lambda_B,\lambda_C,\lambda_D,\rho) &= \mathbb{P}\left(B\log\left(1+SINR^B_0\right)\mathbb{E}\left[e^B_0\right] > \rho | e^B_0 = 1\right)\\
P^C_{rate}(\lambda_A,\lambda_B,\lambda_C,\lambda_D,\rho) &= \mathbb{P}\left(B\log\left(1+SINR^C_0\right)\mathbb{E}\left[e^C_0\right] > \rho | e^C_0 = 1\right)\\
P^D_{rate}(\lambda_A,\lambda_B,\lambda_C,\lambda_D,\rho) &= \mathbb{P}\left(B\log\left(1+SINR^D_0\right)\mathbb{E}\left[e^D_0\right] > \rho | e^D_0 = 1\right)
\end{aligned} \tag{4.5}$$

where $\mathbb{E}[e^A_0]/\mathbb{E}[e^B_0]/\mathbb{E}[e^C_0]/\mathbb{E}[e^D_0]$ in (4.4) account for the fact that the tagged eNB has a channel access for $\mathbb{E}[e^A_0]/\mathbb{E}[e^B_0]/\mathbb{E}[e^C_0]/\mathbb{E}[e^D_0]$ fraction of time on average which signifies that the rate coverage probability with threshold ρ provides the

fraction of links that can support an average data rate of ρ. For the rest of the chapter, since Φ_A, Φ_B, Φ_C and Φ_D are stationary and isotropic, thus the above performance metrics of the typical UE are invariant with respect to the angle of the tagged eNB. Also, we assume in our case that the polar coordinates of the tagged eNB are $(r_0, 0)$.

Table 4.3: Used Symbols and Simulation Values

Symbol	Definition	Simulation Value
P_A, P_B, P_C,P_D	Transmit power for eNBs for priority classes A, B, C, and D	23 dBm
f_c, B	Carrier frequency and bandwidth of the unlicensed band	5 GHz, 20 MHz
α	Path loss exponent	4
μ	Parameter for Rayleigh fading channel	1
σ_N^2	Noise power	0
T_A, T_B, T_C, T_D	Energy detection thresholds	
Φ_A, Φ_B, Φ_C, Φ_D	LAA priority class A, B, C, D PPP	
λ_A, λ_B, λ_C, λ_D	LAA priority class A, B, C, D density	
$B^c(x,r)$,$B^o(x,r)$	Closed (open) ball with center x and radius r	
$G_{i,j}^U$,($G_{i,j}^{UD}$,$G_{i,j}^{UL}$)	Fading of the channel from STA i to STA j (from STA i to AP j, from STA i to eNB (co-existing AP or UE) j respectively)	Exponentially distributed with parameter μ
$G_{i,j}^X$	Fading of the channel from LAA eNB i with priority class X to another LAA eNB j from the same priority class e.g. X = A, B, C, or D	Exponentially distributed with parameter μ
$G_{i,j}^{XY}$	Fading of the channel from LAA eNB i with priority class X to another LAA eNB (or UE) j from priority class Y e.g. Y = A, B, C, or D	Exponentially distributed with parameter μ

Finally we define the following functions to be used throughout the chapter where $N_X(y, T_X, r)$ represents the expected number of eNBs respectively in $\mathbb{R}^2 \backslash B(0,r)$ whose signal power received at $z \in \mathbb{R}^2$ exceeds threshold T_X.

Furthermore, $C_X(x_1, T_1, x_2, T_2, r)$ represents the expected number of eNBs respectively in $\mathbb{R}^2 \backslash B(0,r)$ whose signal power received at $x_1 \in R^2$ and $x_2 \in R^2$ exceeds thresholds T_1 and T_2 respectively. Note that the functions H_N, H_{D_1}, and H_{D_2} are used to simplify the equations of the conditional MAP in the coming sections.

4.1.2 MAP and SINR Coverage Probability

We study in this section the MAP and the SINR coverage performance for the coexisting LAA eNBs with traffic having different channel access priority classes.

Medium Access Probability

The medium access indicator of LAA eNB using LBT for priority class A, B, C and D are given as follows:

$$
\begin{aligned}
e_i^A = & \prod_{x_j \in \Phi_A \setminus \{x_i\}} \left(\mathbb{1}_{t_j^A \geq t_i^A} + \mathbb{1}_{t_j^A < t_i^A} \mathbb{1}_{G_{ji}^A / l(\|x_j - x_i\|) \leq T_A / P_A} \right) \times \prod_{w_k \in \Phi_B} \left(\mathbb{1}_{t_k^B \geq t_i^A} + \mathbb{1}_{t_k^B < t_i^A} \mathbb{1}_{G_{ki}^{BA} / l(\|w_k - x_i\|) \leq T_A / P_B} \right) \\
& \times \prod_{y_n \in \Phi_C} \left(\mathbb{1}_{t_n^C \geq t_i^A} + \mathbb{1}_{t_n^C < t_i^A} \mathbb{1}_{G_{ni}^{CA} / l(\|y_n - x_i\|) \leq T_A / P_C} \right) \times \prod_{z_p \in \Phi_D} \left(\mathbb{1}_{t_p^D \geq t_i^A} + \mathbb{1}_{t_p^D < t_i^A} \mathbb{1}_{G_{pi}^{DA} / l(\|z_p - x_i\|) \leq T_A / P_D} \right) \\
e_l^B = & \prod_{x_j \in \Phi_A} \left(\mathbb{1}_{t_j^A \geq t_l^B} + \mathbb{1}_{t_j^A < t_l^B} \mathbb{1}_{G_{jl}^{AB} / l(\|x_j - w_l\|) \leq T_B / P_A} \right) \times \prod_{w_k \in \Phi_B \setminus \{w_l\}} \left(\mathbb{1}_{t_k^B \geq t_l^B} + \mathbb{1}_{t_k^B < t_l^B} \mathbb{1}_{G_{kl}^B / l(\|w_k - w_l\|) \leq T_B / P_B} \right) \\
& \times \prod_{y_n \in \Phi_C} \left(\mathbb{1}_{t_n^C \geq t_l^B} + \mathbb{1}_{t_n^C < t_l^B} \mathbb{1}_{G_{nl}^{CB} / l(\|y_n - w_l\|) \leq T_B / P_C} \right) \times \prod_{z_p \in \Phi_D} \left(\mathbb{1}_{t_p^D \geq t_l^B} + \mathbb{1}_{t_p^D < t_l^B} \mathbb{1}_{G_{pl}^{DB} / l(\|z_p - w_l\|) \leq T_B / P_D} \right) \\
e_m^C = & \prod_{x_j \in \Phi_A} \left(\mathbb{1}_{t_j^A \geq t_m^C} + \mathbb{1}_{t_j^A < t_m^C} \mathbb{1}_{G_{jm}^{AC} / l(\|x_j - y_m\|) \leq T_C / P_A} \right) \times \prod_{w_k \in \Phi_B} \left(\mathbb{1}_{t_k^B \geq t_m^C} + \mathbb{1}_{t_k^B < t_m^C} \mathbb{1}_{G_{km}^{BC} / l(\|w_k - y_m\|) \leq T_C / P_B} \right) \\
& \times \prod_{y_n \in \Phi_C \setminus \{y_m\}} \left(\mathbb{1}_{t_n^C \geq t_m^C} + \mathbb{1}_{t_n^C < t_m^C} \mathbb{1}_{G_{nm}^C / l(\|y_n - y_m\|) \leq T_C / P_C} \right) \times \prod_{z_p \in \Phi_D} \left(\mathbb{1}_{t_p^D \geq t_m^C} + \mathbb{1}_{t_p^D < t_m^C} \mathbb{1}_{G_{pm}^{DC} / l(\|z_p - y_m\|) \leq T_C / P_D} \right) \\
e_q^D = & \prod_{x_j \in \Phi_A} \left(\mathbb{1}_{t_j^A \geq t_q^D} + \mathbb{1}_{t_j^A < t_q^D} \mathbb{1}_{G_{jq}^{AD} / l(\|x_j - z_q\|) \leq T_D / P_A} \right) \times \prod_{w_k \in \Phi_B} \left(\mathbb{1}_{t_k^B \geq t_q^D} + \mathbb{1}_{t_k^B < t_q^D} \mathbb{1}_{G_{kq}^D / l(\|w_k - z_q\|) \leq T_D / P_B} \right) \\
& \times \prod_{y_n \in \Phi_C} \left(\mathbb{1}_{t_n^C \geq t_q^D} + \mathbb{1}_{t_n^C < t_q^D} \mathbb{1}_{G_{nq}^{CD} / l(\|y_n - z_q\|) \leq T_D / P_C} \right) \times \prod_{z_p \in \Phi_D \setminus \{z_q\}} \left(\mathbb{1}_{t_p^D \geq t_q^D} + \mathbb{1}_{t_p^D < t_q^D} \mathbb{1}_{G_{pq}^D / l(\|z_p - z_q\|) \leq T_D / P_D} \right)
\end{aligned}
\tag{4.6}
$$

Note that the energy detection is implemented based on the strongest interferer which is a reasonable model that is used instead of total interference as shown in [37]. Based on the medium access indicators in (4.6), we provide upper and lower performance bounds for the MAPs of each of the classes A, B, C and D.

Lemma 1: For LTE-LAA downlink with the contention window sizes [Δ_A, $CW_A + \Delta_A$], [Δ_B, $CW_B + \Delta_B$], [Δ_C, $CW_C + \Delta_C$], and [Δ_D, $CW_D + \Delta_D$] corresponding to channel priority class A, B, C, and D respectively, the MAP for a tagged eNB of each priority class is given by:

$$
\begin{aligned}
\mathbb{E}[e_0^A] &= \int_0^\infty H_{_M}\big(x, T_A, A, B, C, D\big) f_{\|x\|}(r_0) \mathrm{d}r_0 \\
\mathbb{E}[e_0^B] &= \int_0^\infty H_{_M}\big(w, T_B, B, A, C, D\big) f_{\|w\|}(r_0) \mathrm{d}r_0 \\
\mathbb{E}[e_0^C] &= \int_0^\infty H_{_M}\big(y, T_C, C, A, B, D\big) f_{\|y\|}(r_0) \mathrm{d}r_0 \\
\mathbb{E}[e_0^D] &= \int_0^\infty H_{_M}\big(z, T_D, D, A, B, C\big) f_{\|z\|}(r_0) \mathrm{d}r_0
\end{aligned}
\tag{4.7}
$$

Proof Given the tagged LAA eNB $x_i = (r_0, 0)$, its MAP is derived as:

$$\begin{aligned}
&\mathbb{E}[e_i^A | t_i^A = t, x_i = (r_0, 0)] \\
&= \mathbb{E}\Bigg[\prod_{x_j \in \Phi_A} \left(\mathbb{1}_{t_j^A \geq t_i^A} + \mathbb{1}_{t_j^A < t_i^A} \mathbb{1}_{G_{ji}^A / l(\|x_j - x_i\|) \leq T_A / P_A} \right) \times \prod_{w_k \in \Phi_B} \left(\mathbb{1}_{t_k^B \geq t_i^A} + \mathbb{1}_{t_k^B < t_i^A} \mathbb{1}_{G_{ki}^{BA} / l(\|w_k - x_i\|) \leq T_A / P_B} \right) \\
&\times \prod_{y_n \in \Phi_C} \left(\mathbb{1}_{t_n^C \geq t_i^A} + \mathbb{1}_{t_n^C < t_i^A} \mathbb{1}_{G_{ni}^{CA} / l(\|y_n - x_i\|) \leq T_A / P_C} \right) \times \prod_{z_p \in \Phi_D} \left(\mathbb{1}_{t_p^D \geq t_i^A} + \mathbb{1}_{t_p^D < t_i^A} \mathbb{1}_{G_{pi}^{DA} / l(\|z_p - x_i\|) \leq T_A / P_D} \right) \Bigg] \\
&\overset{(a)}{=} \mathbb{E}\left[\prod_{x_j \in \Phi_A \cap B^c(0, r_0)} \left(1 - F_{t_A}(t) \exp\left(-\mu \frac{T_A}{P_A} l(\|x_j - x_i\|) \right) \right) \right] \times \mathbb{E}\left[\prod_{w_k \in \Phi_B} \left(1 - F_{t_B}(t) \exp\left(-\mu \frac{T_A}{P_B} l(\|w_k - x_i\|) \right) \right) \right] \\
&\quad \times \mathbb{E}\left[\prod_{y_n \in \Phi_C} \left(1 - F_{t_C}(t) \exp\left(-\mu \frac{T_A}{P_C} l(\|y_n - x_i\|) \right) \right) \right] \times \mathbb{E}\left[\prod_{z_p \in \Phi_D} \left(1 - F_{t_D}(t) \exp\left(-\mu \frac{T_A}{P_D} l(\|z_p - x_i\|) \right) \right) \right] \\
&\overset{(b)}{=} \frac{1}{CW_A} \int_{\Delta_A}^{CW_A + \Delta_A} \exp\Big(- F_{t_A}(t) N_A(x_i, T_A, r_0) - F_{t_B}(t) N_B(x_i, T_A) - F_{t_C}(t) N_C(x_i, T_A) - F_{t_D}(t) N_D(x_i, T_A) \Big) dt
\end{aligned}$$

Where (a) follows by re-writing $x_i = (r_0, 0)$ as $x_i \in \Phi_A, \Phi_A(B^o(0, r_0)) = 0$ and de-conditioning on $\Phi_A(B^o(0, r_0)) = 0$ in addition to the fact that Φ_A, Φ_B, Φ_C, Φ_D are independent and by using slivnyak′s theorem, (b) follows from and the probability generating functional (P.G.FL) of the PPP. Then by de-conditioning on $t \sim U(\Delta_A, CW_A + \Delta_A)$ and r_0 and by using the definition of $N_A(x_i, T_A, r_0)$, $N_B(x_i, T_A)$, $N_C(x_i, T_A)$, and $N_D(x_i, T_A)$ gives the desired result.■

The MAP of eNBs that belong to priority classes B, C, and D can be proved in a similar manner given that $t \sim U(\Delta_B, CW_B + \Delta_B)$, $t \sim U(\Delta_C, CW_C + \Delta_C)$, and $t \sim U(\Delta_D, CW_D + \Delta_D)$ respectively.

However, the expressions of $F_{t_A}(t), F_{t_B}(t), F_{t_C}(t)$, and $F_{t_D}(t)$ depend on the selected values of CW_A, CW_B, CW_C, and CW_D. Thus, given the large number of possible combinations of $[CW_A, CW_B, CW_C, CW_D]$, we restrict our analysis to provide upper and lower performance bounds as will be shown in the rest of the chapter. Note that in the case of the upper performance bound for class X, in general, class X will use the smallest possible contention window size $CW_{X_{min}}$ whereas other classes will utilize the largest possible contention window size. On the other hand, in the case of the lower performance bound for a particular class X, class X will use the largest possible contention window size $CW_{X_{max}}$ where as other classes will utilize the smallest possible contention window size per class.

Upper and Lower MAP Performance Bounds For each of class A, B, C, and D we provide the corresponding expressions of $F_{t_A}(t), F_{t_B}(t), F_{t_C}(t)$, and $F_{t_D}(t)$ based on the values of CW_A,CW_B,CW_C and CW_D. Then the expressions provided can be substituted in (4.7) in order to compute the resulting upper and lower MAP of each class.

Class A: Lower and Upper MAP Bound

In case of the lower MAP bound of class A, we have $CW_A = 7$, $CW_B = 7$, $CW_C = 15$ and $CW_D = 15$. On the other hand, in case of the upper MAP bound of class A, we have $CW_A = 3$, $CW_B = 15$, $CW_C = 63$ and $CW_D = 1023$. Hence

Table 4.4: Class A MAP Timers Distributions

Lower Bound	Upper Bound
$F_{t_A}(t) = \frac{t-\Delta_A}{CW_A-\Delta_A} \quad \forall \quad \Delta_A \leq t \leq \Delta_A + CW_A$	$F_{t_A}(t) = \frac{t-\Delta_A}{CW_A-\Delta_A} \quad \forall \quad \Delta_A \leq t \leq \Delta_A + CW_A$
$F_{t_B}(t) = \frac{t-\Delta_B}{CW_B-\Delta_B} \quad \forall \quad \Delta_B \leq t \leq \Delta_A + CW_A$	$F_{t_B}(t) = \frac{t-\Delta_B}{CW_B-\Delta_B} \quad \forall \quad \Delta_B \leq t \leq \Delta_A + CW_A$
$F_{t_C}(t) = \frac{t-\Delta_C}{CW_C-\Delta_C} \quad \forall \quad \Delta_C \leq t \leq \Delta_A + CW_A$	$F_{t_C}(t) = \frac{t-\Delta_C}{CW_C-\Delta_C} \quad \forall \quad \Delta_C \leq t \leq \Delta_A + CW_A$
$F_{t_D}(t) = \frac{t-\Delta_D}{CW_D-\Delta_D} \quad \forall \quad \Delta_D \leq t \leq \Delta_A + CW_A$	$F_{t_D}(t) = 0 \quad \forall \quad \Delta_A \leq t \leq \Delta_A + CW_A$

Table 4.5: Class B MAP Timers Distributions

Lower Bound	Upper Bound
$F_{t_A}(t) = \begin{cases} \frac{t-\Delta_A}{CW_A-\Delta_A} & \forall \quad \Delta_A \leq t \leq \Delta_A + CW_A \\ 1 & \forall \quad \Delta_A + CW_A \leq t \leq \Delta_B + CW_B \end{cases}$	$F_{t_A}(t) = \frac{t-\Delta_A}{CW_A-\Delta_A} \quad \forall \quad \Delta_A \leq t \leq \Delta_B + CW_B$
$F_{t_B}(t) = \frac{t-\Delta_B}{CW_B-\Delta_B} \quad \forall \quad \Delta_B \leq t \leq \Delta_B + CW_B$	$F_{t_B}(t) = \frac{t-\Delta_B}{CW_B-\Delta_B} \quad \forall \quad \Delta_B \leq t \leq \Delta_B + CW_B$
$F_{t_C}(t) = \frac{t-\Delta_C}{CW_C-\Delta_C} \quad \forall \quad \Delta_C \leq t \leq \Delta_B + CW_B$	$F_{t_C}(t) = \frac{t-\Delta_C}{CW_C-\Delta_C} \quad \forall \quad \Delta_C \leq t \leq \Delta_B + CW_B$
$F_{t_D}(t) = \frac{t-\Delta_D}{CW_D-\Delta_D} \quad \forall \quad \Delta_D \leq t \leq \Delta_B + CW_B$	$F_{t_p^D}(t) = \frac{t-\Delta_D}{CW_D-\Delta_D} \quad \forall \quad \Delta_C \leq t \leq \Delta_B + CW_B$

the derived expressions of $F_{t_A}(t), F_{t_B}(t), F_{t_C}(t)$, and $F_{t_D}(t)$ are shown in Table 4.4.

Class B: Lower and Upper MAP Bound

In case of the lower MAP bound of class B, we have $CW_A = 3$, $CW_B = 15$, $CW_C = 15$ and $CW_D = 15$. On the other hand, in case of the upper MAP bound of class B, we have $CW_A = 7$, $CW_B = 7$, $CW_C = 63$ and $CW_D = 1023$. Hence the derived expressions of $F_{t_A}(t), F_{t_B}(t), F_{t_C}(t)$, and $F_{t_D}(t)$ are shown in Table 4.5.

Class C: Lower and Upper MAP Bound

In case of the lower MAP bound of class C, we have $CW_A = 3$, $CW_B = 7$, $CW_C = 63$ and $CW_D = 15$. Whereas in the case of the upper MAP bound of class A, we have $CW_A = 7$, $CW_B = 15$, $CW_C = 15$ and $CW_D = 1023$. Hence the expressions of $F_{t_A}(t), F_{t_B}(t), F_{t_C}(t)$, and $F_{t_D}(t)$ are shown in Table 4.6.

Class D: Lower and Upper MAP Bound

In case of the lower MAP bound of class D, we have $CW_A = 3$, $CW_B = 7$, $CW_C = 15$ and $CW_D = 1023$. On the other hand, in case of the upper MAP bound of class A, we have $CW_A = 7$, $CW_B = 15$, $CW_C = 63$ and $CW_D = 15$. Hence the derived expressions of $F_{t_A}(t), F_{t_B}(t), F_{t_C}(t)$, and $F_{t_D}(t)$ are shown in Table 4.7. Based on the system parameters in Table 4.3, the MAP for the typical LTE UE in case of different priority classes with upper and lower bound performance are plotted in Fig. 4.2 and 4.3 versus different LTE eNBs density. Fig. 4.2 corresponds to priority classes A and B whereas Fig. 4.3 corresponds to priority classes C and D. The energy detection threshold used is the same for all

Table 4.6: Class C MAP Timers Distributions

Lower Bound	Upper Bound
$F_{t_A}(t) = \begin{cases} \frac{t-\Delta_A}{CW_A-\Delta_A} & \forall \quad \Delta_C \le t \le \Delta_A + CW_A \\ 1 & \forall \quad \Delta_A + CW_A \le t \le \Delta_C + CW_C \end{cases}$	$F_{t_A}(t) = \begin{cases} \frac{t-\Delta_A}{CW_A-\Delta_A} & \forall \quad \Delta_C \le t \le \Delta_A + CW_A \\ 1 & \forall \quad \Delta_A + CW_A \le t \le \Delta_C + CW_C \end{cases}$
$F_{t_B}(t) = \begin{cases} \frac{t-\Delta_B}{CW_B-\Delta_B} & \forall \quad \Delta_C \le t \le \Delta_B + CW_B \\ 1 & \forall \quad \Delta_B + CW_B \le t \le \Delta_C + CW_C \end{cases}$	$F_{t_B}(t) = \begin{cases} \frac{t-\Delta_B}{CW_B-\Delta_B} & \forall \quad \Delta_C \le t \le \Delta_B + CW_B \\ 1 & \forall \quad \Delta_B + CW_B \le t \le \Delta_C + CW_C \end{cases}$
$F_{t_C}(t) = \frac{t-\Delta_C}{CW_C-\Delta_C} \quad \forall \quad \Delta_C \le t \le \Delta_C + CW_C$	$F_{t_C}(t) = \frac{t-\Delta_C}{CW_C-\Delta_C} \quad \forall \quad \Delta_C \le t \le \Delta_C + CW_C$
$F_{t_D}(t) = \begin{cases} \frac{t-\Delta_D}{CW_D-\Delta_D} & \forall \quad \Delta_D \le t \le \Delta_D + CW_D \\ 1 & \forall \quad \Delta_D + CW_D \le t \le \Delta_C + CW_C \end{cases}$	$F_{t_D}(t) = \frac{t-\Delta_D}{CW_D-\Delta_D} \quad \forall \quad \Delta_D \le t \le \Delta_D + CW_D$

Table 4.7: Class D MAP Timers Distributions

Lower Bound	Upper Bound
$F_{t_A}(t) = 1 \quad \forall \quad \Delta_D \le t \le \Delta_D + CW_D$	$F_{t_A}(t) = \begin{cases} \frac{t-\Delta_A}{CW_A-\Delta_A} & \forall \quad \Delta_D \le t \le \Delta_A + CW_A \\ 1 & \forall \quad \Delta_A + CW_A \le t \le \Delta_D + CW_D \end{cases}$
$F_{t_B}(t) = \begin{cases} \frac{t-\Delta_B}{CW_B-\Delta_B} & \forall \quad \Delta_D \le t \le \Delta_B + CW_B \\ 1 & \forall \quad \Delta_B + CW_B \le t \le \Delta_D + CW_D \end{cases}$	$F_{t_B}(t) = \begin{cases} \frac{t-\Delta_B}{CW_B-\Delta_B} & \forall \quad \Delta_D \le t \le \Delta_B + CW_B \\ 1 & \forall \quad \Delta_B + CW_B \le t \le \Delta_D + CW_D \end{cases}$
$F_{t_C}(t) = \begin{cases} \frac{t-\Delta_C}{CW_C-\Delta_C} & \forall \quad \Delta_D \le t \le \Delta_C + CW_C \\ 1 & \forall \quad \Delta_C + CW_C \le t \le \Delta_D + CW_D \end{cases}$	$F_{t_C}(t) = \frac{t-\Delta_C}{CW_C-\Delta_C} \quad \forall \quad \Delta_D \le t \le \Delta_C + CW_C$
$F_{t_p^D}(t) = \frac{t-\Delta_D}{CW_D-\Delta_D} \quad \forall \quad \Delta_D \le t \le \Delta_D + CW_D$	$F_{t_D}(t) == \frac{t-\Delta_D}{CW_D-\Delta_D} \quad \forall \quad \Delta_D \le t \le \Delta_D + CW_D$

priority classes $\left(T_A = T_B = T_C = T_B = -72 \text{ dBm}\right)$ according to [49].

We start first by analyzing the impact of the coexistence of eNBs with different channel access priority classes on their corresponding medium access probability (MAP). From Fig. 4.2 and 4.3, we can see that eNBs that belong to class A have the highest MAP as compared to other classes such as B, C and D where class D has the lowest MAP. Also, it is interesting to see that the lower bound performance of class A is similar to that of the upper bound performance of class B. Similarly, we can see that the lower performance bound of classes B and C are similar to the upper performance bounds of classes C and D respectively. On the other hand, we can see that the range between the lower performance bound and the upper performance bound is about 50 % for a particular class.

On the other hand, from Fig. 4.2 (a) and (b), we can see that the MAP of an eNB that belongs to class A decreases more when the density of eNBs of class A increase than the case when the density of those of classes B, C,and D increase. Also, this effect is the same for other classes. This can be explained by the fact that an eNB that belongs to class A would have higher chance to access the channel given its random waiting time before accessing the channel is selected from a smaller range of values as compared to other classes e.g. $CW_A \le CW_B$. Furthermore, from Fig. 4.2 (c) and (d) we can see that the MAP of eNBs that belong to class B remains acceptable. Whereas, it is clear from Fig. 4.3 that the MAP of an eNB that belongs to either class C or D is significantly

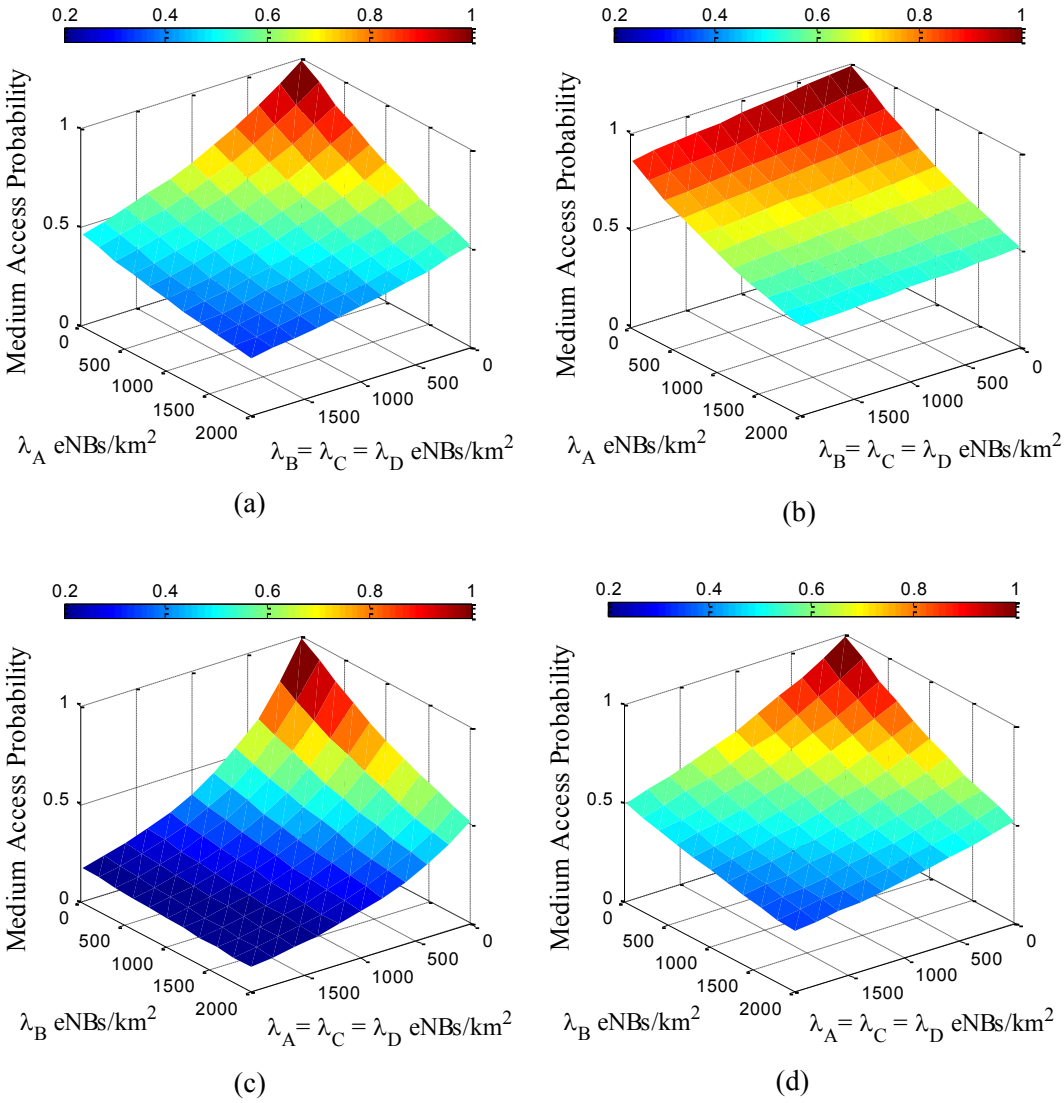

Figure 4.2: MAP For LAA eNB in Case of Channel Access Priority (a) Lower Bound Class A, (b) Upper Bound Class A, (c) Lower Bound Class B, and (d) Upper Bound Class B.

degraded especially when the density of eNBs that belong to class A and B becomes relatively large.

SINR Coverage Probability

The transmitting LAA eNB process for each priority class is a dependent thinning of Φ_A, Φ_B, Φ_C, and Φ_D, whose Laplace functionals are generally unknown in closed form. Thus, in order to approximate the SINR coverage of the typical

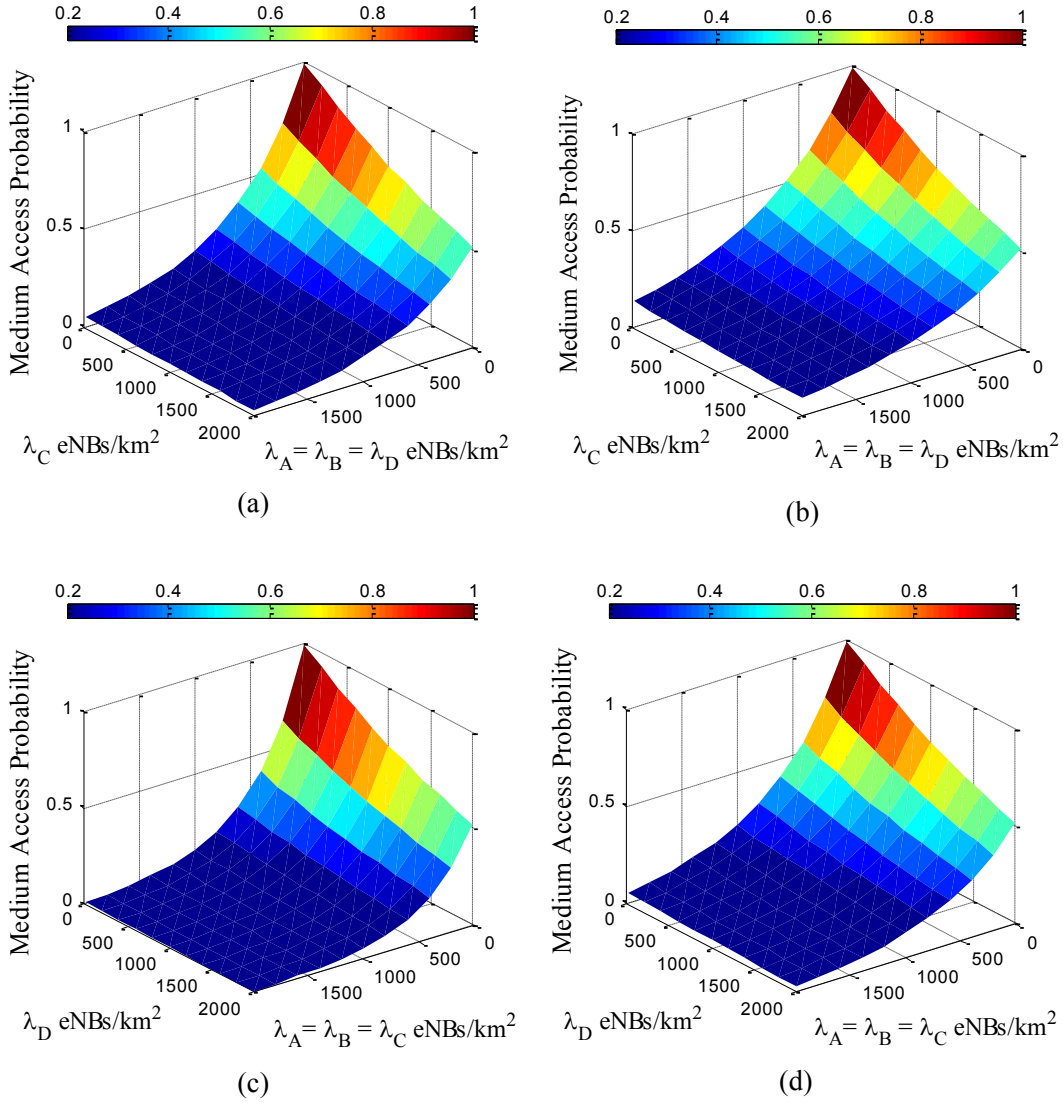

Figure 4.3: MAP For LAA eNB in Case of Channel Access Priority (a) Lower Bound Class C, (b) Upper Bound Class C, (c) Lower Bound Class D, and (d) Upper Bound Class D.

UE, we first derive the conditional MAP for each eNB given the tagged eNB transmits.

SINR Coverage Probability of Typical UE For Channel Priority Class A When deriving the SINR coverage upper and lower performance bounds of class A, the upper bound for class A exists when $CW_A = 3$, $CW_B = 15$, $CW_C = 63$, and $CW_D = 1023$. On the other hand, the lower bound for class A exists when $CW_A = 7$, $CW_B = 7$, $CW_C = 15$, and $CW_D = 15$.

Corollary 1: Conditioned on the fact that the tagged eNB $x_0 = (r_0, 0) \in \Phi_A$ is retained by the MAC protocol, the probability for another eNB $x \in \Phi_A$ to transmit is:

$$\mathbb{P}^{x/x_0}_{MAP} = \frac{H_N\left(x_0, x, \frac{T_A}{P_A}, \Delta_A, CW_A, \Delta_A, CW_A, A, B, C, D\right)}{H_D\left(x_0, x_i, \frac{T_A}{P_A}, A, B, C, D, A\right)} \tag{4.8}$$

Proof For every LTE eNB $x_i \in \Phi_A \cap B^c(0, r_0)$, given that tagged eNB located at $x_0 = (r_0, 0)$, the conditional MAP $P^{x_i}_{\Phi_A}\left[e^A_i = 1 \middle| e^A_0 = 1, x_0 = (r_0, 0)\right]$ is derived as follows:

$$\begin{aligned}
&\mathbb{P}\left[e^A_i = 1 \middle| e^A_0 = 1, x_0 = (r_0, 0), x_i \in \Phi_A\right] \\
&\overset{(a)}{=} \mathbb{P}^{x_i}_{\Phi_A}\left[e^A_i = 1 \middle| e^A_0 = 1, x_0 \in \Phi_A, \Phi_A(B^o(0, r_0)) = 0\right] \\
&\overset{(b)}{=} \frac{\mathbb{P}^{x_i, x_0}_{\Phi_A}\left[\hat{e}^A_i = 1, \hat{e}^A_0 = 1\right]}{\mathbb{P}^{x_i, x_0}_{\Phi_U}\left[\hat{e}^A_0 = 1\right]} \overset{(c)}{=} \frac{\mathbb{E}^{x_i}_{\Phi_A}\left[\hat{e}^A_i \hat{e}^A_0\right]}{\mathbb{E}^{x_i}_{\Phi_A}\left[\hat{e}^A_0\right]}
\end{aligned} \tag{4.9}$$

Where (a) follows from re-writing $x_0 = (r_0, 0)$ as $x_0 \in \Phi_A, \Phi_A(B^o(0, r_0)) = 0$. (b) follows from Bayes rule, and de-conditioning on $\Phi_A(B^o(0, r_0)) = 0$. Step (c) follows from slivnyak′s theorem. The modified access indicators for x_0 and x_i are:

$$\begin{aligned}
\hat{e}^A_i = &\prod_{x_j \in (\Phi_A \cap B^c(0, r_0) + \delta_{x_0}) \setminus \{x_i\}} \left(\mathbb{1}_{t^A_j \geq t^A_i} + \mathbb{1}_{t^A_j < t^A_i} \mathbb{1}_{G^A_{ji} / l(\|x_j - x_i\|) \leq T_A / P_A}\right) \times \prod_{w_k \in \Phi_B} \left(\mathbb{1}_{t^B_k \geq t^A_i} + \mathbb{1}_{t^B_k < t^A_i} \mathbb{1}_{G^{BA}_{ki} / l(\|w_k - x_i\|) \leq T_A / P_B}\right) \\
&\times \prod_{y_n \in \Phi_C} \left(\mathbb{1}_{t^C_n \geq t^A_i} + \mathbb{1}_{t^C_n < t^A_i} \mathbb{1}_{G^{CA}_{ni} / l(\|y_n - x_i\|) \leq T_A / P_C}\right) \times \prod_{z_p \in \Phi_D} \left(\mathbb{1}_{t^D_p \geq t^A_i} + \mathbb{1}_{t^D_p < t^A_i} \mathbb{1}_{G^{DA}_{pi} / l(\|z_p - x_i\|) \leq T_A / P_D}\right) \\
\hat{e}^A_0 = &\prod_{x_j \in \Phi_A \cap B^c(0, r_0)} \left(\mathbb{1}_{t^A_j \geq t^A_0} + \mathbb{1}_{t^A_j < t^A_0} \mathbb{1}_{G^A_{j0} / l(\|x_j - x_0\|) \leq T_A / P_A}\right) \times \prod_{w_k \in \Phi_B} \left(\mathbb{1}_{t^B_k \geq t^A_0} + \mathbb{1}_{t^B_k < t^A_0} \mathbb{1}_{G^{BA}_{k0} / l(\|w_k - x_0\|) \leq T_A / P_B}\right) \\
&\times \prod_{y_n \in \Phi_C} \left(\mathbb{1}_{t^C_n \geq t^A_0} + \mathbb{1}_{t^C_n < t^A_0} \mathbb{1}_{G^{CA}_{n0} / l(\|y_n - x_0\|) \leq T_A / P_C}\right) \times \prod_{z_p \in \Phi_D} \left(\mathbb{1}_{t^D_p \geq t^A_0} + \mathbb{1}_{t^D_p < t^A_0} \mathbb{1}_{G^{DA}_{p0} / l(\|z_p - x_0\|) \leq T_A / P_D}\right)
\end{aligned} \tag{4.10}$$

Therefore, the denominator $E^{x_i}_{\Phi_A}[\hat{e}^A_0]$ is given by:

$$\begin{aligned}
&\mathbb{E}^{x_i}_{\Phi_A}\Bigg[\prod_{x_j \in \Phi_A \cap B^c(0, r_0)} \left(\mathbb{1}_{t^A_j \geq t^A_0} + \mathbb{1}_{t^A_j < t^A_0} \mathbb{1}_{G^A_{j0} / l(\|x_j - x_0\|) \leq T_A / P_A}\right) \times \prod_{w_k \in \Phi_B} \left(\mathbb{1}_{t^B_k \geq t^A_0} + \mathbb{1}_{t^B_k < t^A_0} \mathbb{1}_{G^{BA}_{k0} / l(\|w_k - x_0\|) \leq T_A / P_B}\right) \\
&\times \prod_{y_n \in \Phi_C} \left(\mathbb{1}_{t^C_n \geq t^A_0} + \mathbb{1}_{t^C_n < t^A_0} \mathbb{1}_{G^{CA}_{n0} / l(\|y_n - x_0\|) \leq T_A / P_C}\right) \times \prod_{z_p \in \Phi_D} \left(\mathbb{1}_{t^D_p \geq t^A_0} + \mathbb{1}_{t^D_p < t^A_0} \mathbb{1}_{G^{DA}_{p0} / l(\|z_p - x_0\|) \leq T_A / P_D}\right)\Bigg] \\
&\overset{(a)}{=} \mathbb{E}\Bigg[\prod_{x_j \in \Phi_A \cap B^c(0, r_0) + \delta_{x_i}} \left(\mathbb{1}_{t^A_j \geq t^A_0} + \mathbb{1}_{t^A_j < t^A_0} \mathbb{1}_{G^A_{j0} / l(\|x_j - x_0\|) \leq T_A / P_A}\right) \times \prod_{w_k \in \Phi_B} \left(\mathbb{1}_{t^B_k \geq t^A_0} + \mathbb{1}_{t^B_k < t^A_0} \mathbb{1}_{G^{BA}_{k0} / l(\|w_k - x_0\|) \leq T_A / P_B}\right) \\
&\times \prod_{y_n \in \Phi_C} \left(\mathbb{1}_{t^C_n \geq t^A_0} + \mathbb{1}_{t^C_n < t^A_0} \mathbb{1}_{G^{CA}_{n0} / l(\|y_n - x_0\|) \leq T_A / P_C}\right) \times \prod_{z_p \in \Phi_D} \left(\mathbb{1}_{t^D_p \geq t^A_0} + \mathbb{1}_{t^D_p < t^A_0} \mathbb{1}_{G^{DA}_{p0} / l(\|z_p - x_0\|) \leq T_A / P_D}\right) \Big/ t^A_0 = t\Bigg]
\end{aligned}$$

$$\overset{(b)}{=}\Big(1-F_{t_A}(t)\exp\Big(-\mu\frac{T_A}{P_A}l(\|x_i-x_0\|)\Big)\Big)\times\exp\Big[-\lambda_A\int_{\mathbb{R}^2\setminus B(0,r_0)}F_{t_A}(t)\exp\Big(-\mu\frac{T_A}{P_A}l(\|x_j-x_0\|)\Big)\mathrm{d}x\Big]$$
$$\times\exp\Big[-\lambda_B\int_{\mathbb{R}^2}F_{t_B}(t)\exp\Big(-\mu\frac{T_A}{P_B}l(\|w_k-x_0\|)\Big)\mathrm{d}w\Big]\quad\times\exp\Big[-\lambda_C\int_{\mathbb{R}^2}F_{t_C}(t)\exp\Big(-\mu\frac{T_A}{P_C}l(\|y_n-x_0\|)\Big)\mathrm{d}y\Big]$$
$$\times\exp\Big[-\lambda_D\int_{\mathbb{R}^2}F_{t_D}(t)\exp\Big(-\mu\frac{T_A}{P_D}l(\|z_p-x_0\|)\Big)\mathrm{d}z\Big]$$
$$=\frac{1}{CW_A}\int_{\Delta_A}^{CW_A+\Delta_A}\Big(1-F_{t_A}(t)\exp\Big(-\mu\frac{T_A}{P_A}l(\|x_i-x_0\|)\Big)\Big)\times$$
$$\exp\Big[-F_{t_A}(t)N_A(x_0,T_A,r_0)-F_{t_B}(t)N_B(x_0,T_A)-F_{t_C}(t)N_C(x_0,T_A)-F_{t_D}(t)N_D(x_0,T_A)\Big]\mathrm{d}t$$
$$=H_D\Big(x_0,x_i,T_A/P_A,A,B,C,D,A\Big)$$

Where (a) follows from slivnyaks theorem. (b) follows from setting $t_0^A=t$ and from the P.G.FL of PPP. Next, the numerator $\mathbb{E}^{x_i}_{\Phi_A}(\hat{e}_i^A\hat{e}_0^A)$ can be derived in a similar manner as follows:

$$\mathbb{E}^{x_i}_{\Phi_A}\big[\hat{e}_i^A\hat{e}_0^A\big]=\mathbb{E}\Big[\prod_{x_j\in\Phi_A\cap B^c(0,r_0)}\Big(\mathbb{1}_{t_j^A\geq t_i^A}+\mathbb{1}_{t_j^A<t_i^A}\mathbb{1}_{G_{ji}^A/l(\|x_j-x_i\|)\leq T_A/P_A}\Big)\Big(\mathbb{1}_{t_j^A\geq t_0^A}+\mathbb{1}_{t_j^A<t_0^A}\mathbb{1}_{G_{j0}^A/l(\|x_j-x_0\|)\leq T_A/P_A}\Big)$$
$$\times\prod_{w_k\in\Phi_B}\Big(\mathbb{1}_{t_k^B\geq t_i^A}+\mathbb{1}_{t_k^B<t_i^A}\mathbb{1}_{G_{ki}^{BA}/l(\|w_k-x_i\|)\leq T_A/P_B}\Big)\Big(\mathbb{1}_{t_k^B\geq t_0^A}+\mathbb{1}_{t_k^B<t_0^A}\mathbb{1}_{G_{k0}^{BA}/l(\|w_k-x_0\|)\leq T_A/P_B}\Big)$$
$$\times\prod_{y_n\in\Phi_C}\Big(\mathbb{1}_{t_n^C\geq t_i^A}+\mathbb{1}_{t_n^C<t_i^A}\mathbb{1}_{G_{ni}^{CA}/l(\|y_n-x_i\|)\leq T_A/P_C}\Big)\Big(\mathbb{1}_{t_n^C\geq t_0^A}+\mathbb{1}_{t_n^C<t_0^A}\mathbb{1}_{G_{n0}^{CA}/l(\|y_n-x_0\|)\leq T_A/P_C}\Big)$$
$$\times\prod_{z_p\in\Phi_D}\Big(\mathbb{1}_{t_p^D\geq t_i^A}+\mathbb{1}_{t_p^D<t_i^A}\mathbb{1}_{G_{pi}^{DA}/l(\|z_p-x_i\|)\leq T_A/P_D}\Big)\Big(\mathbb{1}_{t_p^D\geq t_0^A}+\mathbb{1}_{t_p^D<t_0^A}\mathbb{1}_{G_{p0}^{DA}/l(\|z_p-x_0\|)\leq T_A/P_D}\Big)$$
$$\times\Big(\mathbb{1}_{G_{i0}^A/l(\|x_i-x_0\|)\leq T_A/P_A}\Big)\Big/t_0^A=t,t_i^A=t'\Big]$$
$$=\frac{1}{(CW_A)(CW_A)}\int_{\Delta_A}^{CW_A+\Delta_A}\int_{\Delta_A}^{CW_A+\Delta_A}\Big(1-\exp\Big(-\mu\frac{T_A}{P_A}l(\|x_i-x_0\|)\Big)\Big)\times$$
$$\exp\Big(-F_{t_j^A}(t')N_A(x_i,T_A,r_0)-F_{t_k^B}(t')N_B(x_i,T_A)-F_{t_n^C}(t')N_C(x_i,T_A)-F_{t_p^D}(t')N_D(x_i,T_A)$$

$$-F_{t_j^A}(t)N_A(x_0,T_A,r_0)-F_{t_k^B}(t)N_B(x_0,T_A)-F_{t_n^C}(t)N_C(x_0,T_A)-F_{t_p^D}(t)N_D(x_0,T_A)$$
$$+F_{t_j^A}(t)Q_A(x_i,x_0)+F_{t_k^B}(t)Q_B(x_i-x_0)+F_{t_n^C}(t)Q_C(x_i-x_0)+F_{t_p^D}(t)Q_D(x_i-x_0)\Big)\mathrm{d}t\mathrm{d}t'$$
$$=H_N\Big(x-x_0,\frac{T_A}{P_A},\Delta_A,CW_A,\Delta_A,CW_A,A,B,C,D\Big)$$

Where (a) follows from slivnyaks theorem and (b) follows from the P.G.FL of PPP. ■

Note that t is the timer of node x_0 and t' is the timer of node x where the resulting distributions of timers are shown in Table 4.8 and which will be used in computing $\mathbb{P}^{x/x_0}_{MAP}$. The following corollaries throughout the chapter can be proved in a similar manner to Corollary 1, thus we omit the detailed proof and

Table 4.8: Distributions For Timer t (or t') in Corollary 1

Lower Bound	Upper Bound
$F_{t_j^A}(t) = \frac{t-\Delta_A}{CW_A-\Delta_A} \quad \forall \quad \Delta_A \leq t \leq \Delta_A + CW_A$	$F_{t_j^A}(t) = \frac{t-\Delta_A}{CW_A-\Delta_A} \quad \forall \quad \Delta_A \leq t \leq \Delta_A + CW_A$
$F_{t_k^B}(t) = \frac{t-\Delta_B}{CW_B-\Delta_B} \quad \forall \quad \Delta_A \leq t \leq \Delta_A + CW_A$	$F_{t_k^B}(t) = \frac{t-\Delta_B}{CW_B-\Delta_B} \quad \forall \quad \Delta_A \leq t \leq \Delta_A + CW_A$
$F_{t_n^C}(t) = \frac{t-\Delta_C}{CW_C-\Delta_C} \quad \forall \quad \Delta_C \leq t \leq \Delta_A + CW_A$	$F_{t_n^C}(t) = \frac{t-\Delta_C}{CW_C-\Delta_C} \quad \forall \quad \Delta_C \leq t \leq \Delta_A + CW_A$
$F_{t_p^D}(t) = \frac{t-\Delta_D}{CW_D-\Delta_D} \quad \forall \quad \Delta_D \leq t \leq \Delta_A + CW_A$	$F_{t_p^D}(t) = 0 \quad \forall \quad \Delta_A \leq t \leq \Delta_A + CW_A$

Table 4.9: Distributions For Timer t' in Corollary 2

Lower Bound	Upper Bound
$F_{t_j^A}(t') = \frac{t'-\Delta_A}{CW_A-\Delta_A} \quad \forall \quad \Delta_A \leq t' \leq \Delta_A + CW_A$	$F_{t_j^A}(t') = \begin{cases} \frac{t'-\Delta_A}{CW_A-\Delta_A} \quad \forall \quad \Delta_B \leq t' \leq \Delta_A + CW_A \\ 1 \quad \forall \quad \Delta_A + CW_A \leq t' \leq \Delta_B + CW_B \end{cases}$
$F_{t_k^B}(t') = \frac{t'-\Delta_B}{CW_B-\Delta_B} \quad \forall \quad \Delta_A \leq t' \leq \Delta_B + CW_B$	$F_{t_k^B}(t') = \frac{t'-\Delta_B}{CW_B-\Delta_B} \quad \forall \quad \Delta_B \leq t' \leq \Delta_B + CW_B$
$F_{t_n^C}(t') = \frac{t'-\Delta_C}{CW_C-\Delta_C} \quad \forall \quad \Delta_C \leq t' \leq \Delta_B + CW_B$	$F_{t_n^C}(t') = \frac{t'-\Delta_C}{CW_C-\Delta_C} \quad \forall \quad \Delta_C \leq t' \leq \Delta_B + CW_B$
$F_{t_p^D}(t') = \frac{t'-\Delta_D}{CW_D-\Delta_D} \quad \forall \quad \Delta_D \leq t' \leq \Delta_B + CW_B$	$F_{t_n^D}(t') = \frac{t'-\Delta_D}{CW_D-\Delta_D} \quad \forall \quad \Delta_D \leq t' \leq \Delta_B + CW_B$

we concentrate on deriving the timer distributions in each case. In addition, in case of class A, timer t will always correspond to node x_0 and hence its resulting distributions used to compute the conditional MAP in corollaries 2, 3, and 4 can be found in Table 4.8.

Corollary 2: Conditioned on the fact that the tagged LAA eNB $x_0 = (r_0, 0)$ is retained by LBT mechanism, the probability for another LAA eNB $w \in \Phi_B$ to transmit is given by:

$$\mathbb{P}_{MAP}^{w/x_0} = \frac{H_N\left(x_0, w, \frac{T_A}{P_B}, \Delta_A, CW_A, \Delta_B, CW_B, A, B, C, D\right)}{H_D\left(x_0, w, \frac{T_A}{P_B}, A, B, C, D, B\right)} \tag{4.11}$$

Where t' is the timer of node w with the resulting distributions shown in Table 4.9 and which will be used in computing $\mathbb{P}_{MAP}^{w/x_0}$.

Corollary 3: Conditioned on the fact that the tagged LAA eNB $x_0 = (r_0, 0)$ is retained by LBT mechanism, the probability for another LAA eNB $y \in \Phi_C$ to transmit is given by:

$$\mathbb{P}_{MAP}^{y/x_0} = \frac{H_N\left(x_0, y, \frac{T_A}{P_C}, \Delta_A, CW_A, \Delta_C, CW_C, A, B, C, D\right)}{H_D\left(x_0, y, \frac{T_A}{P_C}, A, B, C, D, C\right)} \tag{4.12}$$

Where t' is the timer of node y with the resulting distributions shown in Table

Table 4.10: Distributions For Timer t' in Corollary 3

Lower Bound	Upper Bound
$F_{t_j^A}(t') = \begin{cases} \frac{t'-\Delta_A}{CW_A-\Delta_A} & \forall \quad \Delta_C \le t' \le \Delta_A + CW_A \\ 1 \quad \forall \quad \Delta_A + CW_A \le t' \le \Delta_C + CW_C \end{cases}$	$F_{t_j^A}(t') = \begin{cases} \frac{t'-\Delta_A}{CW_A-\Delta_A} & \forall \quad \Delta_C \le t' \le \Delta_A + CW_A \\ 1 \quad \forall \quad \Delta_A + CW_A \le t' \le \Delta_C + CW_C \end{cases}$
$F_{t_k^B}(t') = \begin{cases} \frac{t'-\Delta_B}{CW_B-\Delta_B} & \forall \quad \Delta_C \le t' \le \Delta_B + CW_B \\ 1 \quad \forall \quad \Delta_B + CW_B \le t' \le \Delta_C + CW_C \end{cases}$	$F_{t_k^B}(t') = \begin{cases} \frac{t'-\Delta_B}{CW_B-\Delta_B} & \forall \quad \Delta_C \le t' \le \Delta_B + CW_B \\ 1 \quad \forall \quad \Delta_B + CW_B \le t' \le \Delta_C + CW_C \end{cases}$
$F_{t_n^C}(t') = \frac{t'-\Delta_C}{CW_C-\Delta_C} \quad \forall \quad \Delta_C \le t' \le \Delta_C + CW_C$	$F_{t_n^C}(t') = \frac{t'-\Delta_C}{CW_C-\Delta_C} \quad \forall \quad \Delta_C \le t' \le \Delta_C + CW_C$
$F_{t_p^D}(t') = \frac{t'-\Delta_D}{CW_D-\Delta_D} \quad \forall \quad \Delta_D \le t' \le \Delta_C + CW_C$	$F_{t_n^D}(t') = \frac{t'-\Delta_D}{CW_D-\Delta_D} \quad \forall \quad \Delta_D \le t' \le \Delta_C + CW_C$

4.10 and which will be used in computing $\mathbb{P}_{MAP}^{y/x_0}$.

Corollary 4: Conditioned on the fact that the tagged LAA eNB $x_0 = (r_0, 0)$ is retained by LBT mechanism, the probability for another LAA eNB $z \in \Phi_D$ to transmit is given by:

$$\mathbb{P}_{MAP}^{z/x_0} = \frac{H_N\left(x_0, z, \frac{T_A}{P_D}, \Delta_A, CW_A, \Delta_D, CW_D, A, B, C, D\right)}{H_D\left(x_0, z, \frac{T_A}{P_D}, A, B, C, D, D\right)} \tag{4.13}$$

Where t' is the timer of node z with the resulting distributions shown in Table 4.11 and which will be used in computing $\mathbb{P}_{MAP}^{z/x_0}$.

Based on Corollaries 1, 2, 3, and 4, the SINR coverage of the typical UE for priority class A is obtained in Lemma 2 as follows:

Lemma 2: Given the tagged LAA eNB is located at $x_0 = (r_0, 0)$, the SINR coverage probability of the typical UE with SINR threshold T for priority class A is approximated as:

$$\mathbb{P}_{SINR}^{A}(T, \lambda_A, \lambda_B, \lambda_C, \lambda_D) \approx \int_0^{\infty} \exp\Big(-\int_{\mathbb{R}^2\setminus B(0,r_0)} \frac{Tl(r_0)\lambda_A \mathbb{P}_{MAP}^{x/x_0}}{l(\|x\|)+Tl(r_0)}\mathrm{d}x\Big)\exp\Big(-\int_{\mathbb{R}^2} \frac{Tl(r_0)\lambda_B \mathbb{P}_{MAP}^{w/x_0}}{\frac{P_A}{P_B}l(\|w\|)+Tl(r_0)}\mathrm{d}w\Big)$$
$$\times\exp\Big(-\int_{\mathbb{R}^2} \frac{Tl(r_0)\lambda_C \mathbb{P}_{MAP}^{y/x_0}}{\frac{P_A}{P_C}l(\|y\|)+Tl(r_0)}\mathrm{d}y\Big) \times \exp\Big(-\int_{\mathbb{R}^2} \frac{Tl(r_0)\lambda_D \mathbb{P}_{MAP}^{z/x_0}}{\frac{P_A}{P_D}l(\|z\|)+Tl(r_0)}\mathrm{d}z\Big) \times \exp\left(-\mu Tl(r_0)\frac{\sigma_N^2}{P_A}\right) \times f_{\|x_0\|}(r_0)\mathrm{d}r_0 \tag{4.14}$$

Proof The conditional SINR coverage of the typical Wi-Fi AP is derived as follows:

$$\mathbb{P}[SINR_0^A > T | x_0 = (r_0, 0), e_0^A = 1]$$
$$= \mathbb{P}\Bigg[\frac{P_A G_{0,0}^{AA'}/l(\|x_0\|)}{\sum\limits_{x_j\in\Phi_A\setminus\{x_0\}} P_A G_{j,0}^{AA'} e_j^A/l(\|x_j\|) + \sum\limits_{w_k\in\Phi_B} P_B G_{k,0}^{BA'} e_k^B/l(\|w_k\|) + \sum\limits_{y_n\in\Phi_C} P_C G_{n,0}^{CA'} e_n^C/l(\|y_n\|) + \sum\limits_{z_p\in\Phi_D} P_D G_{p,0}^{DA'} e_p^D/l(\|z_p\|) + \sigma_N^2}$$
$$> T \Big| x_0 = (r_0, 0), e_0^A = 1\Bigg]$$

Table 4.11: Distributions For Timer t' in Corollary 4

Lower Bound	Upper Bound
$F_{t_j^A}(t') = \begin{cases} \frac{t'-\Delta_A}{CW_A-\Delta_A} \quad \forall \quad \Delta_C \le t' \le \Delta_A + CW_A \\ 1 \quad \forall \quad \Delta_A + CW_A \le t' \le \Delta_D + CW_D \end{cases}$	$F_{t_j^A}(t') = 1 \quad \forall \quad \Delta_D \le t' \le \Delta_D + CW_D$
$F_{t_k^B}(t') = \begin{cases} \frac{t'-\Delta_B}{CW_B-\Delta_B} \quad \forall \quad \Delta_D \le t' \le \Delta_B + CW_B \\ 1 \quad \forall \quad \Delta_B + CW_B \le t' \le \Delta_D + CW_D \end{cases}$	$F_{t_k^B}(t') = \begin{cases} \frac{t'-\Delta_B}{CW_B-\Delta_B} \quad \forall \quad \Delta_D \le t' \le \Delta_B + CW_B \\ 1 \quad \forall \quad \Delta_B + CW_B \le t' \le \Delta_D + CW_D \end{cases}$
$F_{t_n^C}(t') = \begin{cases} \frac{t'-\Delta_C}{CW_C-\Delta_C} \quad \forall \quad \Delta_D \le t' \le \Delta_C + CW_C \\ 1 \quad \forall \quad \Delta_C + CW_C \le t' \le \Delta_D + CW_D \end{cases}$	$F_{t_n^C}(t') = \begin{cases} \frac{t'-\Delta_C}{CW_C-\Delta_C} \quad \forall \quad \Delta_D \le t' \le \Delta_C + CW_C \\ 1 \quad \forall \quad \Delta_C + CW_C \le t' \le \Delta_D + CW_D \end{cases}$
$F_{t_p^D}(t') = \frac{t'-\Delta_D}{CW_D-\Delta_D} \quad \forall \quad \Delta_D \le t' \le \Delta_D + CW_D$	$F_{t_n^D}(t') = \frac{t'-\Delta_D}{CW_D-\Delta_D} \quad \forall \quad \Delta_D \le t' \le \Delta_D + CW_D$

$$\overset{(a)}{=} \mathbb{P}\Bigg[\frac{P_A G_{0,0}^{AA'}/l(\|x_0\|)}{\sum\limits_{x_j \in \Phi_A \setminus \{x_0\}} P_A G_{j,0}^{AA'} e_j^A/l(\|x_j\|) + \sum\limits_{w_k \in \Phi_B} P_B G_{k,0}^{BA'} e_k^B/l(\|w_k\|) + \sum\limits_{y_n \in \Phi_C} P_C G_{n,0}^{CA'} e_n^C/l(\|y_n\|) + \sum\limits_{z_p \in \Phi_D} P_D G_{p,0}^{DA'} e_p^D/l(\|z_p\|) + \sigma_N^2} > T | x_0 \in \Phi_A, \Phi_A(B^o(0,r_0)) = 0, e_0^A = 1 \Bigg]$$

$$\overset{(b)}{=} \mathbb{P}\Bigg[\frac{P_A G_{0,0}^{AA'}/l(\|x_0\|)}{\sum\limits_{x_j \in \Phi_A \cap B^c(0,r_0)} P_A G_{j,0}^{AA'} \hat{e}_j^A/l(\|x_j\|) + \sum\limits_{w_k \in \Phi_B} P_B G_{k,0}^{BA'} \hat{e}_k^B/l(\|w_k\|) + \sum\limits_{y_n \in \Phi_C} P_C G_{n,0}^{CA'} \hat{e}_n^C/l(\|y_n\|) + \sum\limits_{z_p \in \Phi_D} P_D G_{p,0}^{DA'} \hat{e}_p^D/l(\|z_p\|) + \sigma_N^2} > T \Big| \hat{e}_0^A = 1 \Bigg]$$

$$\begin{aligned} \overset{(c)}{\approx} & \mathbb{E}\Big[\exp\Big(-\mu T l(\|r_0\|)\frac{\sigma_N^2}{P_A}\Big)\Big] \times \mathbb{E}\Big[\exp\Big(-\mu T l(\|r_0\|) \sum_{x_j \in \Phi_A \cap B^c(0,r_0)} G_{j,0}^{AA'} \hat{e}_j^A/l(\|x_j\|)\Big)\Big| \hat{e}_0^A = 1\Big] \\ & \times \mathbb{E}\Big[\exp\Big(-\mu T l(\|r_0\|) \sum_{w_k \in \Phi_B} \frac{P_B}{P_A} G_{k,0}^{BA'} \hat{e}_k^B/l(\|w_k\|)\Big)\Big| \hat{e}_0^A = 1\Big] \times \mathbb{E}\Big[\exp\Big(-\mu T l(\|r_0\|) \sum_{y_n \in \Phi_C} \frac{P_C}{P_A} G_{n,0}^{CA'} \hat{e}_n^C/l(\|y_n\|)\Big)\Big| \hat{e}_0^A = 1\Big] \\ & \times \mathbb{E}\Big[\exp\Big(-\mu T l(\|r_0\|) \sum_{z_p \in \Phi_D} \frac{P_D}{P_A} G_{m,0}^{DA'}/l(\|z_p\|)\Big)\Big| \hat{e}_0^A = 1\Big] \end{aligned}$$

Where (a) follows from Bayes rule by re-writing $x_0 = (r_0, 0)$ as $x_0 \in \Phi_A$, $\Phi_A(B^o(0,r_0)) = 0$. Step (b) follows from slivnyak′s theorem and deconditioning on $\Phi_A(B^o(0,r_0)) = 0$. The modified medium access indicator for $x_i \in \Phi_A \cap B^c(0,r_0)$ is provided in (4.10) and the conditional probabilities that eNB $x \in \Phi_A \cap B^c(0,r_0)$, eNB $w \in \Phi_B$, eNB $y \in \Phi_C$, and eNB $z \in \Phi_D$ transmit are derived in corollaries 1, 2, 3 and 4 respectively. Step (c) follows from the fact that channels are Rayleigh fading channels and from the assumption that interference from Φ_A, Φ_B, Φ_C, and Φ_D is independent. Finally (4.14) can be derived by approximating the law of interfering LAA eNBs as a non-homogeneous PPP with intensity $\lambda_A \mathbb{P}_{MAP}^{x/x_0}/\ \lambda_B \mathbb{P}_{MAP}^{w/x_0}/\ \lambda_C \mathbb{P}_{MAP}^{y/x_0}/\ \lambda_D \mathbb{P}_{MAP}^{z/x_0}$ and by deconditioning on r_0. Note that the first term in (4.14) results from the noise, whereas other 4 terms result from the interference of eNBs from priority classes A, B, C, and D respectively. ■

Table 4.12: Distributions For Timer t in Corollary 5

Lower Bound	Upper Bound
$F_{t_j^A}(t) = \begin{cases} \frac{t-\Delta_A}{CW_A-\Delta_A} & \forall \quad \Delta_A \leq t \leq \Delta_A + CW_A \\ 1 \quad \forall \quad \Delta_A + CW_A \leq t \leq \Delta_B + CW_B \end{cases}$	$F_{t_j^A}(t) = \frac{t-\Delta_A}{CW_A-\Delta_A} \quad \forall \quad \Delta_A \leq t \leq \Delta_A + CW_A$
$F_{t_k^B}(t) = \frac{t-\Delta_B}{CW_B-\Delta_B} \quad \forall \quad \Delta_B \leq t \leq \Delta_B + CW_B$	$F_{t_k^B}(t) = \frac{t-\Delta_B}{CW_B-\Delta_B} \quad \forall \quad \Delta_B \leq t \leq \Delta_B + CW_B$
$F_{t_n^C}(t) = \frac{t-\Delta_C}{CW_C-\Delta_C} \quad \forall \quad \Delta_C \leq t \leq \Delta_B + CW_B$	$F_{t_n^C}(t) = \frac{t-\Delta_C}{CW_C-\Delta_C} \quad \forall \quad \Delta_C \leq t \leq \Delta_B + CW_B$
$F_{t_p^D}(t) = \frac{t-\Delta_D}{CW_D-\Delta_D} \quad \forall \quad \Delta_D \leq t \leq \Delta_B + CW_B$	$F_{t_n^D}(t) = \frac{t-\Delta_D}{CW_D-\Delta_D} \quad \forall \quad \Delta_D \leq t \leq \Delta_B + CW_B$

Table 4.13: Distributions For Timer t' in Corollary 5

Lower Bound	Upper Bound
$F_{t_j^A}(t') = \frac{t'-\Delta_A}{CW_A-\Delta_A} \quad \forall \quad \Delta_A \leq t' \leq \Delta_A + CW_A$	$F_{t_j^A}(t') = \frac{t'-\Delta_A}{CW_A-\Delta_A} \quad \forall \quad \Delta_A \leq t' \leq \Delta_A + CW_A$
$F_{t_k^B}(t') = \frac{t'-\Delta_B}{CW_B-\Delta_B} \quad \forall \quad \Delta_B \leq t' \leq \Delta_A + CW_A$	$F_{t_k^B}(t') = \frac{t'-\Delta_B}{CW_B-\Delta_B} \quad \forall \quad \Delta_B \leq t' \leq \Delta_A + CW_A$
$F_{t_n^C}(t') = \frac{t'-\Delta_C}{CW_C-\Delta_C} \quad \forall \quad \Delta_C \leq t' \leq \Delta_A + CW_A$	$F_{t_n^C}(t') = \frac{t'-\Delta_C}{CW_C-\Delta_C} \quad \forall \quad \Delta_C \leq t' \leq \Delta_A + CW_A$
$F_{t_p^D}(t') = 0 \quad \forall \quad \Delta_A \leq t' \leq \Delta_A + CW_A$	$F_{t_p^D}(t') = \frac{t'-\Delta_D}{CW_D-\Delta_D} \quad \forall \quad \Delta_D \leq t' \leq \Delta_A + CW_A$

SINR Coverage Probability of Typical UE For Channel Priority Class B When deriving the SINR coverage upper and lower performance bounds of class B, the upper bound for class B exists when $CW_A = 7$, $CW_B = 7$, $CW_C = 63$, and $CW_D = 1023$. On the other hand, the lower bound for class B exists when $CW_A = 3$, $CW_B = 15$, $CW_C = 15$, and $CW_D = 15$.

Corollary 5: Conditioned on the fact that the tagged LAA eNB $w_0 = (r_0, 0) \in \Phi_B$ is retained by the MAC protocol, the probability for another eNB $x \in \Phi_A$ to transmit is:

$$\mathbb{P}_{MAP}^{x/w_0} = \frac{H_N\left(w_0, x, \frac{T_B}{P_A}, \Delta_B, CW_B, \Delta_A, CW_A, B, A, C, D\right)}{H_D\left(w_0, x, \frac{T_B}{P_A}, B, A, C, D, A\right)} \tag{4.15}$$

Where t is the timer of node w_0 and t' is the timer of node x. The resulting distributions of the timers t and t' are shown in Tables 4.12 and 4.13 respectively and which will be used in computing $\mathbb{P}_{MAP}^{x/w_0}$.

Corollary 6: Conditioned on the fact that the tagged LAA eNB $w_0 = (r_0, 0) \in \Phi_B$ is retained by LBT mechanism, the probability for another LAA eNB $w \in \Phi_B$ to transmit is given by:

Table 4.14: Distributions For Timer t' in Corollary 7

Lower Bound	Upper Bound
$F_{t_j^A}(t') = \begin{cases} \frac{t'-\Delta_A}{CW_A-\Delta_A} \quad \forall \quad \Delta_C \leq t' \leq \Delta_A + CW_A \\ 1 \quad \forall \quad \Delta_A + CW_A \leq t' \leq \Delta_C + CW_C \end{cases}$	$F_{t_j^A}(t') = \begin{cases} \frac{t'-\Delta_A}{CW_A-\Delta_A} \quad \forall \quad \Delta_C \leq t' \leq \Delta_A + CW_A \\ 1 \quad \forall \quad \Delta_A + CW_A \leq t' \leq \Delta_C + CW_C \end{cases}$
$F_{t_k^B}(t') = \begin{cases} \frac{t'-\Delta_B}{CW_B-\Delta_B} \quad \forall \quad \Delta_C \leq t' \leq \Delta_B + CW_B \\ 1 \quad \forall \quad \Delta_B + CW_B \leq t' \leq \Delta_C + CW_C \end{cases}$	$F_{t_k^B}(t') = \begin{cases} \frac{t'-\Delta_B}{CW_B-\Delta_B} \quad \forall \quad \Delta_C \leq t' \leq \Delta_B + CW_B \\ 1 \quad \forall \quad \Delta_B + CW_B \leq t' \leq \Delta_C + CW_C \end{cases}$
$F_{t_n^C}(t') = \frac{t'-\Delta_C}{CW_C-\Delta_C} \quad \forall \quad \Delta_C \leq t' \leq \Delta_C + CW_C$	$F_{t_n^C}(t') = \frac{t'-\Delta_C}{CW_C-\Delta_C} \quad \forall \quad \Delta_C \leq t' \leq \Delta_C + CW_C$
$F_{t_p^D}(t') = \frac{t'-\Delta_D}{CW_D-\Delta_D} \quad \forall \quad \Delta_D \leq t' \leq \Delta_C + CW_C$	$F_{t_n^D}(t') = \frac{t'-\Delta_D}{CW_D-\Delta_D} \quad \forall \quad \Delta_D \leq t' \leq \Delta_C + CW_C$

$$\mathbb{P}_{MAP}^{w/w_0} = \frac{H_N\left(w_0, w, \frac{T_B}{P_B}, \Delta_B, CW_B, \Delta_B, CW_B, B, A, C, D\right)}{H_D\left(w_0, w, \frac{T_B}{P_B}, B, A, C, D, B\right)} \tag{4.16}$$

Where t is the timer of node w_0 and t' is the timer of node w. The resulting distributions of the timers t and t' are the same as those in Table 4.12 and which will be used in computing $\mathbb{P}_{MAP}^{w/w_0}$.

Corollary 7: Conditioned on the fact that the tagged LAA eNB $w_0 = (r_0, 0) \in \Phi_B$ is retained by LBT mechanism, the probability for another LAA eNB $y \in \Phi_C$ to transmit is given by:

$$\mathbb{P}_{MAP}^{y/w_0} = \frac{H_N\left(w_0, y, \frac{T_B}{P_C}, \Delta_B, CW_B, \Delta_C, CW_C, B, A, C, D\right)}{H_D\left(w_0, y, \frac{T_B}{P_C}, B, A, C, D, C\right)} \tag{4.17}$$

Where t is the timer of node w_0 and t' is the timer of node y. The resulting distributions of the timers t and t' are shown in Tables 4.12 and 4.14 respectively and which will be used in computing $\mathbb{P}_{MAP}^{y/w_0}$.

Corollary 8: Conditioned on the fact that the tagged LAA eNB $w_0 = (r_0, 0) \in \Phi_B$ is retained by LBT mechanism, the probability for another LAA eNB $z \in \Phi_D$ to transmit is given by:

$$\mathbb{P}_{MAP}^{z/w_0} = \frac{H_N\left(w_0, z, \frac{T_B}{P_D}, \Delta_B, CW_B, \Delta_D, CW_D, B, A, C, D\right)}{H_D\left(w_0, z, \frac{T_B}{P_D}, B, A, C, D, D\right)} \tag{4.18}$$

Where t' is the timer of node z with the resulting distributions shown in Table 4.15 and which will be used in computing $\mathbb{P}_{MAP}^{z/w_0}$.

Based on Corollaries 5, 6, 7, and 8, the SINR coverage of the typical UE for

Table 4.15: Distributions For Timer t' in Corollary 8

Lower Bound	Upper Bound
$F_{t_j^A}(t') = 1 \quad \forall \quad \Delta_D \leq t' \leq \Delta_D + CW_D$	$F_{t_j^A}(t') = \begin{cases} \frac{t' - \Delta_A}{CW_A - \Delta_A} & \forall \quad \Delta_D \leq t' \leq \Delta_A + CW_A \\ 1 & \forall \quad \Delta_A + CW_A \leq t' \leq \Delta_D + CW_D \end{cases}$
$F_{t_k^B}(t') = \begin{cases} \frac{t' - \Delta_B}{CW_B - \Delta_B} & \forall \quad \Delta_D \leq t' \leq \Delta_B + CW_B \\ 1 & \forall \quad \Delta_B + CW_B \leq t' \leq \Delta_D + CW_D \end{cases}$	$F_{t_k^B}(t') = \begin{cases} \frac{t' - \Delta_B}{CW_B - \Delta_B} & \forall \quad \Delta_D \leq t' \leq \Delta_B + CW_B \\ 1 & \forall \quad \Delta_B + CW_B \leq t' \leq \Delta_D + CW_D \end{cases}$
$F_{t_n^C}(t') = \begin{cases} \frac{t' - \Delta_C}{CW_C - \Delta_C} & \forall \quad \Delta_D \leq t' \leq \Delta_C + CW_C \\ 1 & \forall \quad \Delta_C + CW_C \leq t' \leq \Delta_D + CW_D \end{cases}$	$F_{t_n^C}(t') = \begin{cases} \frac{t' - \Delta_C}{CW_C - \Delta_C} & \forall \quad \Delta_D \leq t' \leq \Delta_C + CW_C \\ 1 & \forall \quad \Delta_C + CW_C \leq t' \leq \Delta_D + CW_D \end{cases}$
$F_{t_p^D}(t') = \frac{t' - \Delta_D}{CW_D - \Delta_D} \quad \forall \quad \Delta_D \leq t' \leq \Delta_D + CW_D$	$F_{t_n^D}(t') = \frac{t' - \Delta_D}{CW_D - \Delta_D} \quad \forall \quad \Delta_D \leq t' \leq \Delta_D + CW_D$

priority class B is obtained in Lemma 3 as follows:

Lemma 3: Given the tagged LAA eNB is located at $w_0 = (r_0, 0) \in \Phi_B$, the SINR coverage probability of the typical UE with SINR threshold T for priority class B is approximated as:

$$\mathbb{P}^B_{SINR}(T, \lambda_A, \lambda_B, \lambda_C, \lambda_D) \approx \int_0^\infty \exp\Big(- \int_{\mathbb{R}^2} \frac{Tl(r_0)\lambda_A \mathbb{P}^{x/w_0}_{MAP}}{\frac{P_B}{P_A} l(\|x\|) + Tl(r_0)} \mathrm{d}x \Big) \exp\Big(- \int_{\mathbb{R}^2 \setminus B(0,r_0)} \frac{Tl(r_0)\lambda_B \mathbb{P}^{w/w_0}_{MAP}}{l(\|w\|) + Tl(r_0)} \mathrm{d}w \Big)$$
$$\times \exp\Big(- \int_{\mathbb{R}^2} \frac{Tl(r_0)\lambda_C \mathbb{P}^{y/w_0}_{MAP}}{\frac{P_B}{P_C} l(\|y\|) + Tl(r_0)} \mathrm{d}y \Big) \times \exp\Big(- \int_{\mathbb{R}^2} \frac{Tl(r_0)\lambda_D \mathbb{P}^{z/w_0}_{MAP}}{\frac{P_B}{P_D} l(\|z\|) + Tl(r_0)} \mathrm{d}z \Big) \times \exp\Big(-\mu T l(r_0) \frac{\sigma_N^2}{P_B} \Big) \times f_{\|w_0\|}(r_0) \mathrm{d}r_0 \tag{4.19}$$

SINR Coverage Probability of Typical UE For Channel Priority Class C When deriving the SINR coverage upper and lower performance bounds of class C, the upper bound for class C exists when $CW_A = 7$, $CW_B = 15$, $CW_C = 15$, and $CW_D = 1023$. On the other hand, the lower bound for class C exists when $CW_A = 3$, $CW_B = 7$, $CW_C = 63$, and $CW_D = 15$.

Corollary 9: Conditioned on the fact that the tagged LAA eNB $y_0 = (r_0, 0) \in \Phi_C$ is retained by the MAC protocol, the probability for another eNB $x \in \Phi_A$ to transmit is:

$$\mathbb{P}^{x/y_0}_{MAP} = \frac{H_N\Big(y_0, x, \frac{T_C}{P_A}, \Delta_C, CW_C, \Delta_A, CW_A, C, A, B, D\Big)}{H_D\Big(y_0, x, \frac{T_C}{P_A}, C, A, B, D, A\Big)} \tag{4.20}$$

Where t is the timer of node y_0 and t' is the timer of node x. The resulting distributions of the timers t' and t are shown in Tables 4.16 and 4.17 respectively and which will be used in computing $\mathbb{P}^{x/y_0}_{MAP}$.

Corollary 10: Conditioned on the fact that the tagged LAA eNB $y_0 = (r_0, 0) \in \Phi_C$ is retained by LBT mechanism, the probability for another LAA eNB $w \in \Phi_B$

Table 4.16: Distributions For Timer t' in Corollary 9

Lower Bound	Upper Bound
$F_{t_j^A}(t') = \frac{t'-\Delta_A}{CW_A-\Delta_A} \quad \forall \quad \Delta_A \leq t' \leq \Delta_A + CW_A$	$F_{t_j^A}(t') = \frac{t'-\Delta_A}{CW_A-\Delta_A} \quad \forall \quad \Delta_A \leq t' \leq \Delta_A + CW_A$
$F_{t_k^B}(t') = \frac{t'-\Delta_B}{CW_B-\Delta_B} \quad \forall \quad \Delta_B \leq t' \leq \Delta_A + CW_A$	$F_{t_k^B}(t') = \frac{t'-\Delta_B}{CW_B-\Delta_B} \quad \forall \quad \Delta_B \leq t' \leq \Delta_A + CW_A$
$F_{t_n^C}(t') = \frac{t'-\Delta_C}{CW_C-\Delta_C} \quad \forall \quad \Delta_C \leq t' \leq \Delta_A + CW_A$	$F_{t_n^C}(t') = \frac{t'-\Delta_C}{CW_C-\Delta_C} \quad \forall \quad \Delta_C \leq t' \leq \Delta_A + CW_A$
$F_{t_p^D}(t') = 0 \quad \forall \quad \Delta_A \leq t' \leq \Delta_A + CW_A$	$F_{t_p^D}(t') = \frac{t'-\Delta_D}{CW_D-\Delta_D} \quad \forall \quad \Delta_D \leq t' \leq \Delta_A + CW_A$

Table 4.17: Distributions For Timer t in Corollary 9

Lower Bound	Upper Bound
$F_{t_j^A}(t) = \begin{cases} \frac{t-\Delta_A}{CW_A-\Delta_A} \quad \forall \quad \Delta_C \leq t \leq \Delta_A + CW_A \\ 1 \quad \forall \quad \Delta_A + CW_A \leq t \leq \Delta_C + CW_C \end{cases}$	$F_{t_j^A}(t) = \begin{cases} \frac{t-\Delta_A}{CW_A-\Delta_A} \quad \forall \quad \Delta_C \leq t \leq \Delta_A + CW_A \\ 1 \quad \forall \quad \Delta_A + CW_A \leq t \leq \Delta_C + CW_C \end{cases}$
$F_{t_k^B}(t) = \begin{cases} \frac{t-\Delta_B}{CW_B-\Delta_B} \quad \forall \quad \Delta_C \leq t \leq \Delta_B + CW_B \\ 1 \quad \forall \quad \Delta_B + CW_B \leq t \leq \Delta_C + CW_C \end{cases}$	$F_{t_k^B}(t) = \begin{cases} \frac{t-\Delta_B}{CW_B-\Delta_B} \quad \forall \quad \Delta_C \leq t \leq \Delta_B + CW_B \\ 1 \quad \forall \quad \Delta_B + CW_B \leq t \leq \Delta_C + CW_C \end{cases}$
$F_{t_n^C}(t) = \frac{t-\Delta_C}{CW_C-\Delta_C} \quad \forall \quad \Delta_C \leq t \leq \Delta_C + CW_C$	$F_{t_n^C}(t) = \frac{t-\Delta_C}{CW_C-\Delta_C} \quad \forall \quad \Delta_C \leq t \leq \Delta_C + CW_C$
$F_{t_p^D}(t) = \frac{t-\Delta_D}{CW_D-\Delta_D} \quad \forall \quad \Delta_D \leq t \leq \Delta_C + CW_C$	$F_{t_n^D}(t) = \frac{t-\Delta_D}{CW_D-\Delta_D} \quad \forall \quad \Delta_D \leq t \leq \Delta_C + CW_C$

to transmit is given by:

$$\mathbb{P}_{MAP}^{w/y_0} = \frac{H_N\left(y_0, w, \frac{T_C}{P_B}, \Delta_C, CW_C, \Delta_B, CW_B, C, A, B, D\right)}{H_D\left(y_0, w, \frac{T_C}{P_B}, C, A, B, D, B\right)} \tag{4.21}$$

Where t is the timer of node y_0 and t' is the timer of node w. The resulting distributions of the timers t and t' are shown in Tables 4.17 and 4.18 respectively and which will be used in computing $\mathbb{P}_{MAP}^{w/y_0}$.

Corollary 11: Conditioned on the fact that the tagged LAA eNB $y_0 = (r_0, 0) \in \Phi_C$ is retained by LBT mechanism, the probability for another LAA eNB $y \in \Phi_C$

Table 4.18: Distributions For Timer t' in Corollary 10

Lower Bound	Upper Bound
$F_{t_j^A}(t') = \begin{cases} \frac{t'-\Delta_A}{CW_A-\Delta_A} \quad \forall \quad \Delta_A \leq t' \leq \Delta_A + CW_A \\ 1 \quad \forall \quad \Delta_A + CW_A \leq t' \leq \Delta_B + CW_B \end{cases}$	$F_{t_j^A}(t') = \begin{cases} \frac{t'-\Delta_A}{CW_A-\Delta_A} \quad \forall \quad \Delta_B \leq t' \leq \Delta_A + CW_A \\ 1 \quad \forall \quad \Delta_A + CW_A \leq t' \leq \Delta_B + CW_B \end{cases}$
$F_{t_k^B}(t') = \frac{t'-\Delta_B}{CW_B-\Delta_B} \quad \forall \quad \Delta_B \leq t' \leq \Delta_B + CW_B$	$F_{t_k^B}(t') = \frac{t'-\Delta_B}{CW_B-\Delta_B} \quad \forall \quad \Delta_B \leq t' \leq \Delta_B + CW_B$
$F_{t_n^C}(t') = \frac{t'-\Delta_C}{CW_C-\Delta_C} \quad \forall \quad \Delta_C \leq t' \leq \Delta_B + CW_B$	$F_{t_n^C}(t') = \frac{t'-\Delta_C}{CW_C-\Delta_C} \quad \forall \quad \Delta_C \leq t' \leq \Delta_B + CW_B$
$F_{t_p^D}(t') = \frac{t'-\Delta_D}{CW_D-\Delta_D} \quad \forall \quad \Delta_D \leq t' \leq \Delta_B + CW_B$	$F_{t_n^D}(t') = \frac{t'-\Delta_D}{CW_D-\Delta_D} \quad \forall \quad \Delta_D \leq t' \leq \Delta_B + CW_B$

Table 4.19: Distributions For Timer t' in Corollary 12

Lower Bound	Upper Bound
$F_{t_j^A}(t') = 1 \quad \forall \quad \Delta_D \leq t' \leq \Delta_D + CW_D$	$F_{t_j^A}(t') = \begin{cases} \frac{t' - \Delta_A}{CW_A - \Delta_A} & \forall \quad \Delta_D \leq t' \leq \Delta_A + CW_A \\ 1 & \forall \quad \Delta_A + CW_A \leq t' \leq \Delta_D + CW_D \end{cases}$
$F_{t_k^B}(t') = \begin{cases} \frac{t' - \Delta_B}{CW_B - \Delta_B} & \forall \quad \Delta_D \leq t' \leq \Delta_B + CW_B \\ 1 & \forall \quad \Delta_B + CW_B \leq t' \leq \Delta_D + CW_D \end{cases}$	$F_{t_k^B}(t') = \begin{cases} \frac{t' - \Delta_B}{CW_B - \Delta_B} & \forall \quad \Delta_D \leq t' \leq \Delta_B + CW_B \\ 1 & \forall \quad \Delta_B + CW_B \leq t' \leq \Delta_D + CW_D \end{cases}$
$F_{t_n^C}(t') = \frac{t' - \Delta_C}{CW_C - \Delta_C} \quad \forall \quad \Delta_D \leq t' \leq \Delta_C + CW_C$	$F_{t_n^C}(t') = \begin{cases} \frac{t' - \Delta_C}{CW_C - \Delta_C} & \forall \quad \Delta_D \leq t' \leq \Delta_C + CW_C \\ 1 & \forall \quad \Delta_C + CW_C \leq t' \leq \Delta_D + CW_D \end{cases}$
$F_{t_p^D}(t') = \frac{t' - \Delta_D}{CW_D - \Delta_D} \quad \forall \quad \Delta_D \leq t' \leq \Delta_D + CW_D$	$F_{t_n^D}(t') = \frac{t' - \Delta_D}{CW_D - \Delta_D} \quad \forall \quad \Delta_D \leq t' \leq \Delta_D + CW_D$

to transmit is given by:

$$\mathbb{P}_{MAP}^{y/y_0} = \frac{H_N\left(y_0, y, \frac{T_C}{P_C}, \Delta_C, CW_C, \Delta_C, CW_C, C, A, B, D\right)}{H_D\left(y_0, y, \frac{T_C}{P_C}, C, A, B, D, C\right)} \tag{4.22}$$

Where t is the timer of node y_0 and t' is the timer of node y. The resulting distributions of both timers t and t' are those in Table 4.17 respectively and which will be used in computing $\mathbb{P}_{MAP}^{y/y_0}$.

Corollary 12: Conditioned on the fact that the tagged LAA eNB $y_0 = (r_0, 0) \in \Phi_C$ is retained by LBT mechanism, the probability for another LAA eNB $z \in \Phi_D$ to transmit is given by:

$$\mathbb{P}_{MAP}^{z/y_0} = \frac{H_N\left(y_0, z, \frac{T_C}{P_D}, \Delta_C, CW_C, \Delta_D, CW_D, C, A, B, D\right)}{H_D\left(y_0, z, \frac{T_C}{P_D}, C, A, B, D, D\right)} \tag{4.23}$$

Where t is the timer of node y_0 and t' is the timer of node z. The resulting distributions of the timers t and t' are shown in Tables 4.17 and 4.19 respectively and which will be used in computing $\mathbb{P}_{MAP}^{z/y_0}$.

Based on Corollaries 9, 10, 11, and 12, the SINR coverage of the typical UE for priority class C is obtained in Lemma 4 as follows:

Lemma 4: Given the tagged LAA eNB is located at $y_0 = (r_0, 0) \in \Phi_C$, the SINR coverage probability of the typical UE with SINR threshold T for priority class C is approximated as:

$$\mathbb{P}_{SINR}^{C}(T, \lambda_A, \lambda_B, \lambda_C, \lambda_D) \approx \int_0^\infty \exp\Big(-\int_{\mathbb{R}^2} \frac{Tl(r_0)\lambda_A \mathbb{P}_{MAP}^{x/y_0}}{\frac{P_C}{P_A} l(\|x\|) + Tl(r_0)} \mathrm{d}x\Big) \exp\Big(-\int_{\mathbb{R}^2} \frac{Tl(r_0)\lambda_B \mathbb{P}_{MAP}^{w/y_0}}{\frac{P_C}{P_B} l(\|w\|) + Tl(r_0)} \mathrm{d}w\Big)$$
$$\times \exp\Big(-\int_{\mathbb{R}^2 \setminus B(0,r_0)} \frac{Tl(r_0)\lambda_C \mathbb{P}_{MAP}^{y/y_0}}{l(\|y\|) + Tl(r_0)} \mathrm{d}y\Big) \times \exp\Big(-\int_{\mathbb{R}^2} \frac{Tl(r_0)\lambda_D \mathbb{P}_{MAP}^{z/y_0}}{\frac{P_C}{P_D} l(\|z\|) + Tl(r_0)} \mathrm{d}z\Big) \times \exp\left(-\mu T l(r_0) \frac{\sigma_N^2}{P_C}\right) \times f_{\|y_0\|}(r_0) \mathrm{d}r_0 \tag{4.24}$$

Table 4.20: Distributions For Timer t in Corollary 13

Lower Bound	Upper Bound
$F_{t_j^A}(t) = 1 \quad \forall \quad \Delta_D \leq t \leq \Delta_D + CW_D$	$F_{t_j^A}(t) = \begin{cases} \frac{t-\Delta_A}{CW_A - \Delta_A} \quad \forall \quad \Delta_D \leq t \leq \Delta_A + CW_A \\ 1 \quad \forall \quad \Delta_A + CW_A \leq t \leq \Delta_D + CW_D \end{cases}$
$F_{t_k^B}(t) = \begin{cases} \frac{t-\Delta_B}{CW_B - \Delta_B} \quad \forall \quad \Delta_D \leq t \leq \Delta_B + CW_B \\ 1 \quad \forall \quad \Delta_B + CW_B \leq t \leq \Delta_D + CW_D \end{cases}$	$F_{t_k^B}(t) = \begin{cases} \frac{t-\Delta_B}{CW_B - \Delta_B} \quad \forall \quad \Delta_D \leq t \leq \Delta_B + CW_B \\ 1 \quad \forall \quad \Delta_B + CW_B \leq t \leq \Delta_D + CW_D \end{cases}$
$F_{t_n^C}(t) = \begin{cases} \frac{t-\Delta_C}{CW_C - \Delta_C} \quad \forall \quad \Delta_D \leq t \leq \Delta_C + CW_C \\ 1 \quad \forall \quad \Delta_C + CW_C \leq t \leq \Delta_D + CW_D \end{cases}$	$F_{t_n^C}(t) = \frac{t-\Delta_C}{CW_C - \Delta_C} \quad \forall \quad \Delta_D \leq t \leq \Delta_C + CW_C$
$F_{t_p^D}(t) = \frac{t-\Delta_D}{CW_D - \Delta_D} \quad \forall \quad \Delta_D \leq t \leq \Delta_D + CW_D$	$F_{t_n^D}(t) = \frac{t-\Delta_D}{CW_D - \Delta_D} \quad \forall \quad \Delta_D \leq t \leq \Delta_D + CW_D$

SINR Coverage Probability of Typical UE For Channel Priority Class D When deriving the SINR coverage upper and lower performance bounds of class D, the upper bound for class D exists when $CW_A = 7$, $CW_B = 15$, $CW_C = 63$, and $CW_D = 15$. On the other hand, the lower bound for class D exists when $CW_A = 3$, $CW_B = 7$, $CW_C = 15$, and $CW_D = 1023$.

Corollary 13: Conditioned on the fact that the tagged LAA eNB $z_0 = (r_0, 0) \in \Phi_D$ is retained by the MAC protocol, the probability for another eNB $x \in \Phi_A$ to transmit is:

$$\mathbb{P}_{MAP}^{x/z_0} = \frac{H_N\left(z_0, x, \frac{T_D}{P_A}, \Delta_D, CW_D, \Delta_A, CW_A, D, A, B, C\right)}{H_D\left(z_0, x, \frac{T_D}{P_A}, D, A, B, C, A\right)} \tag{4.25}$$

Where t is the timer of node y_0 and t' is the timer of node x. The resulting distributions of the timer t' were found to be similar to those in Table 4.17. On the other hand, the resulting distributions of the timer t are shown in Table 4.20. The distributions in Table 4.17 and Table 4.20 can then be used to compute $\mathbb{P}_{MAP}^{x/z_0}$.

Corollary 14: Conditioned on the fact that the tagged LAA eNB $z_0 = (r_0, 0) \in \Phi_D$ is retained by LBT mechanism, the probability for another LAA eNB $w \in \Phi_B$ to transmit is given by:

$$\mathbb{P}_{MAP}^{w/z_0} = \frac{H_N\left(z_0, w, \frac{T_D}{P_B}, \Delta_D, CW_D, \Delta_B, CW_B, D, A, B, C\right)}{H_D\left(z_0, w, \frac{T_D}{P_B}, D, A, B, C, B\right)} \tag{4.26}$$

Where t is the timer of node y_0 and t' is the timer of node w. The resulting distributions of the timers t' and t were found to be similar to those in Tables 4.18 and 4.20 which can used to compute $\mathbb{P}_{MAP}^{w/z_0}$.

Corollary 15: Conditioned on the fact that the tagged LAA eNB $z_0 = (r_0, 0) \in$

Φ_D is retained by LBT mechanism, the probability for another LAA eNB $y \in \Phi_C$ to transmit is given by:

$$\mathbb{P}^{y/z_0}_{MAP} = \frac{H_N\left(z_0, y, \frac{T_D}{P_C}, \Delta_D, CW_D, \Delta_C, CW_C, D, A, B, C\right)}{H_D\left(z_0, y, \frac{T_D}{P_C}, D, A, B, C, C\right)} \tag{4.27}$$

Where t is the timer of node y_0 and t' is the timer of node y. The resulting distributions of the timers t' and t were found to be similar to those in Tables 4.17 and 4.20 which can used to compute $\mathbb{P}^{y/z_0}_{MAP}$.

Corollary 16: Conditioned on the fact that the tagged LAA eNB $z_0 = (r_0, 0) \in \Phi_D$ is retained by LBT mechanism, the probability for another LAA eNB $z \in \Phi_D$ to transmit is given by:

$$\mathbb{P}^{z/z_0}_{MAP} = \frac{H_N\left(z_0, z, \frac{T_D}{P_D}, \Delta_D, CW_D, \Delta_D, CW_D, D, A, B, C\right)}{H_D\left(z_0, z, \frac{T_D}{P_D}, D, A, B, C, D\right)} \tag{4.28}$$

Where t is the timer of node y_0 and t' is the timer of node z. The resulting distributions of the timers t' and t were derived in Table 4.20 which can used to compute $\mathbb{P}^{z/z_0}_{MAP}$.

Based on Corollaries 13, 14, 15, and 16, the SINR coverage of the typical UE for priority class D is obtained in Lemma 5 as follows:

Lemma 5: Given the tagged LAA eNB is located at $z_0 = (r_0, 0) \in \Phi_D$, the SINR coverage probability of the typical UE with SINR threshold T for priority class D is approximated as:

$$\begin{aligned}\mathbb{P}^{D}_{SINR}(T, \lambda_A, \lambda_B, \lambda_C, \lambda_D) \approx \int_0^\infty \exp\Big(-\int_{\mathbb{R}^2} \frac{Tl(r_0)\lambda_A \mathbb{P}^{x/z_0}_{MAP}}{\frac{P_D}{P_A} l(\|x\|) + Tl(r_0)} \mathrm{d}x\Big) \exp\Big(-\int_{\mathbb{R}^2} \frac{Tl(r_0)\lambda_B \mathbb{P}^{w/z_0}_{MAP}}{\frac{P_D}{P_B} l(\|w\|) + Tl(r_0)} \mathrm{d}w\Big) \\ \times \exp\Big(-\int_{\mathbb{R}^2} \frac{Tl(r_0)\lambda_C \mathbb{P}^{y/z_0}_{MAP}}{\frac{P_D}{P_C} l(\|y\|) + Tl(r_0)} \mathrm{d}y\Big) \times \exp\Big(-\int_{\mathbb{R}^2 \setminus B(0,r_0)} \frac{Tl(r_0)\lambda_D \mathbb{P}^{z/z_0}_{MAP}}{l(\|z\|) + Tl(r_0)} \mathrm{d}z\Big) \times \exp\left(-\mu T l(r_0) \frac{\sigma_N^2}{P_D}\right) \times f_{\|z_0\|}(r_0) \mathrm{d}r_0\end{aligned} \tag{4.29}$$

Based on the parameters in Table 4.3 and upper performance bound channel access parameters (for demonstration purpose), we show in Fig. 4.4 the SINR coverage probability of the typical LAA UE in the downlink for different LTE eNB densities corresponding to different channel access priority classes. The simulation results are obtained from the definition of SINR in (4.1), (4.2), (4.3), and (4.4). It can be observed from Fig. 4.4 that the approximation in Lemma 2, 3, 4, and 5 give an accurate estimation of the actual SINR coverage. In addition, we can see that in general the best performance is achieved when the density of eNBs from any class is dominating over that of the other classes as shown in Fig. 4.4 (a) and (d).

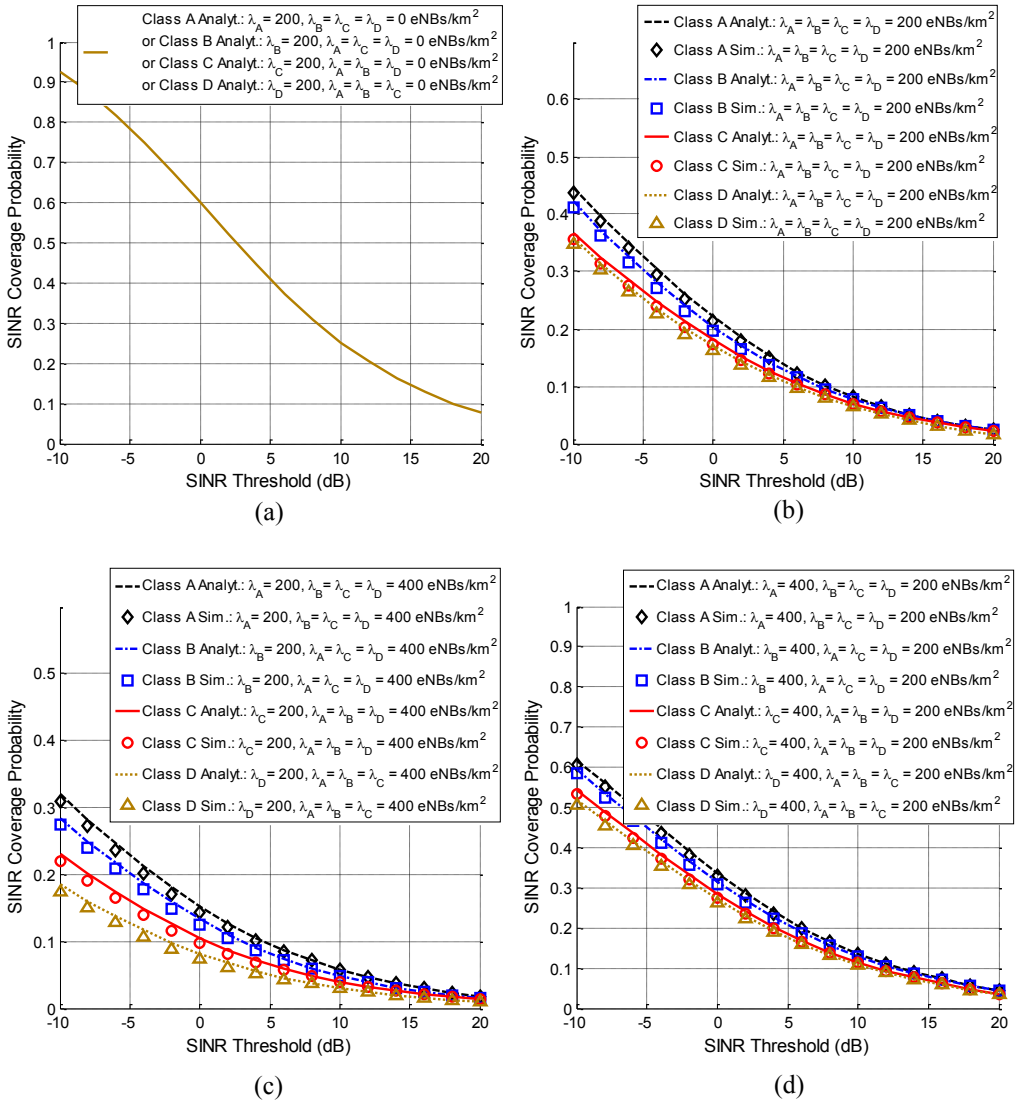

Figure 4.4: SINR Coverage For Typical LTE-LAA UE with Different Priority Classes

Also, the coexistence of LTE eNBs from other classes in the same channel show a diverse impact on the downlink transmissions of any class. The SINR performance of the typical UE appears to be worse when the density of LAA eNBs of a particular class is smaller where the the effect of interference from other LAA channel access priority classes is higher when a class has $\lambda = 200$ eNBs/km^2 than the case where it has $\lambda = 400$ eNBs/km^2 as shown in Fig. 4.4. Furthermore, we can see that the SINR performance for class A is the best whereas class B follows the same trend as that of class A with an extra acceptable degradation that is highest especially in the low SINR regime (below 0 dB) when the density of eNBs that belong to class B is smaller than that of other classes

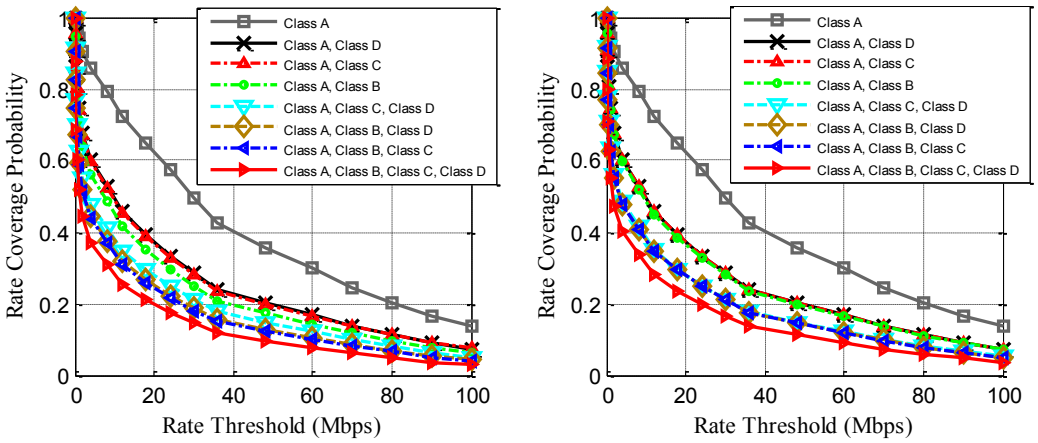

Figure 4.5: Rate Coverage Probability For Typical LTE-LAA UE in Case of Channel Priority Class A: (a) Lower Performance Bound (b) Upper Performance Bound.

as shown in Fig. 4.4 (c). Also, we can see that the SINR performance for class C shows a large degradation compared to that of class A and B especially in the low SINR regime (below 0 dB) when the density of eNBs that belong to class C (200 eNBs/km^2) is smaller than that of other classes (400 eNBs/km^2). Finally, we can see that the SINR performance for class D shows a large degradation compared to that of class A and B and a closer performance to that of class C. However, class D suffers from the lowest SINR performance when coexisting with classes A, B, and C. The worst being when class D has lower density of eNBs than the density of other classes as shown in Fig. 4.4 (c).

4.1.3 Numerical Results and Evaluation

In this section, based on the MAP and the SINR coverage probability, we investigate the effect of the different channel access priority classes on the rate coverage probability that was defined in section 4.1.1. We focus in our analysis on a dense network deployment with $\lambda_A = 200$ eNBs/km^2, $\lambda_B = 200$ eNBs/km^2, $\lambda_C = 200$ eNBs/km^2, and $\lambda_D = 200$ eNBs/km^2. Note that since we consider the effect of the channel access priority on the performance of different classes, we consider same density of eNBs for all classes. The Rayleigh fading parameter μ is equal to 1 and we assume that the noise power is negligible as compared to interference power ($\sigma_N^2 = 0$).

One way to interpret these classes would be to assign them to different traffic types as in [64]. For example, class A may be used for signaling, voice, and real-time gaming. While class B may be used for streaming and interactive gaming. In addition, class C may be used for best-effort data whereas class D may be used for background traffic. In figures 4.5, 4.6, 4.7 and 4.8, we present the

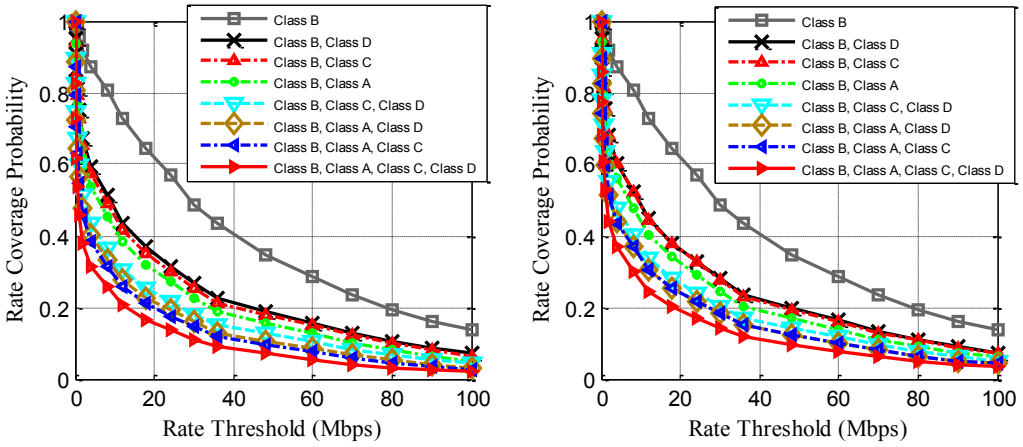

Figure 4.6: Rate Coverage Probability For Typical LTE-LAA UE in Case of Channel Priority Class B: (a) Lower Performance Bound (b) Upper Performance Bound.

rate coverage probability of the typical UE under different channel access priority classes which are based on 3GPP release 14 specifications for LAA downlink as described in Table 4.21. In each figure, we show the performance of all possible coexistence scenarios corresponding to each channel access priority class. This is important as the operator may decide to select particular traffic to be offloaded to the unlicensed band through LAA while aiming to maintain the quality of service requested by users.

First, we start by analyzing Fig. 4.5 where the performance of class A having highest channel access priority is presented. In Fig. 4.5, we can see that the operator achieves the best performance when one traffic class is used. This is the same in case of classes B, C, and D as shown in figures 4.6, 4.7 and 4.8. However when other classes coexist with class A, the rate coverage probability of class A decreases rapidly especially in the low rate threshold regime (≤ 30 Mbps). In particular, in the case where class A coexists with exactly one another class $\{$(class A, class B), (class A, class C, (class A, class D)$\}$, we can realize that although class B has the worst effect on class A, the effect of the coexistence of classes C and D are close to that of B. On the other hand, when class A coexists with two other classes, the performance of class A is more degraded but also with close effect on the performance of class A from the combinations of $\{$(class A, class C, class D), (class A, class B, class D), (class A, class B, class C)$\}$ where the last has the worst performance. Finally, for the case of coexisting with three other classes, we can see that class A has the worst rate coverage probability. Also, by inspecting Fig. 4.6, we can see that the effect of the performance on class B with other classes follows the same trend as that of class A but with an extra degradation in the rate coverage probability whenever coexisting with class A. We can

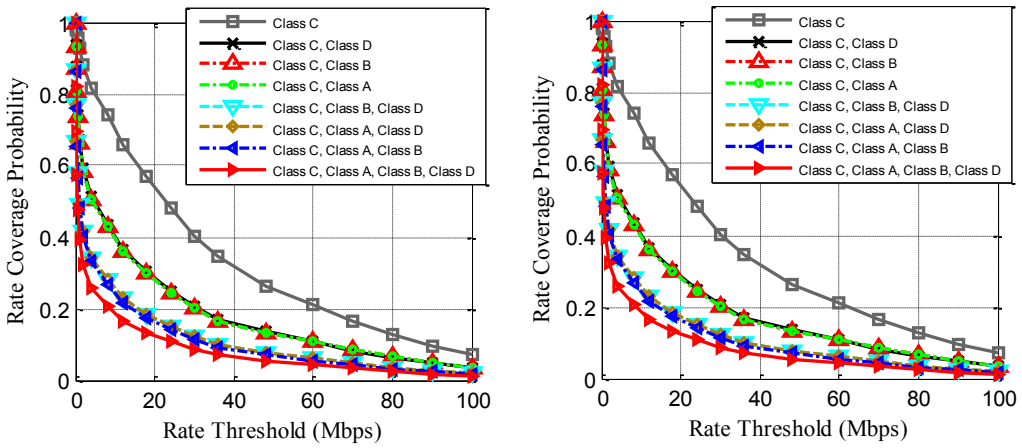

Figure 4.7: Rate Coverage Probability For Typical LTE-LAA UE in Case of Channel Priority Class C: (a) Lower Performance Bound (b) Upper Performance Bound.

see that the effect of coexistence with class A only is equivalent to the effect of coexisting with two other classes like C and D. This can be explained by the fact that class A has the higher channel access priority than class B and hence the presence of eNBs that belongs to class A will diversely affect the performance of eNBs from class B. As for the performance of class C and D, we can see that class C maintains an acceptable performance when coexisting with class D. However, when class C coexists with either class A and B its performance starts degrading and becomes more severe in case of coexisting with other two or three classes. For class D, we can see that its performance is severely affected by the presence of any combination of all other classes. The worst being the case where class D coexists with classes A, B, and C. Note that the lower and upper performance bounds are similar in classes A, B, and C. Whereas in class D, we can see that in case of the upper performance bound, we have an enhancement in about 20% in the rate coverage probability.

4.1.4 Summary

In this chapter, we have presented and validated a framework using stochastic geometry to analyze the effect of different channel access priorities on the performance of four different coexisting LAA networks in the unlicensed band. The coexistence of LAA networks with each other is a major issue on the road toward 5G. Based on this, we adopted 3GPP release 14 specification for LAA downlink. Throughout the analysis, we used several performance metrics such as MAP, SINR coverage probability, and rate coverage probability. Results show that operators may exploit the unlicensed bands using different traffic types but with a trade off between the achieved performance and the number of traffic classes

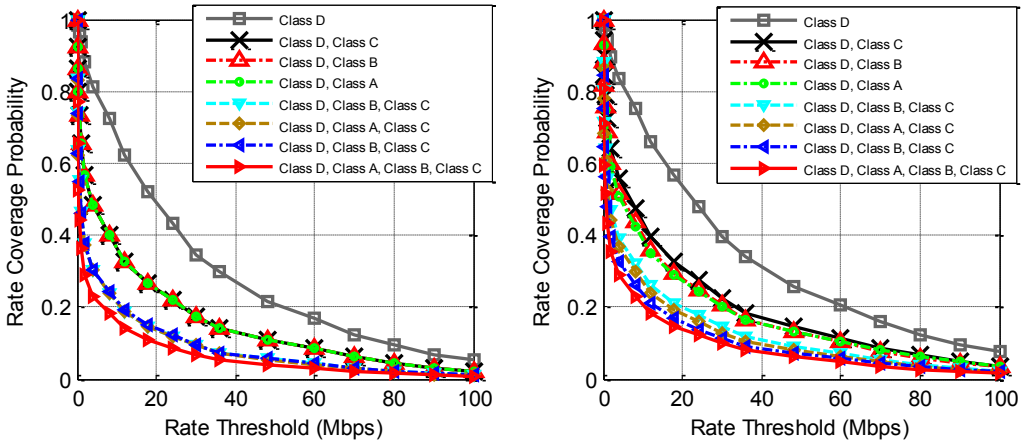

Figure 4.8: Rate Coverage Probability For Typical LTE-LAA UE in Case of Channel Priority Class D: (a) Lower Performance Bound (b) Upper Performance Bound.

used. We showed that most of the traffic classes may maximize their benefit from the unlicensed channel when a single traffic class is used. However, the diverse impact on the performance of each class starts when increasing the number of classes being transmitted. Results showed that classes A and B retain an acceptable performance and are better than that of classes C and D when coexisting with one or two other classes having different types. However, when all classes coexist, there is a severe impact on the LAA network in the case of all classes. Also, when analyzing the lower and upper performance bounds, we can see that they are similar in case of classes A, B, and C. Whereas in case of class D, we have an improvement in the rate coverage probability by about 20% in the upper performance bound.

4.2 LTE-LAA Coexistence: Generalized M-operator Approach

In this section, we provide a stochastic geometry framework for analyzing the performance attained by an arbitrary number of LTE operators sharing an unlicensed band in licensed assisted access. We derive closed-form expressions for the medium access and coverage probabilities and the network throughput per unit area. These performance metrics address the impact of multi-operator coexistence. Our results identify coexistence issues not accounted for in the standard and provide analytical tools to help overcome them.

4.2.1 System Model

We consider a downlink scenario with M LAA operators coexisting in an unlicensed band of bandwidth W. Coordinators (eNBs) are assumed to have persistent traffic. Each user equipment (UE) is associated with the eNB providing the strongest average received power.

Network Model

The location of a node n (eNB or UE) is denoted by $x_n \in \mathbb{R}^2$. The locations of eNBs for each operator i are modeled as independent realizations $\Phi_i = \{x_n\}$ of a homogeneous Poisson point processes (PPP) of intensity $\hat{\lambda}_i$ on $\mathbb{R}^2$. The served UEs are also modeled as independent homogeneous PPPs with λ_i^{UE} for each operator. Only eNBs that have at least one UE to serve are considered in our analysis. The density of these active eNBs is $\lambda_i = \delta\hat{\lambda}_i$, where $\delta = 1 - \left(1 - \frac{\lambda_i^{\mathrm{UE}}}{\lambda_i^{\mathrm{UE}} + \kappa\hat{\lambda}_i}\right)^{\kappa}$ is the activation probability with $\kappa = 3.575$ [70].

The signal path loss between an eNB located at x_n and a UE located at x_m is defined as $\ell_{nm} := \ell(x_n, x_m)$ or $\ell(x_n) := \ell(x_n, 0)$ and modeled as $\ell(x_n, x_m) = \frac{c}{4\pi f_c}\|x_n - x_m\|^{\alpha}$ with f_c standing for the carrier frequency, c for the speed of light, and α for the path loss exponent. We consider path loss exponent $\alpha = 4$. The probability density function of the distance between these two nodes, defined as $r := \|x_n - x_m\|$ is $f_R(r) = 2\pi r\lambda_i e^{-\lambda_i \pi r^2}$ [37]. We assume that channels are subject to Rayleigh fading, such that the power fading coefficient h_{nm}^i between eNB n and UE m from operator i is exponentially distributed with parameter μ. For simplicity, we neglect shadowing effects in this letter.

Based on Slivnyak′s theorem [39], we study the performance of a typical UE assumed to be located in the origin without affecting the distribution of the rest of the UEs process. The typical UE is denoted as UE_0. The coordinator associated to UE_0 is called tagged eNB, denoted by $\mathrm{eNB}_0 = x_0$.

Channel Access

We consider the Load Based Equipment (LBE) medium access control (MAC) protocol for LAA [20], where an LAA eNB performs a carrier sensing before transmission. A channel observation time of at least 20 μs is employed to detect the presence of active transmitters. The received signal power is compared against a given energy detection threshold level threshold ξ_i [20, 49]. The channel for operator i is determined busy if a signal above the threshold ξ_i is detected. If the channel is found idle, the eNB transmits. However, if busy, the eNB waits a back-off period t before transmission, which is a randomly selected multiple of the channel observation time from a contention window $[0; q_i]$. Parameter q_i is selected based on the traffic type carried by the LAA eNB in the range [4; 32] which determines its channel access priority [21]. Each eNB $x_n \in \Phi_i$ has an independent mark t_n^i that represents its random back-off, uniformly distributed in

the interval $[0, q_i]$. Although this channel access model may have some limitations with its fixed contention window size, it allows us to highlight interesting LAA design issues.

The contenders of an eNB from operator i are the eNBs from other operators for which a power above ξ_i is received. The MAC protocol retains the eNB with the smallest back-off from all contenders. In this way, a medium access indicator e_n^i equal to one is assigned to the eNB $x_n \in \Phi_i$ if the eNB is selected to transmit, and equal to zero otherwise.

Performance Metrics

If the tagged eNB $x_0 \in \Phi_i$ transmits with power p_i, the received SINR at UE_0 is:

$$\mathrm{SINR}_0^i = \frac{p_i h_{00}^i / \ell(x_0)}{I_i + \sigma_N^2}, \tag{4.30}$$

where I_i is the interference resulting from other eNBs of the same operator and from the eNBs of the coexisting operators, and σ_N^2 stands for the thermal noise power at UE_0, which is assumed to be much smaller than the interference power and therefore neglected in the following. The interference can be further written as

$$I_i = \sum_{x_n \in \Phi_i \setminus \{x_0\}} p_i h_{n0}^i e_n^i / \ell(x_n) + \sum_{j \neq i} \sum_{x_l \in \Phi_j} p_j h_{l0}^{ji} e_l^j / \ell(x_l). \tag{4.31}$$

From (4.30), the SINR coverage probability for operator i, with an SINR threshold θ, is defined as $\mathbb{P}_{\mathrm{SINR}}^i(\theta) = \Pr(\mathrm{SINR}_0^i > \theta | e_0^i = 1)$. Based on this definition and that of the medium access probability (MAP) $\mathbb{P}_{\mathrm{MAP}}^i = \mathrm{E}[e_0^i]$ (derived in the following section), the area system throughput (AST) for operator i is defined as [70]:

$$\mathrm{AST}^i = \lambda_i \, \mathbb{P}_{\mathrm{MAP}}^i \, W \int_0^\infty \mathbb{P}_{\mathrm{SINR}}^i (2^\rho - 1) \mathrm{d}\rho. \tag{4.32}$$

Note that the MAP accounts for the expected fraction of time that the tagged eNB has access to the channel. It therefore measures the expected fraction of active eNBs per operator, over a fully overlapped coverage area.

Since $\Phi_i \; \forall \, i = 1 \ldots M$ are stationary and isotropic, the introduced performance metrics of UE_0 are invariant with respect to the angle of the tagged eNB, which we therefore, locate at $(r_0, 0)$. We also define the following functions to be used. First,

$$N_{ij}(x_n, r) = \lambda_i \int_{\mathbb{R}^2 \setminus B(0,r)} \exp\left(-\mu \frac{\xi_j}{p_i} \ell(x, x_n) \right) \mathrm{d}x \tag{4.33}$$

represents the expected number of eNBs that belong to operator i (in $\mathbb{R}^2 \setminus B(0, r)$), whose signal power at $x_n \in \mathbb{R}^2$ exceeds its activity threshold ξ_j. Second,

$$\begin{aligned} &Q_{ij}(x_n, x_m, r) = \\ &\lambda_i \int_{\mathbb{R}^2 \setminus B(0,r)} \exp\left(-\mu \frac{\xi_i}{p_i} \ell(x, x_n) - \mu \frac{\xi_j}{p_j} \ell(x, x_m) \right) \mathrm{d}x \end{aligned} \tag{4.34}$$

represents the expected number of eNBs in $\mathbb{R}^2 \backslash B(0,r)$ whose signal power at $x_n \in \mathbb{R}^2$ and $x_m \in \mathbb{R}^2$ exceeds thresholds ξ_i and ξ_j, respectively. Equations (4.33) and (4.34) are used to simplify the expressions of the conditional MAP later on.

4.2.2 MAP and SINR Coverage Probability

The medium access indicator e_n^i for the n-th LAA eNB from operator i, using LBE MAC is:

$$\begin{aligned} e_n^i = & \prod_{x_i \in \Phi_i \backslash \{x_n\}} \left(\mathbb{1}_{t_m^i \geq t_n^i} + \mathbb{1}_{t_m^i < t_n^i} \mathbb{1}_{h_{mn}^i / \ell_{mn} \leq \xi_i / p_i} \right) \\ & \cdot \prod_{j \neq i}^{M} \prod_{x_l \in \Phi_j} \left(\mathbb{1}_{t_l^j \geq t_n^i} + \mathbb{1}_{t_l^j < t_n^i} \mathbb{1}_{h_{ln}^{ji} / \ell_{ln} \leq \xi_i / p_j} \right), \end{aligned} \tag{4.35}$$

with $\mathbb{1}$ standing for the indicator function. e_n^i is equal to one only when the back-off timer of the n-th LAA eNB is smaller than that of all other eNBs or if it does not detect the transmissions of other eNBs even if its back-off timer is larger than that of other eNBs. e_n^i is equal to zero otherwise.

Lemma 1: When LAA operators $1, 2, \ldots, M$ adopt the contention window parameters $q_1, q_2, \ldots, q_M$, respectively, the MAP for eNB that belongs to operator i is given by:

$$\mathbb{P}_{\text{MAP}}^i = \int_0^\infty \frac{1 - \exp\left(- N_{ii}(x, r_0) - \sum_{j \neq i} \frac{q_i}{q_j} N_{ji}(x, 0) \right)}{N_{ii}(x, r_0) + \sum_{j \neq i} \frac{q_i}{q_j} N_{ji}(x, 0)} f_R(r_0) \mathrm{d}r_0. \tag{4.36}$$

Given the tagged eNB from operator i we have:

$$\begin{aligned} & \mathbb{E}\left[e_n^i | t_n^i = t, x_n = (r_0, 0) \right] \\ & \overset{(a)}{=} \mathbb{E}\left[\prod_{x_m \in \Phi_i \cap B^c(0, r_0)} \left(1 - \frac{t}{q_i} \exp\left(-\mu \frac{\xi_i}{p_i} \ell_{mn} \right) \right) \right. \\ & \left. \cdot \prod_{j \neq i}^{M} \left(\mathbb{E}\left[\prod_{x_l \in \Phi_j} \left(1 - \frac{t}{q_j} \exp\left(-\mu \frac{\xi_i}{p_j} \ell_{ln} \right) \right) \right] \right) \right] \\ & \overset{(b)}{=} \exp\left(-\frac{t}{q_i} N_{ii}(x_n, r_0) - \sum_{j \neq i}^{M} \frac{t}{q_j} N_{ji}(x_n, 0) \right), \end{aligned} \tag{4.37}$$

where (a) follows by re-writing $x_n = (r_0, 0)$ as $x_n \in \Phi_i$, $\Phi_i(B^o(0, r_0)) = 0$, and de-conditioning on $\Phi_i(B^o(0, r_0)) = 0$. Using Slivnyak's theorem and the

Table 4.21: Scenario of 10 LAA operators

Operator i	1	2	3	4	5	6	7	8	9	10
q_i	1	2	4	8	12	16	20	24	28	32

$$\mathbb{E}^{x_n}_{\Phi_i}\left[\hat{e}^i_n \hat{e}^i_0\right] = \frac{1}{q_i \times q_k}\int_0^{q_i}\int_0^{q_k}\left(1-\exp\left(-\mu\frac{\xi_k}{p_i}\ell(x,x_0)\right)\right) \times\exp\left(-t'\left(\frac{N_{ii}(x,r_0)}{q_i}+\sum_{j\neq i}^{M}\frac{N_{ji}(x,0)}{q_j}\right)-t\left(\frac{N_{ii}(x_0,r_0)}{q_i}+\sum_{j\neq i}^{M}\frac{N_{ji}(x_0,0)}{q_j}\right)\right. \left.+\min\left(t,t'\right)\left(\frac{Q_{ii}(x,x_0,r_0)}{q_i^2}+\sum_{j\neq i}^{M}\frac{Q_{ji}(x,x_0,0)}{q_j^2}\right)\right)\mathrm{d}t\mathrm{d}t' \tag{4.39}$$

$$\mathbb{E}^{x_n}_{\Phi_i}[\hat{e}^i_0] = \frac{1}{q_i}\int_0^{q_i}\left(1-\frac{t}{q_k}\exp\left(-\mu\frac{\xi_i}{p_k}\ell(x,x_0)\right)\right)\exp\left[-\frac{t}{q_i}N_{ii}(x_0,r_0)-\sum_{j\neq i}^{M}\frac{t}{q_j}N_{ji}(x_0,0)\right]\mathrm{d}t \tag{4.40}$$

independence of Φ_i and $\Phi_{j\neq i}$, (b) follows from the probability generating functional (P.G.FL) of the PPP. De-conditioning on $t \sim U(0, q_i)$ and on x_0, and using $N_{ij}(x_n, r)$ from (4.33) gives the result. Hence, by adding extra LAA operators each with eNBs density λ_j, the MAP of an operator i is degraded by $-\sum_{j\neq i}^{M}\frac{t}{q_j}N_{ji}$. The process of the transmitting eNB for each operator is a dependent thinning of the Φ_is, whose Laplace functionals are unknown in closed form. We approximate the SINR coverage probability of UE_0 by first deriving MAP for each eNB conditioned on the tagged eNB being active.

Corollary 1: Conditioned on the retention of the tagged eNB x_0 from operator i by the MAC protocol, the MAP for an eNB from operator k is:

$$\mathbb{P}^{k|\,i}_{\mathrm{MAP}} = \frac{\mathbb{E}^{x_n}_{\Phi_i}\left[\hat{e}^i_n \hat{e}^i_0\right]}{\mathbb{E}^{x_n}_{\Phi_i}[\hat{e}^i_0]}, \tag{4.38}$$

with the expectation expressions given in (4.39) and (4.40).

Proof For every eNB $x_n \in \Phi_i \cap B^c(0, r_0)$, given that eNB_0 is located at x_0, the conditional MAP is derived as follows:

$$\begin{aligned}\mathbb{P}^{k|\,i}_{\text{MAP}} &= \mathbb{P}\big[e^i_n = 1 \big| e^i_0 = 1, x_0 = (r_0, 0), x_n \in \Phi_i\big] \\ &\overset{(a)}{=} \mathbb{P}^{x_n}_{\Phi_i}\big[e^i_n = 1 \big| e^i_0 = 1, x_0 \in \Phi_i, \Phi_i(B^o(0, r_0)) = 0\big] \\ &\overset{(b)}{=} \frac{\mathbb{P}^{x_n, x_0}_{\Phi_i}\big[\hat{e}^i_n = 1, \hat{e}^i_0 = 1\big]}{\mathbb{P}^{x_n, x_0}_{\Phi_i}\big[\hat{e}^i_0 = 1\big]} \overset{(c)}{=} \frac{\mathbb{E}^{x_n}_{\Phi_i}\big[\hat{e}^i_n \hat{e}^i_0\big]}{\mathbb{E}^{x_n}_{\Phi_i}\big[\hat{e}^i_0\big]},\end{aligned} \tag{4.41}$$

where (a) follows from re-writing $x_0 = (r_0, 0)$ as $x_0 \in \Phi_i, \Phi_i(B^o(0, r_0)) = 0$. (b) follows from Bayes rule and de-conditioning on $\Phi_i(B^o(x_0, r_0)) = 0$. Step (c) follows from Slivnyak′s theorem. The modified access indicators are:

$$\begin{aligned}\hat{e}^i_n = &\prod_{x_m \in (\Phi_i \cap B^c(0,r_0) + \delta_{x_0}) \setminus \{x_n\}} \left(\mathbb{1}_{t^i_m \geq t^i_n} + \mathbb{1}_{t^i_m < t^i_n} \mathbb{1}_{h^i_{mn}/\ell_{mn} \leq \xi_i/p_i}\right) \\ &\cdot \prod_{j \neq i}^{M} \prod_{x_l \in \Phi_j} \left(\mathbb{1}_{t^j_l \geq t^i_n} + \mathbb{1}_{t^j_l < t^i_n} \mathbb{1}_{h^{ji}_{ln}/\ell_{ln} \leq \xi_i/p_j}\right),\end{aligned} \tag{4.42}$$

$$\begin{aligned}\hat{e}^i_0 = &\prod_{x_m \in \Phi_i \cap B^c(0,r_0)} \left(\mathbb{1}_{t^i_m \geq t^i_0} + \mathbb{1}_{t^i_m < t^i_0} \mathbb{1}_{h^i_{m0}/\ell_{m0} \leq \xi_i/p_i}\right) \\ &\cdot \prod_{j \neq i}^{M} \prod_{x_l \in \Phi_j} \left(\mathbb{1}_{t^j_l \geq t^i_0} + \mathbb{1}_{t^j_l < t^i_0} \mathbb{1}_{h^{ji}_{l0}/\ell_{l0} \leq \xi_i/p_j}\right).\end{aligned} \tag{4.43}$$

Inserting (4.43) in the denominator expectation $\mathbb{E}^{x_n}_{\Phi_i}[\hat{e}^i_0]$, (4.40) follows from Slivnyak′s theorem, setting $t^i_0 = t$, then de-conditioning on t, and using the P.G.FL of a PPP. The numerator of (4.41) is derived similarly to obtain (4.39).

From Corollary 1, we can approximate the SINR coverage probability of UE_0 with threshold θ as:

$$\begin{aligned}\mathbb{P}^i_{\text{SINR}}(\theta) \approx \int_0^\infty \exp\Bigg(&-\sum_{i \neq j}^{M} \int_{\mathbb{R}^2} \frac{\theta \ell(r_0) \lambda_j \mathbb{P}^{j|\,i}_{\text{MAP}}}{\frac{p_i}{p_j}\ell(x) + \theta \ell(r_0)} \mathrm{d}x - \\ &\int_{\mathbb{R}^2 \setminus B(0,r_0)} \frac{\theta \ell(r_0) \lambda_i \mathbb{P}^{j|\,i}_{\text{MAP}}}{\ell(x) + \theta \ell(r_0)} \mathrm{d}x - \mu \theta \ell(r_0) \frac{\sigma^2_N}{p_i}\Bigg) f_R(r_0) \mathrm{d}r_0.\end{aligned} \tag{4.44}$$

Performance Evaluation

Simulation results are presented to assess the accuracy of our expressions for the SINR distributions and to get insights into the performance of coexisting LAA networks. We focus on a very dense network deployment of $200\,\text{eNBs/km}^2$ per operator. We consider a total user density of $\lambda^{\text{UE}} = 5000\,\text{UEs/km}^2$ divided equally over the number of operators. The power fading parameter is set to $\mu = 1$.

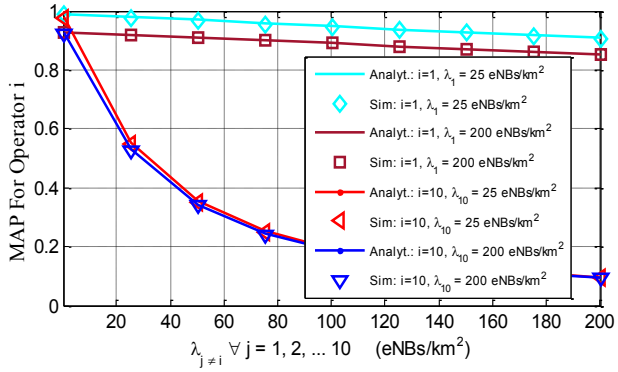

Figure 4.9: Medium Access Probability (MAP) for LAA eNBs of Operator 1 ($q_1 = 1$) and Operator 10 ($q_{10} = 32$).

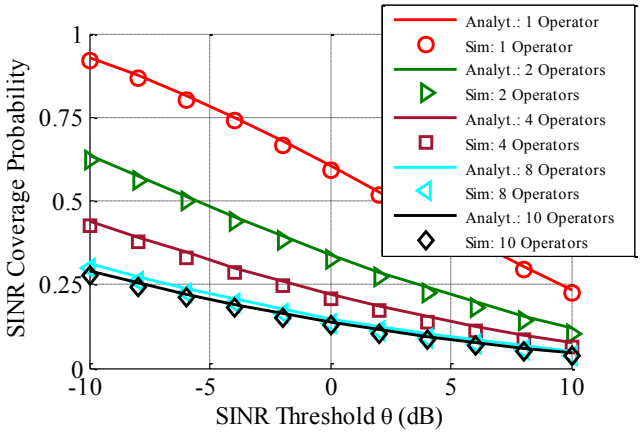

Figure 4.10: SINR coverage probability of UE_0 for Operator 1

For demonstration purposes, we fix the number of coexisting LAA operators to 10, where a scenario for the adopted contention window parameters is shown in Table 4.21. The accuracy of the analytical results from Section 4.2.2 were validated against the simulation results using a spatial discrete event simulator for LAA as in [32, 37].

Figures 4.9 and 4.10 shows the MAP and the SINR coverage probability of UE_0. We can observe that (4.36) as well as the approximation in (4.44) provide an accurate fit to the simulation points for the several operators scenarios.

The impact of the coexistence of these operators on the MAP of the eNBs of each operator is shown in Fig. 4.9 for a sensing threshold $\xi_i = -72$ dBm $\forall\, i \in [1, M]$. In particular, we present the MAP of Operators 1 and 10. We can see that the MAP is constant over the operators own λ_i, and that MAP of Operator 1 is much higher than that of Operator 10. This is expected given the much lower back-off range from Operator 1. It highlights that (while an LBT mechanism is key to enable coexistence) further regulatory steps may be required to ensure the harmonious coexistence of LAA operators given the major impact

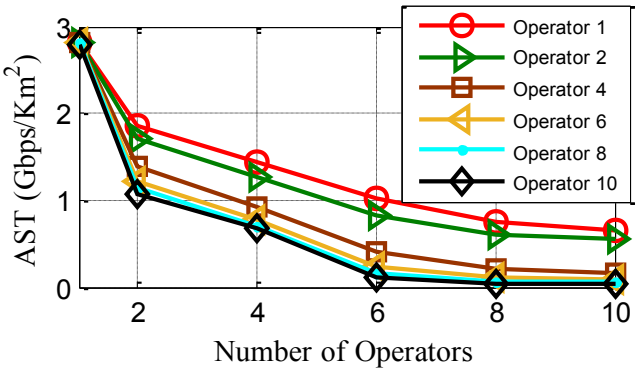

Figure 4.11: Area system throughput per operator

that the contention window size could have on the performance of some operators.

We also note from Fig. 4.10 that as the number of coexisting LAA operators increases from 1 to 8, there is a large decrease in the SINR coverage probability for a given SINR threshold. However, this coverage difference is small when the number of coexisting operators is above 8.

Based on the MAP and SINR coverage probability, we further analyze the performance of the coexistence scenario of 10 operators. Fig. 4.11 shows the AST per operator versus the number of operators. We investigate the trade-off between having many operators and few operators for a fixed density of subscribers in the service area. We can see that, on average, the AST per operator is higher when the number of operators M is small and hence the number of users per operator ($\lambda_i^{\mathrm{UE}} = \lambda^{\mathrm{UE}}/M$) is large. This effect is more evident on operators using larger contention windows (larger q_i), such as Operator 10 where the AST drops by 2 Gbps/km^2 from the starting scenario of 2 operators. Note that the AST of Operators 6, 8, and 10 gets drastically reduced as the number of operators increase to 10 whereas Operators 1 and 2 maintain the best performance. These results indicate that there is a need to set a limit on the number of operators expected to serve the same area, as an over-population of operators can lead to a severe degradation of their performance.

4.2.3 Summary

We have presented a framework based on stochastic geometry for analyzing the performance of coexisting LAA networks in an unlicensed band. It shows, as expected, that an increasing number of operators, whose devices use different contention window sizes within the same band, impacts the area system throughput of most operators and that the AST of some operators may get drastically reduced.

Chapter 5

Coexistence of DSRC and IEEE 802.11ax Wi-Fi in the Unlicensed Band

We discuss in this chapter the impact of the possible coexistence of the DSRC and Wi-Fi networks on each other in these bands through an analytical framework that is based on performance metrics obtained using stochastic geometry. The proposed framework helps in increasing the awareness among regulatory bodies regarding the possible benefits and drawbacks of approving such proposal.

5.1 System Model

In this section we describe the channel access model, the spatial location model, and the radio channel model, for both the IEEE 802.11p DSRC and the IEEE 802.11ax Wi-Fi networks.

5.1.1 Channel Access Model

IEEE 802.11p

This 802.11 amendment is termed as the Dedicated Short Range Communication (DSRC) standard, and defines the lower MAC and PHY layer protocols. This standard falls actually under the umbrella of a wider scope standard, namely the Wireless Access in Vehicular Environments (WAVE) standard, which also covers the set of IEEE 1609.x protocols that define the upper MAC and network layers.

The DSRC bandwidth comprises seven channels, six of which are service channels (SCHs) and one is the control channel (CCH). Each channel bandwidth is 10 MHz, the first channel (Channel 172) starts at 5.855 GHz, while the center Channel 178 is the control channel, which is allocated mainly for communicating road safety. These channels and their allocations are identified in Figure 5.1.

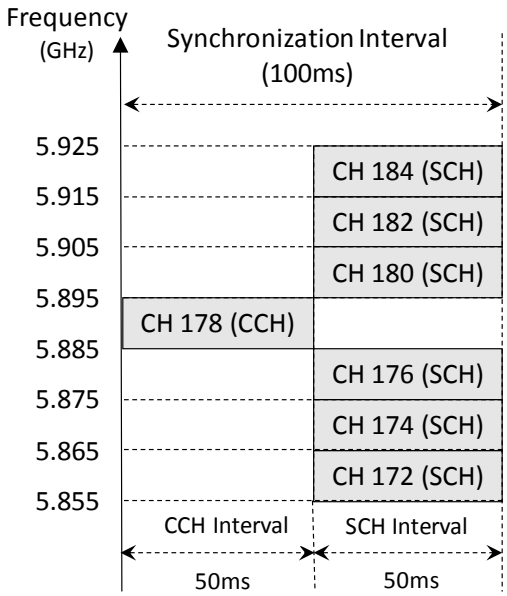

Figure 5.1: DSRC Channel Allocation

Vehicles with a single radio use time division to operate on the CCH and SCHs. Details related to multi-channel operations are defined in the upper layer IEEE 1609.x protocols. Fig. 1 illustrates the basic time division concept defined in the IEEE 1609.4 protocol, where time is segmented into synchronized periods, the default duration of each is 100 millisecond (ms). Each synchronized period consists of one CCH interval followed by an SCH interval, and the default duration for each interval is 50 ms. Each CCH and SCH interval begins with a 4 ms guard interval, which is used by the radio to transfer control from one channel to another.

Compared to other 802.11 standards, 802.11p has a number of distinguishing features. For example, the transmitter broadcasts packets on the CCH to all other nodes in the network. In order to prevent the network from flooding with Acknowledgment messages (ACKs), 802.11p receivers do not send ACKs to the transmitter. Thus, there is no feedback mechanism provided by the receiver, and hence, the Contention Window size of the 802.11p transmitter remains fixed.

Moreover the IEEE 802.11p protocol employs the EDCA mechanism for contention based prioritized QoS support. According to EDCA, a station (node) can implement up to four access categories (ACs) with different priorities corresponding to voice (AC 3), video (AC 2), best effort (AC 1), and background traffic (AC 0) [72]. Each AC has an independent MAC queue entity, which can be identified by a set of distinct channel access parameters, including the CW, AIFS, and Arbitrary Inter-Frame Space Number (AIFSN[AC]). When using the CSMA/CA protocol, a DSRC node performs the clear channel assessment (CCA) process

to detect the presence of active transmitters for which the received signal power exceeds a certain detection threshold. However, 802.11p nodes cannot decode the 20 MHz Wi-Fi preambles. Hence the DSRC node uses energy detection to detect the presence of any Wi-Fi interferer by using an energy detection threshold Γ_{ed}. Using the CCA process, a channel is determined busy if the intending transmitter detects another DSRC signal above the carrier sense (CS) threshold Γ_{cs}, or if any other signal that is not decodable, such as the Wi-Fi signal that is detected above the energy detection (ED) threshold Γ_{ed}. If the channel is found idle, the DSRC node will follow before transmission a random back-off period that is selected randomly from a contention window, which is a set of possible values with a predefined maximum and minimum, depending on the channel access class, to determine the priority for a the DSRC node to access the medium.
We define the contender of a DSRC node x_n as the other DSRC nodes, Wi-Fi APs, and Wi-Fi users from which the received power at x_n exceeds thresholds Γ_{cs}, Γ_{ed}, and Γ_{ed} respectively. Each DSRC node x_n has an independent mark t_n^V that is uniformly distributed in the interval $[0, CW_V]$ where CW is the contention window size. Given that safety messages ought to be treated with high priority, which is the priority of voice traffic (AC 3) in EDCA, we classified the CCH traffic in our analysis as voice. On the other hand, we considered the worst-case scenario for Wi-Fi traffic, namely voice traffic. Hence, in this chapter we conduct the coexistence study using voice traffic for both DSRC and Wi-Fi. Consequently, we consider t_{VO} to be uniformly distributed in the intervals [0, 7], as in [44], [72]. Each DSRC node is retained when contending for channel access if it has a smaller timer (or back-off period) than all of its contenders. A medium access indicator e_n^V is assigned to each DSRC node which is equal to one if the DSRC node is allowed to transmit by the corresponding MAC layer protocol, and zero otherwise.

IEEE 802.11ax - Next Generation Wireless LANs

The IEEE 802.11ax standard presents several enhancements for high efficiency WLANs where it defines two modes of operation namely, the single-user (SU) mode and the multi-user (MU) mode [47, 48, 13]. In the SU mode, Wi-Fi users/APs send and receive data one at a time once they secure access to the medium using the CSMA/CA protocol, as defined in the legacy IEEE 802.11 standard. On the other hand, the MU mode defines simultaneous operations of multiple WiFi users. The MU mode is further divided into downlink (DL) and uplink (UL) MU modes.

The MU mode is enabled by the OFDMA technology that builds on the existing OFDM digital modulation scheme, where the 802.11ax standard further assigns a specific set of subcarriers to individual users. Hence, it divides the existing 802.11 channels with 20, 40, 80 and 160 MHz widths into smaller sub-

channels called resource units (RUs) with a predefined number of subcarriers. In this context, the AP decides how to allocate the channel based on MU traffic needs, where it may allocate the whole channel e.g. 20 MHz to one user at a time (as in the case of 802.11ac), or it may partition it to serve multiple users simultaneously. For example, in case of 20 MHz channel, the AP may partition the channel into $N_{RU} = 2$, 4 or 9 RUs.

In the DL MU mode, the AP serves multiple data transmissions associated with Wi-Fi users at the same time. On the other hand, in the UL MU mode there are simultaneous UL transmissions of data from multiple users to the AP. Hence, in the MU mode, the AP acts as a central coordinator for scheduling transmissions, and hence users will not transmit in this case unless the AP assigns them RUs. In the case of simultaneous DL transmissions, after successful access to the channel, the AP will send DL data to several users simultaneously on different RUs. Whereas in case of simultaneous UL transmissions, the AP will transmit a trigger frame (TF) after accessing the channel. Hence, in both cases the AP will initially contend using the EDCA parameters for channel access as in the case of SU mode, and it is clear therefore that the access of the user depends on the probability of the AP in accessing the channel.

In order to schedule UL transmissions, the AP polls the users with a TF. After receiving the trigger frame, two channel access mechanisms may be used by the user, specifically the trigger-based deterministic access (DA) and the trigger-based random access (RA). In the trigger-based DA mechanism, the user will send a data frame on the scheduled RUs that were indicated in the TF, while in the trigger-based RA, users that receive the TF will contend for channel access on the specified RUs using the CSMA/CA protocol. Next, users that win access to the medium on a randomly selected RU from a set of specified RUs, will send their data frames to the AP. As the AP has to contend for channel access, it could choose any access category (AC) that may give the AP higher priority in accessing the channel as compared to its associated users. The different ACs are defined based on the parametrized arbitration inter-frame spacing (AIFS[AC]) interval and the contention window size to differentiate between traffic types (voice, video, best effort, and background traffic) within each user/AP.

Using the CSMA/CA protocol, a Wi-Fi AP/user performs also the Clear Channel Access (CCA) process to detect the presence of active transmitters for which the received signal power exceeds a certain detection threshold. Using the CCA process, a channel is determined busy if the intending transmitter detects another Wi-Fi signal above the CS threshold Γ_{cs}, or if any other signal that is not decodable, such as a DSRC signal (Wi-Fi transmitters have no support for preamble detection of DSRC 10 MHz-wide signals) that is detected above the ED threshold Γ_{ed}.
If the channel is found idle, the Wi-Fi device will then follow before transmission a random back-off period that is selected randomly from a contention window

of the corresponding channel access class. As mentioned earlier, we define the contender of a Wi-Fi AP z_i as the other Wi-Fi APs, Wi-Fi user, and DSRC nodes from which the received power at z_i exceeds thresholds Γ_{cs}, Γ_{cs}, and Γ_{ed} respectively. Similarly, we define the contenders of a Wi-Fi user y_p as the other Wi-Fi users, Wi-Fi APs, and DSRC nodes from which the received power at y_p exceeds thresholds Γ_{cs}, Γ_{cs}, and Γ_{ed} respectively.

Each Wi-Fi AP z_i has an independent mark t_i^D that represents the random back-off period, which is uniformly distributed in the interval $[0, 7]$ in case of voice traffic [73]. Also, each Wi-Fi user z_n has an independent mark t_n^U that is uniformly distributed in the interval $[0, 7]$. Each Wi-Fi user/AP is retained when contending for channel access if it has a smaller timer (or back-off period) than all its contenders. A medium access indicator e_p^U is assigned to each Wi-Fi user (e_i^D to each AP) which is equal to one if the Wi-Fi user or AP are allowed to transmit by the corresponding MAC layer protocol and zero otherwise.

In the considered model for Wi-Fi channel access, the derivation of the SINR coverage probability at the AP in the UL accounts for hidden node transmissions where two Wi-Fi users that operate using EDCA and are associated with the same AP may get access to the channel simultaneously given that they are not in the contention domain of each other. Note that we denote by medium access probability (MAP), the Palm probability [39] that the medium access indicator of a Wi-Fi user/AP/DSRC node is equal to 1. This channel access model, which may have some limitations with its fixed contention window size (that does not capture the exponential backoff and the dynamics of the timer history), has shown its ability as a conservative model for the CSMA/CA in IEEE 802.11 standard. This was demonstrated in [32], where the authors showed that the stochastic geometry models for the MAP provided an accurate matching versus the simulation results generated using the NS-2 simulator.

5.1.2 Spatial Location Model

We consider mainly a scenario in which a DSRC network coexists with an IEEE 802.11ax Wi-Fi network in a single unlicensed frequency band where the 10 MHz DSRC CCH is overlapped by a 20 MHz Wi-Fi channel.

In the considered DSRC network, the wireless DSRC nodes are located on a system of roads, which we model as lines with corresponding line density λ_l. In addition, the wireless DSRC nodes, including vehicular nodes and road side units (RSUs), on each line (road) are modeled using a density λ_v. Then, the location of DSRC nodes having traffic for transmission are modeled using an equivalent independent homogeneous 2D Poisson point process (PPP) $\Phi_{D_i} = \{\zeta_{d_i}^{D_i}\}$ with density $\lambda_{D_i} = \lambda_l \times \lambda_{d_i}$, where the sub-index $i \in \{1, 2\}$ is used to identify the DSRC network throughout the chapter.

Although other models may be more accurate, the authors in [71] showed that in case of high road density and low node density, the 2D homogeneous

PPP model shows similar results when compared to more sophisticated models, such as the Cox process-based model that is based on modeling the roads using a Poisson line process (PLP) and the location of nodes on each road as a 1D PPP. This is due to the fact that when the density of nodes on each line is low, a small number of nodes may appear to be aligned on a straight line. Hence, nodes will look uniformly distributed in the whole 2D plane just as a PPP. Nevertheless, we still believe it will be worthwhile to study the use of PLP for modeling the roads and its effect on performance, but due to the steep complexity of the PLP derivations, we elected to treat this in a future work that would build upon this work.

On the other hand, we model the locations of 802.11ax Wi-Fi APs and users (mostly pedestrians), having traffic for transmission and co-existing in the same band, as realizations of two independent 2D homogeneous PPP on $\mathbb{R}^2$. The Wi-Fi users process with persistent uplink (UL) traffic is denoted as $\Phi_U = \{\zeta_u\}$ and has intensity λ_U, while the Wi-Fi APs process with persistent downlink (DL) traffic is denoted as $\Phi_W = \{\zeta_w\}$ with intensity λ_W.

Thus, based on Slyvniak′s theorem [39], we study the performance of the typical receiving node without affecting the distribution of the rest of the receiving nodes process. In particular, we analyze the performance of a typical receiving DSRC node as well as that of the typical Wi-Fi user/AP in the DL/UL, respectively . The typical receiving node is assumed to be at the origin, and it is associated with its closest transmitting node, which provides the strongest average received power [71]. For the UL of Wi-Fi, we consider the scenario where the Wi-Fi user connects to the Internet through the closest AP and that no direct user-user (i.e., device-to-device (D2D)) communication exists. Furthermore, index 0 is used for the typical receiver and its serving (transmitting) node which will be called the tagged node in the rest of the chapter. The link between the tagged DSRC node $\zeta_0^{D_1}/\zeta_0^{D_2}$ and the typical DSRC node is referred to as the typical DSRC link ($\zeta_0^{D_1}$ and $\zeta_0^{D_2}$ are DSRC nodes belonging to two different networks represented by the processes Φ_{D_1} and Φ_{D_2}, respectively). In addition, the link between the tagged AP ζ_0^W/user ζ_0^U and the typical Wi-Fi user/AP in the DL/UL is referred to as the typical Wi-Fi DL/UL, respectively.

Given that Φ_{D_i} is a PPP with intensity λ_{D_i}, the probability density function (PDF) of the distance from the tagged DSRC node to the typical DSRC node is $f_{\|\zeta_0^{D_i}\|}(r) = 2\pi r\lambda_{D_i} e^{-\lambda_{D_i}\pi r^2}$. Similarly, the PDF of the distance from the tagged AP to the typical user in the DL is $f_{\|\zeta_0^W\|}(r) = 2\pi r\lambda_W e^{-\lambda_W \pi r^2}$. Also, given that the Wi-Fi users that are associated with an AP should be those ones inside the Voronoi cell of this AP, the distribution of $\|\zeta_0^W\|$ can be approximated by that of $\|\zeta_0^U\|$, where UL and DL links are assumed to be reciprocal. Hence the PDF of the distance from the the tagged Wi-Fi user to the typical AP in the UL is $f_{\|\zeta_0^U\|}(r) = 2\pi r\lambda_W e^{-\lambda_W \pi r^2}$.

5.1.3 Radio Channel Model

We denote by $l(d)$ the path loss between the transmitter and the receiver which are separated by a distance d. We use here a common free space path loss model with reference distance of one meter for both DSRC and Wi-Fi links. Hence, the path loss $l(d)$ is given by $l(d) = \left(\frac{4\pi}{\Lambda_c}\right)^2 \times d^{\alpha}$ where Λ_c represents the wavelength and α is the path-loss exponent. Also, we assume that all channels are subject to i.i.d Rayleigh fading where each fading variable is exponentially distributed with parameter μ.

5.1.4 Performance Metrics

Given that the tagged DSRC node $\zeta_0^{D_1} \in \Phi_{D_1}$ transmits with power P_{D_1}, the received SINR at the typical receiving DSRC node is:

$$\mathrm{SINR}_0^{D_1} = \frac{P_{D_1} G_{0,0}^{D_1} / \ell(\|\zeta_0^{D_1}\|)}{I_{D_1} + \sigma_N^2}, \tag{5.1}$$

where I_{D_1} is the interference resulting from the coexisting transmissions, and σ_N^2 is the thermal noise power at the typical receiving node, which is assumed to be much smaller than the interference power, and hence, we neglect it. The interference in case of DSRC-only networks can be stated as

$$I_{D_1} = \sum_{\zeta_{d_1} \in \Phi_{D_1} \setminus \{\zeta_0^{D_1}\}} P_{D_1} G_{d_1,0}^{D_1} e_{d_1}^{D_1} / \ell(\|\zeta_{d_1}\|) + \sum_{\zeta_{d_2} \in \Phi_{D_2}} P_{D_2} G_{d_2,0}^{D_2 D_1} e_{d_2}^{D_2} / \ell(\|\zeta_{d_2}\|) \tag{5.2}$$

where as in case of DSRC-Wi-Fi coexistence, it can be stated as:

$$I_{D_1} = \sum_{\zeta_{d_1} \in \Phi_{D_1} \setminus \{\zeta_0^{D_1}\}} P_{D_1} G_{d_1,0}^{D_1} e_{d_1}^{D_1} / \ell(\|\zeta_{d_1}\|) + \sum_{\zeta_w \in \Phi_W} P_W G_{w,0}^{W D_1} e_w^W / \ell(\|\zeta_w\|) + \sum_{\zeta_u \in \Phi_U} P_U G_{u,0}^{U D_1} e_u^U / \ell(\|\zeta_u\|) \tag{5.3}$$

On the other hand, given that the tagged AP $\zeta_0^W \in \Phi_W$ transmits with power P_W, the received SINR at the receiving Wi-Fi user is:

$$\mathrm{SINR}_0^W = \frac{P_W G_{0,0}^W / \ell(\|\zeta_0^W\|)}{I_W + \sigma_N^2}, \tag{5.4}$$

where

$$I_W = \sum_{\zeta_w \in \Phi_W \setminus \{\zeta_0^w\}} P_W G_{w,0}^W e_w^W / \ell(\|\zeta_w\|) + \sum_{\zeta_{d_1} \in \Phi_{D_1}} P_{D_1} G_{d_1,0}^{D_1 W} e_{d_1}^{D_1} / \ell(\|\zeta_{d_1}\|) + \sum_{\zeta_u \in \Phi_U} P_U G_{u,0}^{UW} e_u^U / \ell(\|\zeta_u\|) \tag{5.5}$$

Similarly, given that the tagged user $\zeta_0^W \in \Phi_U$ transmits with power P_U, the received SINR at the receiving Wi-Fi AP is:

$$\mathrm{SINR}_0^U = \frac{P_U G_{0,0}^U / \ell(\|\zeta_0^U\|)}{I_U + \sigma_N^2}, \tag{5.6}$$

where

$$I_U = \sum_{\zeta_u \in \Phi_U \setminus \{\zeta_0^u\}} P_U G_{u,0}^U e_u^U / \ell(\|\zeta_u\|) + \sum_{\zeta_{d_1} \in \Phi_{D_1}} P_{D_1} G_{d_1,0}^{D_1 U} e_{d_1}^{D_1} / \ell(\|\zeta_{d_1}\|) + \sum_{\zeta_w \in \Phi_W} P_W G_{w,0}^{WU} e_w^W / \ell(\|\zeta_w\|) \tag{5.7}$$

From (5.1), (5.4), and (5.6), the SINR coverage probability with a SINR threshold θ, is defined as $\Pr(\mathrm{SINR}_0^{\mathrm{X}} > \theta | e_0^X = 1)$. Based on this definition and that of the medium access probability (MAP) $\mathbb{P}_{\mathrm{MAP}}^X = \mathrm{E}[e_0^X]$ (derived in the following section), the area system throughput (AST) is defined as:

$$\mathrm{AST}^i = \lambda_X \; \mathbb{P}_{\mathrm{MAP}}^X \; BW \int_0^\infty \mathbb{P}_{\mathrm{SINR}}^X (2^\rho - 1) \mathrm{d}\rho. \tag{5.8}$$

Where X is D_1, W, or U, depending on the scenario considered. The MAP accounts for the expected fraction of time that the tagged DSRC node/Wi-Fi AP/Wi-Fi user has access to the channel, and hence it is a measure of the expected fraction of active transmitters, over a fully overlapped coverage area.

Since Φ_{D_1}, Φ_W, and Φ_U are stationary and isotropic, the introduced performance metrics are invariant with respect to the angle of the tagged transmitter, which we therefore, locate at the polar coordinate $(r_0, 0)$. We also define the following functions to be used throughout the chapter. First,

$$N_X(\zeta_1, r, \Gamma) = \lambda_X \int_{\mathbb{R}^2 \setminus B(0,r)} \exp\left(-\mu \frac{\Gamma_X}{P_X} \ell(\zeta, \zeta_1)\right) \mathrm{d}x, \tag{5.9}$$

represents the expected number of transmitters in $\mathbb{R}^2 \setminus B(0,r)$ whose signal power at $\zeta \in \mathbb{R}^2$ exceeds the activity threshold Γ_X. Second,

$$C_X(\zeta_1, \Gamma_1, \zeta_2, \Gamma_2, r) = \lambda_X \int_{\mathbb{R}^2 \setminus B(0,r)} \exp\left(-\mu \frac{\Gamma_1}{P_1} \ell(\zeta, \zeta_1) - \mu \frac{\Gamma_2}{P_2} \ell(\zeta, \zeta_2)\right) \mathrm{d}x, \tag{5.10}$$

represents the expected number of transmitters in $\mathbb{R}^2 \setminus B(0,r)$ whose signal power at $\zeta_1 \in \mathbb{R}^2$ and $\zeta_2 \in \mathbb{R}^2$ in general exceeds thresholds Γ_1 and Γ_2, respectively. Equations (5.9) and (5.10) in addition to (5.11) and (5.12) below are used to simplify the expressions of the conditional MAP later on.

$$\begin{aligned} &\Theta_N\Big(\zeta_1, \zeta_2, \zeta_3, \Delta_1, CW_1, \Delta_2, CW_2, N_1(t), N_2(t')\Big) = \\ &\frac{1 - \exp\big(-\mu \zeta_3 l(\|\zeta_1 - \zeta_2\|)\big)}{CW_1 CW_2} \int_{\Delta_2}^{CW_2 + \Delta_2} \int_{\Delta_1}^{CW_1 + \Delta_1} \exp\Big[-N_1(t) - N_2(t')\Big] \mathrm{d}t \mathrm{d}t' \end{aligned} \tag{5.11}$$

$$\begin{aligned} &\Theta_D\Big(\zeta_1, \zeta_2, \Delta, CW, N_1(t), N_2(t)\Big) = \\ &\frac{1}{CW} \int_{\Delta}^{CW + \Delta} \Big(1 - N_1(t) \exp\big[-\mu \zeta_2 l(\|\zeta_1\|)\big]\Big) \exp\big[-N_2(t)\big] \mathrm{d}t \end{aligned} \tag{5.12}$$

5.2 Baseline Scenario: Analysis of DSRC IEEE 802.11p Networks

In this section, we analyze the possible co-existence of two DSRC networks with each others. Here, by a DSRC network we mean a set of road side units (RSUs) along with their respective users (vehicles), whereby these RSUs are managed by an operator in a similar manner as a network of WiFi access points (APs). Hence, in a particular geographic area, there may be one or more DSRC networks that are managed by different operators to offer services to subscribing vehicles (and perhaps limited services to non-subscribers). From an analysis point of view, we extend the following definition of fair coexistence that was used in the context of LTE License-Assisted Access (LAA) - Wi-Fi coexistence: "LAA network should not impact a Wi-Fi network more than an additional Wi-Fi network" [60]. Hence, we apply it for DSRC-Wi-Fi coexistence through constructing a baseline scenario of two DSRC networks where a fair coexistence would be defined as: "A Wi-Fi network should not impact a DSRC network more than an additional DSRC network".

When DSRC nodes (vehicles and RSUs) co-exist with each other in the same band, each node will contend using the EDCA mechanism to access the channel. Hence, a DSRC node $\zeta_{d_1'} \in \Phi_{D_1} / \zeta_{d_2'} \in \Phi_{D_2}$ will have the medium access indicator $e_{d_1'}^{D_1}$ / $e_{d_2'}^{D_2}$ in the case of coexistence with other DSRC nodes that is derived as follows:

$$
\begin{aligned}
e_{d_1'}^{D_1} &= \prod_{\zeta_{d_1} \in \Phi_{D_1} \setminus \{\zeta_{d_1'}\}} \left(\mathbb{1}_{t_{d_1}^{D_1} \geq t_{d_1'}^{D_1}} + \mathbb{1}_{t_{d_1}^{D_1} < t_{d_1'}^{D_1}} \mathbb{1}_{G_{d_1 d_1'}^{D_1} / l\left(\|\zeta_{d_1} - \zeta_{d_1'}\|\right) \leq \Gamma_{cs}/P_{D_1}} \right) \\
&\times \prod_{\zeta_{d_2} \in \Phi_{D_2}} \left(\mathbb{1}_{t_{d_2}^{D_2} \geq t_{d_1'}^{D_1}} + \mathbb{1}_{t_{d_2}^{D_2} < t_{d_1'}^{D_1}} \mathbb{1}_{G_{d_2 d_1'}^{D_2 D_1} / l\left(\|\zeta_{d_2} - \zeta_{d_1'}\|\right) \leq \Gamma_{cs}/P_{D_2}} \right) \\
e_{d_2'}^{D_2} &= \prod_{\zeta_{d_1} \in \Phi_{D_1}} \left(\mathbb{1}_{t_{d_1}^{D_1} \geq t_{d_2'}^{D_2}} + \mathbb{1}_{t_{d_1}^{D_1} < t_{d_2'}^{D_2}} \mathbb{1}_{G_{d_1 d_2'}^{D_1 D_2} / l\left(\|\zeta_{d_1} - \zeta_{d_2'}\|\right) \leq \Gamma_{cs}/P_{D_1}} \right) \\
&\times \prod_{\zeta_{d_2} \in \Phi_{D_2} \setminus \{\zeta_{d_1'}\}} \left(\mathbb{1}_{t_{d_2}^{D_2} \geq t_{d_2'}^{D_2}} + \mathbb{1}_{t_{d_2}^{D_2} < t_{d_2'}^{D_2}} \mathbb{1}_{G_{d_2 d_2'}^{D_2} / l\left(\|\zeta_{d_2} - \zeta_{d_2'}\|\right) \leq \Gamma_{cs}/P_{D_2}} \right)
\end{aligned}
\tag{5.13}
$$

Note that $\mathbb{1}_A$ is the indicator function of the event A, which is equal to one if A exists and zero otherwise. Thus, given that a DSRC node $\zeta_{d_1} / \zeta_{d_2}$ has a timer $t_{d_1}^{D_1} \in [0,7]$ / $t_{d_2}^{D_2} \in [0,7]$, with cumulative distribution function (CDF) $F_{D_1}(t) = F_{D_2}(t) = \frac{t}{7}$, the MAP in the baseline scenario for a tagged DSRC node that belongs to Operator 1 or Operator 2 is given by:

$$
\begin{aligned}
P_{MAP}^{D_1}(\lambda_{D_1}, \lambda_{D_2}) &= \frac{1}{7} \int_0^{\infty} \int_0^{7} \exp\big[- \frac{t}{7} N_{D_1}(\zeta_0^{D_1}, \Gamma_{cs}, r_0) - \frac{t}{7} N_{D_2} \big] \mathrm{d}t \mathrm{d}r_0 \\
P_{MAP}^{D_2}(\lambda_{D_1}, \lambda_{D_2}) &= \frac{1}{7} \int_0^{\infty} \int_0^{7} \exp\big[- \frac{t}{7} N_{D_1} - \frac{t}{7} N_{D_2}(\zeta_0^{D_2}, \Gamma_{cs}, r_0) \big] \mathrm{d}t \mathrm{d}r_0
\end{aligned}
\tag{5.14}
$$

Proof Given that a DSRC node ζ_{d_1}/ζ_{d_2} has a timer $t_{d_1}^{D_1} \in [0,7]$ / $t_{d_2}^{D_2} \in [0,7]$, with cumulative distribution function (CDF) $F_{D_1}(t)=F_{D_2}(t)=\frac{t}{7}$, the MAP in the baseline scenario for a tagged DSRC node is given by:

$$
\begin{aligned}
&\hat{P}_{MAP}^{D_1}(\lambda_{D_1},\lambda_{D_2}) = \mathbb{P}[e_{d_1'}^{D_1}=1 | t_{d_1'}^{D_1}=t, \zeta_0^{D_1}=(0,r_0)] = \mathbb{E}_{\Phi_{D_1}}^{\zeta_{d_1'}}(e_{d_1}^{D_1}) \\
&= \mathbb{E}_{\Phi_{D_1}}^{\zeta_{d_1'}}\Bigg[\prod_{\zeta_{d_1}\in\Phi_{D_1}\setminus\{\zeta_{d_1'}\}} \left(\mathbb{1}_{t_{d_1}^{D_1}\geq t_{d_1'}^{D_1}} + \mathbb{1}_{t_{d_1}^{D_1}<t_{d_1'}^{D_1}} \mathbb{1}_{G_{d_1d_1'}^{D_1}/l\left(\|\zeta_{d_1}-\zeta_{d_1'}\|\right)\leq \Gamma_{cs}/P_{D_1}} \right) \\
&\qquad \times \prod_{\zeta_{d_2}\in\Phi_{D_2}} \left(\mathbb{1}_{t_{d_2}^{D_2}\geq t_{d_1'}^{D_1}} + \mathbb{1}_{t_{d_2}^{D_2}<t_{d_1'}^{D_1}} \mathbb{1}_{G_{d_2d_1'}^{D_2D_1}/l\left(\|\zeta_{d_2}-\zeta_{d_1'}\|\right)\leq \Gamma_{cs}/P_{D_2}} \right) \Bigg] \\
&\overset{(a)}{=} \mathbb{E}_{\Phi_{D_1}}^{!\zeta_{d_1'}}\left[\prod_{\zeta_{d_1}\in\Phi_{D_1}\cap B^c(\zeta_0^{D_1},r_0)} \left(1-F_{D_1}(t)\exp\left(-\mu\frac{\Gamma_{cs}}{P_{D_1}} l(\|\zeta_{d_1}-\zeta_{d_1'}\|)\right)\right)\right] \\
&\qquad \times \mathbb{E}\left[\prod_{d_2\in\Phi_{D_2}} \left(1-F_{D_2}(t)\exp\left(-\mu\frac{\Gamma_{cs}}{P_{D_2}} l(\|\zeta_{d_2}-\zeta_{d_1'}\|)\right)\right)\right] \\
&\overset{(b)}{=} \frac{1}{7}\int_0^7 \exp\Big(- F_{D_1}(t) N_{D_1}(\zeta_0^{D_1},\Gamma_{cs},r_0) - F_{D_2}(t) N_{D_2}\Big)\mathrm{d}t
\end{aligned}
\tag{5.15}
$$

where (a) follows from the fact that Φ_{D_1} and Φ_{D_2} are independent. (b) follows from Slyvniak′s theorem, the probability generating functional (P.G.FL) of the PPP, and by de-conditioning on $t \in [0,7]$ gives the desired result. Then by de-conditioning over r_0 we get the expression in (5.14). ■
However, conditioned on the fact that the tagged DSRC node $\zeta_0^{D_1}=(r_0,0)$ is retained by the CSMA/CA protocol, the probabilities $P_{MAP}^{\zeta_{d_1}/\zeta_0^{D_1}}$ for a DSRC node $\zeta_{d_1}\in\Phi_{D_1}$ and $P_{MAP}^{\zeta_{d_2}/\zeta_0^{D_2}}$ for a DSRC node $\zeta_{d_2}\in\Phi_{D_2}$ to transmit are derived as follows:

$$
\begin{aligned}
P_{MAP}^{\zeta_{d_1}/\zeta_0^{D_1}} &= \frac{\Theta_N\big(\zeta_{d_1},\zeta_0^{D_1},\Gamma_{cs}/P_{D_1},0,7,0,7,N_{D_1^1}(t),N_{D_1^2}(t')\big)}{\Theta_D\big(\zeta_{d_1}-\zeta_0^{D_1},\Gamma_{cs}/P_{D_1},0,7,F_{D_1}(t),N_{D_1^3}(t)\big)} \\
P_{MAP}^{\zeta_{d_2}/\zeta_0^{D_1}} &= \frac{\Theta_N\big(\zeta_{d_2},\zeta_0^{D_1},\Gamma_{cs}/P_{D_2},0,7,0,7,N_{D_2^1}(t),N_{D_1^2}(t')\big)}{\Theta_D\big(\zeta_{d_2}-\zeta_0^{D_1},\Gamma_{cs}/P_{D_2},0,7,F_{D_2}(t),N_{D_1^3}(t)\big)}
\end{aligned}
\tag{5.16}
$$

Where $N_{D_1^1}(t) = \frac{t}{7}\big(- N_{D_2} + C_{D_2}(\zeta_{d_1}-\zeta_0^{D_1}) - N_{D_1}(r_0) + C_{D_1}(\zeta_{d_1},\zeta_0^{D_1})\big)$ and $N_{D_1^2}(t') = \frac{t'}{7}\big(- N_{D_2} - N_{D_1}(r_0)\big)$ and $N_{D_1^3}(t) = -\frac{t}{7}\big(N_{D_1}(\zeta_0^{D_1}) - N_{D_2}\big)$. Similarly, $N_{D_2^1}(t) = \frac{t}{7}\big(- N_{D_2} + C_{D_2}(\zeta_{d_2}-\zeta_0^{D_1}) - N_{D_1}(r_0) + C_{D_1}(\zeta_{d_2},\zeta_0^{D_1})\big)$.

Proof For every DSRC node $\zeta_{d_1'} \in \Phi_{D_1} \cap B^c(\zeta_0^{D_1}, r_0)$, given that the tagged user located at $\zeta_0^{D_1} = (r_0, 0)$, the conditional MAP is derived as in (5.17).

$$\begin{aligned} &\mathbb{P}\big[e_{d_1'}^{D_1} = 1 \big| e_0^{D_1} = 1, \zeta_0^{D_1} = (r_0, 0), \zeta_{d_1'} \in \Phi_{D_1}\big] \\ &\overset{(a)}{=} \frac{\mathbb{P}_{\Phi_{D_1}}^{\zeta_{d_1'}, \zeta_0^{D_1}}\big[\hat{e}_{d_1'}^{D_1} = 1, \hat{e}_0^{D_1} = 1\big]}{\mathbb{P}_{\Phi_U}^{\zeta_{d_1'}, \zeta_0^{D_1}}\big[\hat{e}_0^{D_1} = 1\big]} \overset{(b)}{=} \frac{\mathbb{E}_{\Phi_{D_1}}^{\zeta_{d_1'}}\big[\hat{e}_{d_1}^{D_1}\hat{e}_0^{D_1}\big]}{\mathbb{E}_{\Phi_{D_1}}^{\zeta_{d_1'}}\big[\hat{e}_0^{D_1}\big]} \end{aligned} \tag{5.17}$$

where (a) follows from re-writing $\zeta_0^{D_1} = (r_0, 0)$ as $\zeta_0^{D_1} \in \Phi_{D_1}, \Phi_{D_1}(B^o(\zeta_0^{D_1}, r)) = 0$. Then by using Bayes rule and de-conditioning on $\Phi_{D_1}(B^o(\zeta_0^{D_1}, r_0)) = 0$. Step (b) follows from Slyvniak's theorem. The modified access indicators for $\zeta_0^{D_1}$ and $\zeta_{d_1'}$ are shown in (5.18). Then, the numerator $\mathbb{E}_{\Phi_U}^{z_n}(\hat{e}_n^U \hat{e}_0^U)$ and the denominator $E_{\Phi_U}^{z_n}[\hat{e}_0^U]$can be derived using Slyvniak's theorem,P.G.FL of PPP, and by deconditioning on t.■

$$\begin{aligned} \hat{e}_{d_1'}^{D_1} &= \prod_{\zeta_{d_1} \in (\Phi_{D_1} \cap B^c(\zeta_0^{D_1}, r_0) + \delta_{\zeta_0^{D_1}}) \setminus \{\zeta_{d_1'}\}} \left(\mathbb{1}_{t_{d_1}^{D_1} \geq t_{d_1'}^{D_1}} + \mathbb{1}_{t_{d_1}^{D_1} < t_{d_1'}^{D_1}} \mathbb{1}_{G_{d_1 d_1'}^{D_1} / l\left(\|\zeta_{d_1} - \zeta_{d_1'}\|\right) \leq \Gamma_{cs}/P_{D_1}} \right) \\ &\times \prod_{\zeta_{d_2} \in \Phi_{D_2}} \left(\mathbb{1}_{t_{d_2}^{D_2} \geq t_{d_1'}^{D_1}} + \mathbb{1}_{t_{d_2}^{D_2} < t_{d_1'}^{D_1}} \mathbb{1}_{G_{d_2 d_1'}^{D_2 D_1} / l\left(\|\zeta_{d_2} - \zeta_{d_1'}\|\right) \leq \Gamma_{cs}/P_{D_2}} \right) \\ \hat{e}_0^{D_1} &= \prod_{\zeta_{d_1} \in \Phi_{D_1} \cap B^c(\zeta_0^{D_1}, r_0)} \left(\mathbb{1}_{t_{d_1}^{D_1} \geq t_0^{D_1}} + \mathbb{1}_{t_{d_1}^{D_1} < t_0^{D_1}} \mathbb{1}_{G_{d_1 0}^{D_1} / l\left(\|\zeta_{d_1} - \zeta_0^{D_1}\|\right) \leq \Gamma_{cs}/P_{D_1}} \right) \\ &\times \prod_{\zeta_{d_2} \in \Phi_{D_2}} \left(\mathbb{1}_{t_{d_2}^{D_2} \geq t_0^{D_1}} + \mathbb{1}_{t_{d_2}^{D_2} < t_0^{D_1}} \mathbb{1}_{G_{d_2 0}^{D_2 D_1} / l\left(\|\zeta_{d_2} - \zeta_0^{D_1}\|\right) \leq \Gamma_{cs}/P_{D_2}} \right) \end{aligned} \tag{5.18}$$

Hence, given the tagged DSRC node is located at $\zeta_0^{D_1} = (r_0, 0)$, the SINR coverage probability of the typical receiving DSRC node with SINR threshold T is approximated as follows:

$$\begin{aligned} \hat{p}_{SINR}^{D_1}(T, \lambda_{D_1}, \lambda_{D_2}) \approx \int_0^\infty &\exp\left(- \int_{\mathbb{R}^2 \setminus B(0, r_0)} \frac{T l(r_0) \lambda_{D_1} P_{MAP}^{\zeta_{d_1}/\zeta_0^{D_1}}}{l(\|\zeta\|) + T l(r_0)} \mathrm{d}\zeta \right) \\ &\exp\left(- \int_{\mathbb{R}^2} \frac{T l(r_0) \lambda_{D_2} P_{MAP}^{\zeta_{d_2}/\zeta_0^{D_1}}}{\frac{P_{D_1}}{P_{D_2}} l(\|\zeta\|) + T l(r_0)} \mathrm{d}\zeta \right) \exp\left(-\mu T l(r_0) \frac{\sigma_N^2}{P_{D_1}} \right) f_{\|\zeta_0^{D_1}\|}(r_0) \mathrm{d}r_0 \end{aligned} \tag{5.19}$$

Note that (4.18) can be derived by approximating the distribution of interfering DSRC nodes processes as non-homogenous PPP with intensity $\lambda_{D_1} P_{MAP}^{\zeta_{d_1}/\zeta_0^{D_1}}$ $big/\lambda_{D_2} P_{MAP}^{\zeta_{d_2}/\zeta_0^{D_1}}$.

5.3 Coexistence Scenario: Analysis of DSRC IEEE 802.11p Network with IEEE 802.11ax Wi-Fi

In this section, we analyze the possible co-existence of a DSRC network with IEEE 802.11ax Wi-Fi UL and DL transmissions. This is done by deriving the MAP, SINR coverage probability, then the AST.

5.3.1 IEEE 802.11ax Wi-Fi DL and UL with SU Operation Mode

When DSRC nodes co-exist with Wi-Fi users and APs in the same band, the DSRC nodes (in the CCH) will contend using the EDCA mechanism with each other and with co-exisiting Wi-Fi users and APs to access the channel. In the 802.11ax SU operation mode, each Wi-Fi user and/or AP will also contend for channel access using EDCA. Hence, a DSRC node $\zeta_{d_1'}$ will have the medium access indicator $e_{d_1'}^{D_1}$, in case of coexistence with Wi-Fi APs and Wi-Fi users, that is derived as follows:

$$\begin{aligned} e_{d_1'}^{D_1} = & \prod_{\zeta_{d_1}\in\Phi_{D_1}\setminus\{\zeta_{d_1'}\}} \left(\mathbb{1}_{t_{d_1}^{D_1}\geq t_{d_1'}^{D_1}} + \mathbb{1}_{t_{d_1}^{D_1}<t_{d_1'}^{D_1}} \mathbb{1}_{G_{d_1d_1'}^{D_1}/l\left(\|\zeta_{d_1}-\zeta_{d_1'}\|\right)\leq \Gamma_{cs}/P_{D_1}} \right) \\ & \times \prod_{\zeta_u\in\Phi_U} \left(\mathbb{1}_{t_u^U\geq t_{d_1'}^{D_1}} + \mathbb{1}_{t_u^U<t_{d_1'}^{D_1}} \mathbb{1}_{G_{ud_1'}^{UD_1}/l\left(\|\zeta_u-\zeta_{d_1'}\|\right)\leq \Gamma_{ed}/P_U} \right) \\ & \times \prod_{\zeta_w\in\Phi_W} \left(\mathbb{1}_{t_w^W\geq t_{d_1'}^{D_1}} + \mathbb{1}_{t_w^W<t_{d_1'}^{D_1}} \mathbb{1}_{G_{wd_1'}^{WD_1}/l\left(\|\zeta_w-\zeta_{d_1'}\|\right)\leq \Gamma_{ed}/P_W} \right) \end{aligned} \tag{5.20}$$

The medium access indicator of a WiFi AP in SU mode is given by e_w^W and derived as follows:

$$\begin{aligned} e_w^W = & \prod_{\zeta_u\in\Phi_U} \left(\mathbb{1}_{t_u^U\geq t_{w'}^W} + \mathbb{1}_{t_u^U<t_{w'}^W} \mathbb{1}_{G_{uw'}^{UW}/l(\|\zeta_u-\zeta_{w'}\|)\leq \Gamma_{cs}/P_U} \right) \\ & \times \prod_{\zeta_w\in\Phi_W\setminus\{\zeta_{w'}\}} \left(\mathbb{1}_{t_w^W\geq t_{w'}^W} + \mathbb{1}_{t_w^W<t_{w'}^W} \mathbb{1}_{G_{ww'}^W/l(\|\zeta_w-\zeta_{w'}\|)\leq \Gamma_{cs}/P_W} \right) \\ & \times \prod_{\zeta_{d_1}\in\Phi_{D_1}} \left(\mathbb{1}_{t_{d_1}^{D_1}\geq t_{w'}^W} + \mathbb{1}_{t_{d_1}^{D_1}<t_{w'}^W} \mathbb{1}_{G_{d_1w'}^{D_1W}/l\left(\|\zeta_{d_1}-\zeta_{w'}\|\right)\leq \Gamma_{ed}/P_{D_1}} \right) \end{aligned} \tag{5.21}$$

Whereas for the WiFi user, the medium access indicator e_u^U is derived as:

$$\begin{aligned} e_u^U = & \prod_{\zeta_u \in \Phi_U \setminus \{\zeta_{u'}\}} \left(\mathbb{1}_{t_u^U \geq t_{u'}^W} + \mathbb{1}_{t_u^U < t_{u'}^W} \mathbb{1}_{G_{uu'}^U / l(\|\zeta_u - \zeta_{u'}\|) \leq \Gamma_{cs}/P_U} \right) \\ & \times \prod_{\zeta_w \in \Phi_W} \left(\mathbb{1}_{t_w^W \geq t_{u'}^{D_1}} + \mathbb{1}_{t_w^W < t_{u'}^{D_1}} \mathbb{1}_{G_{wu'}^{WU_1} / l(\|\zeta_w - \zeta_{u'}\|) \leq \Gamma_{cs}/P_W} \right) \\ & \times \prod_{\zeta_{d_1} \in \Phi_{D_1}} \left(\mathbb{1}_{t_{d_1}^{D_1} \geq t_{u'}^W} + \mathbb{1}_{t_{d_1}^{D_1} < t_{u'}^W} \mathbb{1}_{G_{d_1 w'}^{D_1 W} / l\left(\|\zeta_{d_1} - \zeta_{w'}\|\right) \leq \Gamma_{ed}/P_{D_1}} \right) \end{aligned} \tag{5.22}$$

Thus, given that a DSRC node ζ_{d_1}, Wi-Fi AP ζ_w, and Wi-Fi user ζ_u have, respectively, timer $t_{d_1}^{D_1} \in [0,7]$, $t_w^W \in [0,7]$, and $t_u^U \in [0,7]$, with CDFs $F_{D_1}(t) = F_W(t) = F_U(t) = \frac{t}{7}$, the MAP in the scenario for a tagged DSRC node, Wi-Fi AP, and Wi-Fi user is given by:

$$\begin{aligned} & P_{SU,MAP}^{D_1}(\lambda_{D_1}, \lambda_W, \lambda_U) = \\ & \frac{1}{7} \int_0^\infty \int_0^7 \exp\big[- F_{D_1}(t) N_{D_1}(\zeta_0^{D_1}, \Gamma_{cs}, r_0) - F_W(t) N_W(\Gamma_{ed}) - F_U(t) N_U(\Gamma_{ed}) \big] \mathrm{d}t \mathrm{d}r_0 \\ & P_{SU,MAP}^{W}(\lambda_{D_1}, \lambda_W, \lambda_U) = \\ & \frac{1}{7} \int_0^\infty \int_0^7 \exp\big[- F_W(t) N_W(\zeta_0^{W}, \Gamma_{cs}, r_0) - F_{D_1}(t) N_{D_1}(\Gamma_{ed}) - F_U(t) N_U(\Gamma_{cs}) \big] \mathrm{d}t \mathrm{d}r_0 \\ & P_{SU,MAP}^{U}(\lambda_{D_1}, \lambda_W, \lambda_U) = \\ & \frac{1}{7} \int_0^\infty \int_0^7 \exp\big[- F_U(t) N_U(\zeta_0^{U}, \Gamma_{cs}, r_0) - F_{D_1}(t) N_{D_1}(\Gamma_{ed}) - F_W(t) N_W(\Gamma_{cs}) \big] \mathrm{d}t \mathrm{d}r_0 \end{aligned} \tag{5.23}$$

Hence, given the tagged DSRC node is located at $\zeta_0^{D_1} = (r_0, 0)$, the SINR coverage probability of the typical receiving DSRC node with SINR threshold T is approximated as follows:

$$\begin{aligned} & \hat{p}_{SINR,SU}^{D_1} \left(T, \lambda_{D_1} P_{MAP}^{\zeta_{d_1}/\zeta_0^{D_1}}, \lambda_W P_{MAP}^{\zeta_w/\zeta_0^{D_1}}, \lambda_U P_{MAP}^{\zeta_u/\zeta_0^{D_1}} \right) \approx \int_0^\infty \exp\Big(- \int_{\mathbb{R}^2 \setminus B(0,r_0)} \frac{T l(r_0) \lambda_{D_1} P_{MAP}^{\zeta_{d_1}/\zeta_0^{D_1}}}{l(\|\zeta\|) + T l(r_0)} \mathrm{d}\zeta \Big) \\ & \times \exp\Big(- \int_{\mathbb{R}^2} \frac{T l(r_0) \lambda_W P_{MAP}^{\zeta_w/\zeta_0^{D_1}}}{\frac{P_{D_1}}{P_W} l(\|\zeta\|) + T l(r_0)} \mathrm{d}\zeta \Big) \times \exp\Big(- \int_{\mathbb{R}^2} \frac{T l(r_0) \lambda_U P_{MAP}^{\zeta_u/\zeta_0^{D_1}}}{\frac{P_{D_1}}{P_U} l(\|\zeta\|) + T l(r_0)} \mathrm{d}\zeta \Big) \\ & \times \exp\left(-\mu T l(r_0) \frac{\sigma_N^2}{P_{D_1}} \right) f_{\|\zeta_0^{D_1}\|}(r_0) \mathrm{d}r_0 \end{aligned} \tag{5.24}$$

$$\begin{aligned} & \hat{p}_{SINR,SU}^{W} \left(T, \lambda_{D_1} P_{MAP}^{\zeta_{d_1}/\zeta_0^{W}}, \lambda_W P_{MAP}^{\zeta_w/\zeta_0^{W}}, \lambda_U P_{MAP}^{\zeta_u/\zeta_0^{W}} \right) \approx \int_0^\infty \exp\Big(- \int_{\mathbb{R}^2} \frac{T l(r_0) \lambda_{D_1} P_{MAP}^{\zeta_{d_1}/\zeta_0^{W}}}{\frac{P_W}{P_{D_1}} l(\|\zeta\|) + T l(r_0)} \mathrm{d}\zeta \Big) \\ & \times \exp\Big(- \int_{\mathbb{R}^2 \setminus B(0,r_0)} \frac{T l(r_0) \lambda_W P_{MAP}^{\zeta_w/\zeta_0^{W}}}{l(\|\zeta\|) + T l(r_0)} \mathrm{d}\zeta \Big) \times \exp\Big(- \int_{\mathbb{R}^2} \frac{T l(r_0) \lambda_U P_{MAP}^{\zeta_u/\zeta_0^{W}}}{\frac{P_W}{P_U} l(\|\zeta\|) + T l(r_0)} \mathrm{d}\zeta \Big) \\ & \times \exp\left(-\mu T l(r_0) \frac{\sigma_N^2}{P_W} \right) f_{\|\zeta_0^{W}\|}(r_0) \mathrm{d}r_0 \end{aligned} \tag{5.25}$$

$$\hat{p}^{U}_{SINR,SU}\left(T,\lambda_{D_1}P_{MAP}^{\zeta_{d_1}/\zeta_0^U},\lambda_W P_{MAP}^{\zeta_w/\zeta_0^U},\lambda_U P_{MAP}^{\zeta_u/\zeta_0^U}\right)\approx\int_0^{\infty}\exp\Big(-\int_{\mathbb{R}^2}\frac{Tl(r_0)\lambda_{D_1}P_{MAP}^{\zeta_{d_1}/\zeta_0^U}}{\frac{P_U}{P_{D_1}}l(\|\zeta\|)+Tl(r_0)}\mathrm{d}\zeta\Big)$$
$$\times\exp\Big(-\int_{\mathbb{R}^2}\frac{Tl(r_0)\lambda_W P_{MAP}^{\zeta_w/\zeta_0^U}}{\frac{P_U}{P_W}l(\|\zeta\|)+Tl(r_0)}\mathrm{d}\zeta\Big)\times\exp\Big(-\int_{\mathbb{R}^2\setminus B(0,r_0)}\frac{Tl(r_0)\lambda_U P_{MAP}^{\zeta_u/\zeta_0^U}}{l(\|\zeta\|)+Tl(r_0)}\mathrm{d}\zeta\Big)$$
$$\times\exp\left(-\mu Tl(r_0)\frac{\sigma_N^2}{P_U}\right)f_{\|\zeta_0^U\|}(r_0)\mathrm{d}r_0 \tag{5.26}$$

Where conditioned on the fact that the tagged DSRC node $\zeta_0^{D_1}=(r_0,0)$, tagged Wi-Fi AP $\zeta_0^W=(r_0,0)$, tagged Wi-Fi user $\zeta_0^U=(r_0,0)$ is retained by the CSMA/CA protocol, the probabilities $P_{MAP}^{\zeta_{d_1}/\zeta_0^{D_1}}$ for a DSRC node $\zeta_{d_1}\in\Phi_{D_1}$, $P_{MAP}^{\zeta_w/\zeta_0^{D_1}}$ for a Wi-Fi AP $\zeta_w\in\Phi_W$, and $P_{MAP}^{\zeta_u/\zeta_0^{D_1}}$ for a Wi-Fi user $\zeta_u\in\Phi_U$ to transmit are derived as follows:

$$\begin{aligned}
P_{MAP}^{\zeta_{d_1}/\zeta_0^{D_1}}&=\frac{\Theta_N\big(\zeta_{d_1},\zeta_0^{D_1},\Gamma_{cs}/P_{D_1},0,7,0,7,N_{D_1^1}^{SU}(t),N_{D_1^2}^{SU}(t')\big)}{\Theta_D\big(\zeta_{d_1}-\zeta_0^{D_1},\Gamma_{cs}/P_{D_1},0,7,F_{D_1}(t),N_{D_1^3}^{SU}(t)\big)}\\
P_{MAP}^{\zeta_w/\zeta_0^{D_1}}&=\frac{\Theta_N\big(\zeta_w,\zeta_0^{D_1},\Gamma_{ed}/P_W,0,7,0,7,N_{W^1}^{SU}(t),N_{W^2}^{SU}(t')\big)}{\Theta_D\big(\zeta_w-\zeta_0^{D_1},\Gamma_{ed}/P_W,0,7,F_W(t),N_{W^3}^{SU}(t)\big)}\\
P_{MAP}^{\zeta_u/\zeta_0^{D_1}}&=\frac{\Theta_N\big(\zeta_u,\zeta_0^{D_1},\Gamma_{ed}/P_U,0,7,0,7,N_{U^1}^{SU}(t),N_{D^2}^{SU}(t')\big)}{\Theta_D\big(\zeta_u-\zeta_0^{D_1},\Gamma_{ed}/P_U,0,7,F_U(t),N_{D^3}^{SU}(t)\big)}
\end{aligned} \tag{5.27}$$

Where $N_{D_1^1}^{SU}(t)=\frac{t}{7}\big(-N_W+C_W(\zeta_{d_1}-\zeta_0^{D_1})-N_U+C_U(\zeta_{d_1}-\zeta_0^{D_1})-N_{D_1}(r_0)+C_{D_1}(\zeta_{d_1},\zeta_0^{D_1})\big)$ and $N_{D_1^2}(t')=\frac{t'}{7}\big(-N_W-N_U-N_{D_1}(r_0)\big)$ and $N_{D_1^3}(t)=-\frac{t}{7}\big(N_{D_1}(\zeta_0^{D_1})+N_U+N_W\big)$.

Similarly, $N_{W^1}^{SU}(t)=\frac{t}{7}\big(-N_W+C_W(\zeta_w-\zeta_0^{D_1})-N_U+C_U(\zeta_w-\zeta_0^{D_1})-N_{D_1}(r_0)+C_{D_1}(\zeta_w,\zeta_0^{D_1})\big)$, $N_{W^2}^{SU}(t')=N_{D_1^2}^{SU}(t')$, and $N_{W^3}^{SU}(t)=N_{D_1^3}^{SU}(t)$. and $N_{W^3}^{SU}(t)=-\frac{t}{7}\big(N_{D_1}(\zeta_0^{D_1})+N_U\big)$.

Finally, $N_{U^1}^{SU}(t)=\frac{t}{7}\big(-N_W+C_W(\zeta_u-\zeta_0^{D_1})-N_U+C_U(\zeta_u-\zeta_0^{D_1})-N_{D_1}(r_0)+C_{D_1}(\zeta_u,\zeta_0^{D_1})\big)$, $N_{U^2}^{SU}(t')=N_{D_1^2}^{SU}(t')$, and $N_{U^3}^{SU}(t)=N_{D_1^3}^{SU}(t)$.

$$\begin{aligned}
P_{MAP}^{\zeta_{d_1}/\zeta_0^{W}}&=\frac{\Theta_N\big(\zeta_{d_1},\zeta_0^{W},\Gamma_{ed}/P_W,0,7,0,7,N_{D_1^4}^{SU}(t),N_{D_1^5}^{SU}(t')\big)}{\Theta_D\big(\zeta_{d_1}-\zeta_0^{W},\Gamma_{ed}/P_{D_1},0,7,F_{D_1}(t),N_{D_1^6}^{SU}(t)\big)}\\
P_{MAP}^{\zeta_w/\zeta_0^{W}}&=\frac{\Theta_N\big(\zeta_w,\zeta_0^{W},\Gamma_{cs}/P_W,0,7,0,7,N_{W^4}^{SU}(t),N_{W^5}^{SU}(t')\big)}{\Theta_D\big(\zeta_w-\zeta_0^{W},\Gamma_{cs}/P_W,0,7,F_W(t),N_{W^6}^{SU}(t)\big)}\\
P_{MAP}^{\zeta_u/\zeta_0^{W}}&=\frac{\Theta_N\big(\zeta_u,\zeta_0^{W},\Gamma_{cs}/P_U,0,7,0,7,N_{U^4}^{SU}(t),N_{U^5}^{SU}(t')\big)}{\Theta_D\big(\zeta_u-\zeta_0^{W},\Gamma_{cs}/P_U,0,7,F_U(t),N_{U^6}^{SU}(t)\big)}
\end{aligned} \tag{5.28}$$

Where $N_{D_1^4}^{SU}(t) = \frac{t}{7}\big(-N_W(r_0)+C_W(\zeta_{d_1},\zeta_0^W) -N_U+C_U(\zeta_{d_1}-\zeta_0^W) -N_{D_1}+C_{D_1}(\zeta_{d_1}-\zeta_0^{D_1})\big)$ and $N_{D_1^5}^{SU}(t') = \frac{t'}{7}\big(- N_W(r_0) - N_U-N_{D_1}\big)$ and $N_{D_1^3}^{SU}(t) = -\frac{t}{7}\big(N_{D_1} + N_U + N_W(\zeta_0^{D_1})\big)$.

Similarly, $N_{W^4}^{SU}(t) = \frac{t}{7}\big(- N_W(r_0) + C_W(\zeta_w,\zeta_0^W) -N_U + C_U(\zeta_w - \zeta_0^W) -N_{D_1} + C_{D_1}(\zeta_w - \zeta_0^{D_1})\big)$, $N_{W^5}^{SU}(t') = N_{D_1^5}^{SU}(t')$, and $N_{W^6}^{SU}(t) = N_{D_1^6}^{SU}(t)$.

Finally, $N_{U^5}^{SU}(t) = \frac{t}{7}\big(- N_W(r_0) + C_W(\zeta_u,\zeta_0^{D_1}) -N_U + C_U(\zeta_u - \zeta_0^{D_1}) -N_{D_1} + C_{D_1}(\zeta_u - \zeta_0^{D_1})\big)$, $N_{U^5}^{SU}(t') = N_{D_1^5}^{SU}(t')$, and $N_{U^6}^{SU}(t) = N_{D_1^6}^{SU}(t)$.

$$
\begin{aligned}
P_{MAP}^{\zeta_{d_1}/\zeta_0^U} &= \frac{\Theta_N\big(\zeta_{d_1},\zeta_0^U,\Gamma_{ed}/P_U,0,7,0,7,N_{D_1^7}^{SU}(t),N_{D_1^8}^{SU}(t')\big)}{\Theta_D\big(\zeta_{d_1}-\zeta_0^U,\Gamma_{ed}/P_{D_1},0,7,F_{D_1}(t),N_{D_1^9}^{SU}(t)\big)} \\
P_{MAP}^{\zeta_w/\zeta_0^U} &= \frac{\Theta_N\big(\zeta_w,\zeta_0^U,\Gamma_{cs}/P_U,0,7,0,7,N_{W^7}^{SU}(t),N_{W^8}^{SU}(t')\big)}{\Theta_D\big(\zeta_w-\zeta_0^U,\Gamma_{cs}/P_U,0,7,F_W(t),N_{W^9}^{SU}(t)\big)} \\
P_{MAP}^{\zeta_u/\zeta_0^U} &= \frac{\Theta_N\big(\zeta_u,\zeta_0^U,\Gamma_{cs}/P_U,0,7,0,7,N_{U^7}^{SU}(t),N_{U^8}^{SU}(t')\big)}{\Theta_D\big(\zeta_u-\zeta_0^U,\Gamma_{cs}/P_U,0,7,F_U(t),N_{U^9}^{SU}(t)\big)}
\end{aligned}
\tag{5.29}
$$

Where $N_{D_1^7}^{SU}(t) = \frac{t}{7}\big(-N_W+C_W(\zeta_{d_1}-\zeta_0^U) -N_U(r_0)+C_U(\zeta_{d_1},\zeta_0^U) -N_{D_1}+C_{D_1}(\zeta_{d_1}-\zeta_0^U)\big)$
and $N_{D_1^8}^{SU}(t') = \frac{t'}{7}\big(-N_W-N_U(r_0)-N_{D_1}\big)$ and $N_{D_1^9}^{SU}(t) = -\frac{t}{7}\big(N_{D_1}+N_U(\zeta_0^U)+N_W\big)$.

Similarly, $N_{W^7}^{SU}(t) = \frac{t}{7}\big(- N_W + C_W(\zeta_w - \zeta_0^U) -N_U(r_0) + C_U(\zeta_w,\zeta_0^U) -N_{D_1} + C_{D_1}(\zeta_w - \zeta_0^U)\big)$, $N_{W^8}^{SU}(t') = N_{D_1^8}^{SU}(t')$, and $N_{W^9}^{SU}(t) = N_{D_1^9}^{SU}(t)$.

Finally, $N_{U^7}^{SU}(t) = \frac{t}{7}\big(- N_W + C_W(\zeta_u - \zeta_0^{D_1}) -N_U(r_0) + C_U(\zeta_u,\zeta_0^{D_1}) -N_{D_1} + C_{D_1}(\zeta_u - \zeta_0^U)\big)$, $N_{U^8}^{SU}(t') = N_{D_1^8}^{SU}(t')$, and $N_{U^9}^{SU}(t) = N_{D_1^9}^{SU}(t)$.

5.3.2 IEEE 802.11ax Wi-Fi DL And UL with MU Operation Mode

In this analysis, we consider that a DSRC network coexists with another DSRC network in the baseline scenario or it coexists with a Wi-Fi network when analyzing the DSRC-Wi-Fi coexistence. In case of the IEEE 802.11ax network, we consider either MU DL transmissions, MU UL transmissions, or both. In the MU operation mode, the AP will initially contend using EDCA parameters for channel access as in the case of SU mode. This is the same in both MU uplink and MU downlink scenarios. Accordingly, by assuming that β APs are associated with MU DL traffic and (1-β) APs are associated with MU UL traffic, we derive initially the MAP of a Wi-Fi AP in the MU mode as follows:

$$
P_{MU,MAP}^{W}(\lambda_{D_1},\lambda_W) = P_{SU,MAP}^{W}(\lambda_{D_1},\lambda_W,\lambda_U=0) \tag{5.30}
$$

The MAP of a DSRC node in this scenario is derived as:

$$P^{D_1}_{MU,MAP}\left(\lambda_{D_1},\lambda_W,\lambda_U\right) = P^{D_1}_{SU,MAP}(\lambda_{D_1},\lambda_W,\lambda_U=0) \tag{5.31}$$

For the case of simultaneous UL transmissions in MU mode, the AP first sends a trigger frame to the users assigning them corresponding RU grants. Then, users may operate based on two different trigger-based access schemes. The first is the trigger-based deterministic access (TR-DA) in which the user will transmit directly on the allocated RUs. Thus, in the TR-DA, the MAP of a user in the UL is:

$$\hat{p}^{U-DA}_{MU,MAP}\left(\lambda_{D_1},\lambda_W,\lambda_U\right) = \hat{p}^{W}_{MU,MAP}\left(\lambda_{D_1},\lambda_W\right) \times P_{DA}(\lambda_U) \tag{5.32}$$

Where $P_{DA}(\lambda_U)$ is the average probability that a user is selected to be scheduled on a particular RU. We assume that the AP uniformly schedules a user on a particular RU. Thus, in case that the number of users k in a certain BSS is smaller than or equal the available number of channels N_{RU}, the probability for a node to be scheduled by an AP is equal to one. On the other hand, when k is larger than N_{RU}, the probability for a node to be scheduled by an AP is equal to $\frac{N_{RU}}{k}$. Therefore, according to [52], P_{DA} can be computed as follows:

$$P_{DA}(\lambda_U) = \frac{\exp(-N_U)}{N_U}\left[N_{RU}\big(\exp(N_U)-1\big) - \sum_{k=1}^{N_{RU}} \frac{(N_{RU}-k)(N_U)^k}{k!}\right] \tag{5.33}$$

On the other hand, the second scheme is the trigger-based random access (TR-RA) mechanism where users will contend for channel access on the assigned set of RUs where we assume in this case that a user selects a particular RU uniformly. Hence, if the AP assigns N_{RU} to users, and after the user contends and wins access to the channel, he will select a particular RU with probability P_{RA} in order to transmit its data to the AP. Thus, in the TR-RA, the MAP of a user in the UL is:

$$\hat{p}^{U-RA}_{MU,MAP}\left(\lambda_{D_1},\lambda_W,\lambda_U\right) = \hat{p}^{W}_{MU,MAP}\left(\lambda_{D_1},\lambda_W\right) \times \hat{p}^{U}_{SU,MAP}\left(\lambda_{D_1},\beta\lambda_W,\lambda_U\right) \times P_{RA} \tag{5.34}$$

where P_{RA} is the average probability that a user uniquely selects a particular RU that is not selected by any other user. Hence, given that the number of users is k in a certain BSS and that the assigned number of channels is N_{RU}, the probability the first user selects a random RU is 1. Then the probability that the second node will select a different RU out of N_{RU} is $\frac{N_{RU}-1}{N_{RU}}$. Furthermore the probability for the k^{th} node to uniquely select a particular RU that is not selected by any other user is $\frac{N_{RU}-k+1}{N_{RU}}$. Therefore, by generalizing the above, P_{RA} can be derived

as follows:

$$\begin{aligned} P_{RA} &= \sum_{k=1}^{N_{RU}} \frac{N_{RU}!(N_U)^k}{(N_{RU})^k(N_{RU}-k)!}\frac{\exp(-N_U)}{k!} \\ &= \frac{N_{RU}!}{\exp(N_U)}\sum_{k=1}^{N_{RU}} \frac{\left(\frac{N_U}{N_{RU}}\right)^k}{k!(N_{RU}-k)!} \end{aligned} \tag{5.35}$$

Also, given that the tagged DSRC node is located at $\zeta_0^{D_1} = (r_0, 0)$ in MU mode the SINR coverage probability of the typical DRSC receiving node with SINR threshold T is:

Case 1: TR-DA UL scheme

$$\hat{p}^{D_1}_{SINR,MU}\left(T, \lambda_{D_1}, \lambda_W\right) = \hat{p}^{D_1}_{SINR,SU}\left(T, \lambda_{D_1}, \beta\lambda_W, \lambda_U^{DA}\right) \tag{5.36}$$

Case 2: TR-RA UL scheme

$$\hat{p}^{D_1}_{SINR,MU}\left(T, \lambda_{D_1}, \lambda_W\right) = \hat{p}^{D_1}_{SINR,SU}\left(T, \lambda_{D_1}, \beta\lambda_W, \lambda_U^{RA}\right) \tag{5.37}$$

Where $\lambda_U^{DA} = \hat{p}^{U-DA}_{MU,MAP}\left(\lambda_{D_1}, \lambda_W, \lambda_U\right) \times \lambda_U$ and $\lambda_U^{RA} = \hat{p}^{U-RA}_{MU,MAP}\left(\lambda_{D_1}, \lambda_W, \lambda_U\right) \times \lambda_U$.

Next, given that the tagged Wi-Fi AP is located at $\zeta_0^W = (r_0, 0)$, during MU mode, the SINR coverage probability of the typical Wi-Fi user with SINR threshold T in the DL is:

Case 1: TR-DA UL scheme

$$\hat{p}^{W}_{SINR,MU}\left(T, \lambda_{D_1}, \lambda_W\right) = \hat{p}^{W}_{SINR,SU}\left(T, \lambda_{D_1}, \beta\lambda_W, \lambda_U^{DA}\right) \tag{5.38}$$

Case 2: TR-RA UL scheme

$$\hat{p}^{W}_{SINR,MU}\left(T, \lambda_{D_1}, \lambda_W\right) = \hat{p}^{W}_{SINR,SU}\left(T, \lambda_{D_1}, \beta\lambda_W, \lambda_U^{RA}\right) \tag{5.39}$$

Finally, with the tagged Wi-Fi user located at $\zeta_0^U = (r_0, 0)$, during MU mode, the SINR coverage probability of the typical Wi-Fi AP with SINR threshold T in the UL is:

Case 1: TR-DA UL scheme

$$\hat{p}^{U}_{SINR,MU}\left(T, \lambda_{D_1}, \lambda_W, \lambda_U\right) = \hat{p}^{U}_{SINR,SU}\left(T, \lambda_{D_1}, \beta\lambda_W, \lambda_U^{DA}\right) \tag{5.40}$$

Case 2: TR-RA UL scheme

$$\hat{p}^{U}_{SINR,MU}\left(T, \lambda_{D_1}, \lambda_W, \lambda_U\right) = \hat{p}^{U}_{SINR,SU}\left(T, \lambda_{D_1}, \beta\lambda_W, \lambda_U^{RA}\right) \tag{5.41}$$

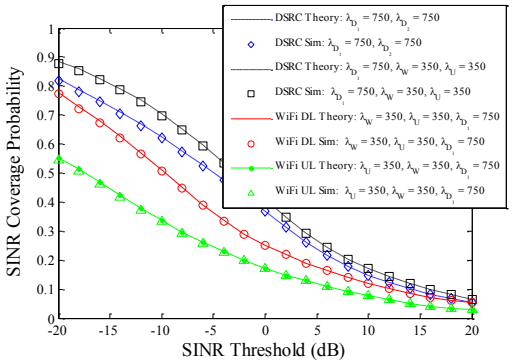

Figure 5.2: SINR Coverage Performance For Typical DSRC link, Typical Wi-Fi UL, Typical Wi-Fi DL

5.4 Performance Evaluation of The Coexistence of DSRC and IEEE 802.11ax Wi-Fi

In this section, we study the impact of IEEE 802.11ax Wi-Fi transmissions on DSRC performance using the developed framework. From Wi-Fi perspective we consider the single user and multi user operation modes of the IEEE 802.11ax. Initially we start by validating the analytical model versus simulations. Then, we study the impact of each coexistence scenario with respect to the DSRC-only (Baseline) scenario.

5.4.1 Scenario Settings

In this study, we consider an area of 2x2 km^2. We also consider a line density λ_l km/km^2 and DSRC node density λ_n nodes/km. In line with the literature (e.g., [44]), the path-loss exponent is set to $\alpha = 4$, and the transmission (Tx) power of the DSRC nodes is $P_D = 20$ dBm in the CCH. For the 802.11ax AP the Tx power is $P_W = 23$ dBm, while for the 802.11ax STAs it is $P_U = 18$ dBm. The power fading parameter is set to $\mu = 1$. The carrier sensing threshold is Γ_{cs} = -82 dBm, whereas the energy detection threshold is Γ_{ed} = - 62 dBm.

5.4.2 Validation of the SINR Model

We start by validating the analytical SINR coverage probability model. Fig. 5.2 presents the analytical and the Monte-Carlo simulation results for the SINR coverage probability of a typical DSRC node receiver, typical Wi-Fi STA in the downlink, and typical Wi-Fi AP in the uplink. The figure shows that the analytical and the simulation results match.

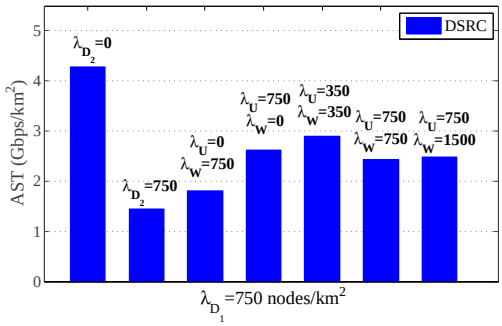

Figure 5.3: Area System Throughput (AST) For DSRC Link

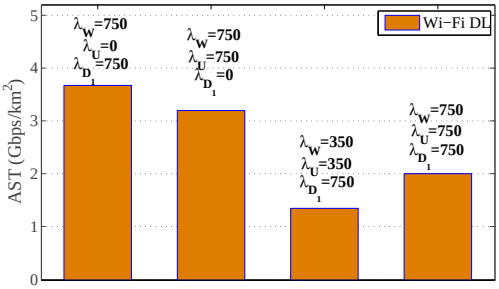

Figure 5.4: Area System Throughput (AST) For Wi-Fi DL

5.4.3 Impact of IEEE 802.11ax SU operation mode

Fig. 5.3 shows the impact of the IEEE802.11ax SU operation mode on the DSRC network performance in terms of AST (Gbps/km^2) when $\lambda_{D_1} = 750$ nodes/km^2. In this case we compare the AST of the two DSRC networks baseline scenario without Wi-Fi ($\lambda_{D_1}, \lambda_{D_2}$) to that when coexisting with Wi-Fi ($\lambda_{D_1}, \lambda_W, \lambda_U$). We observe in Fig. 5.3 that naturally when there is a single DSRC network with no coexisting Wi-Fi network in case of the ($\lambda_{D_1} = 750, \lambda_{D_2} = \lambda_W = \lambda_U = 0$) the network achieves its best AST performance, reaching 4.3 Gbps/km^2. However when comparing this scenario with the coexistence with another DSRC network (baseline scenario) or with a Wi-Fi network, there is about 40% or more decrease in the AST performance.

Furthermore, compared to the ($\lambda_{D_1} = 750, \lambda_{D_2} = 750$) scenario, the DSRC network shows better performance when it coexists with the same density of Wi-Fi APs ($\lambda_{D_1} = 750, \lambda_U = 0, \lambda_W = 750$) or Wi-Fi users ($\lambda_{D_1} = 750, \lambda_U = 750, \lambda_W = 0$) or both ($\lambda_{D_1} = 750, \lambda_U = 350, \lambda_W = 350$). This can be explained by the fact that DSRC nodes use energy detection to determine if the channel is busy or not when coexisiting with Wi-Fi APs and users, whereas it uses carrier sensing with DSRC nodes. Hence, DSRC nodes are more sensitive to other DSRC nodes when trying to access the channel, knowing that the energy detection threshold is smaller by about 20 dB than the carrier sensing threshold. This results in a lower area system throughput. In addition, we observe that Wi-Fi users have less impact on DSRC performance than Wi-Fi APs. This is due

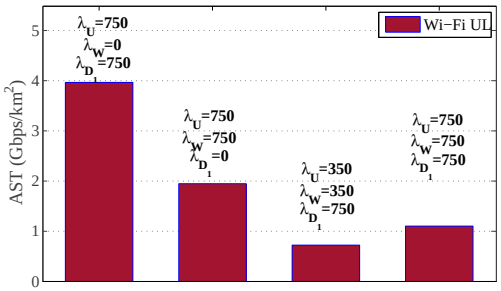

Figure 5.5: Area System Throughput (AST) For Wi-Fi UL

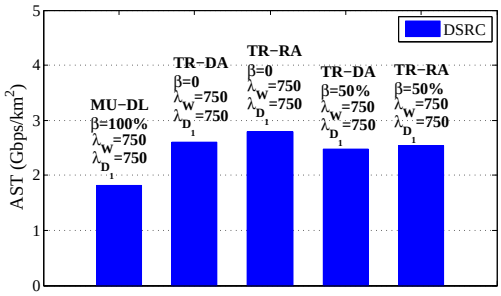

Figure 5.6: Area System Throughput (AST) For DSRC

to the fact that the transmission power of Wi-Fi users is less than that of Wi-Fi APs, and hence the resulting interference power is smaller. On the other hand, Fig 5.4 and Fig. 5.5 shows the impact of the IEEE802.11ax SU operation mode on the Wi-Fi uplink and downlink performance. The AST is higher in this case due to the fact that Wi-Fi uses a 20 MHz bandwidth. We can also see that the AST of the Wi-Fi DL is the highest when coexisting with the DSRC network ($\lambda_W = 750, \lambda_U = 0, \lambda_{D_1} = 750$) even when compared to the Wi-Fi only scenario where we have similar Wi-Fi UL density ($\lambda_W = 750, \lambda_U = 750, \lambda_{D_1} = 0$). However, as the density of Wi-Fi APs is less or equal to that of the DSRC nodes and Wi-Fi users ($\lambda_W = 350, \lambda_U = 350, \lambda_{D_1} = 750$), we observe a further decrease in the AST of Wi-Fi DL. Similar trend can be observed in the case of Wi-Fi UL in Fig. 5.5 with a lower performance in case of Wi-Fi UL due to the lower transmission power as compared to Wi-Fi APs.

5.4.4 Impact of IEEE 802.11ax MU operation mode

Fig. 5.6 presents the impact of the IEEE802.11ax MU operation mode on the DSRC network performance. Similarly, we compare the AST of the DSRC network without Wi-Fi to that in case of coexistence with Wi-Fi. We consider different values of β (β fraction of APs that are associated with MU DL, and $1 - \beta$ is the fraction of APs that are associated with MU UL). We can see that the DSRC performance in case of MU operation is better than when there is

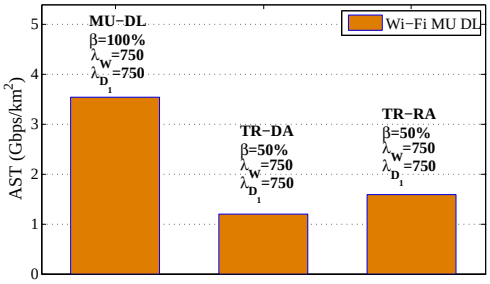

Figure 5.7: Area System Throughput (AST) For Wi-Fi MU DL

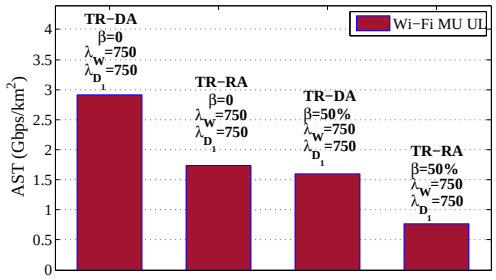

Figure 5.8: Area System Throughput (AST) For Wi-Fi MU UL

another DSRC network (already presented in Fig. 5.2). In addition, we see that the DSRC AST is lowest in case of MU-DL scenario only (β=100%), whereas it the highest in case of TR-DA UL scenario with $\beta = 0$. The DSRC AST is lower in case of TR-DA UL than the case of TR-RA due to the increased interference from Wi-Fi UL transmissions in case of TR-DA UL operation mode. On the other hand, in case of Wi-Fi MU DL we can see that the highest performance is achieved when β=100% whereas in the case where β=50%, the performance decreases significantly especially in the case of TR-DA UL. As for the case of MU UL, we observe that TR-DA enables higher DST for UL with different values of β, where the highest AST achieved is when β=0 and where a larger number of Wi-Fi users are able to access the channel and transmit.

5.5 Discussion

Throughout the analysis, we can see that when there is a single DSRC network with no coexisting DSRC or Wi-Fi network, the DSRC network achieves its best AST performance, reaching 4.3 Gbps/km^2. However when a DSRC network coexists with another DSRC network (baseline scenario) with the same node density there is about 65% decrease in the AST performance. Whereas, when a DSRC network coexists with a Wi-Fi network instead of a DSRC one, there is about 40%-55% decrease in the AST performance which is lower than the effect of another DSRC network for the same node density. In addition, Wi-

Fi users showed less impact on the DSRC performance than Wi-Fi APs. On the other hand, trigger-based deterministic access uplink transmissions showed slightly more impact by about 5% on the AST performance of the DSRC network than the tigger-based random access uplink transmissions.
In contrast, the impact of the DSRC transmissions on the AST performance of Wi-Fi DL transmissions is less than that of Wi-Fi UL transmissions on DL transmissions by about 10% for the same node density. Also, the impact of DSRC transmissions on Wi-Fi UL is less than that of Wi-Fi DL transmissions on Wi-Fi UL by about 50% for the same density. Thus, compared to the baseline scenario (two coexisitng DSRC networks), we can see that Wi-Fi can fairly coexist with DSRC. Whereas compared to the performance of a single DSRC network, it is clear that there is a need for extra mechanisms to enable the fair coexistence of DSRC and Wi-Fi.

5.6 Summary

In this chapter, we presented and validated an analytical framework that uses stochastic geometry to assess the impact of allowing 802.11ax Wi-Fi to coexist in the unlicensed ITS band with DSRC. Throughout the analysis, we used the area system throughput (AST) as a performance metric to evaluate the impact of coexistence. The results showed the impact of the different operation modes of Wi-Fi for both uplink and downlink directions and involving access points and users. In the future, this work can be extended by assuming non-full buffer DSRC and Wi-Fi traffic and by extending the analysis to a more sophisticated model for the distribution of DSRC nodes, such as the Poisson line process (PLP).

Chapter 6

Conclusion and Future Directions

In this chapter, we summarize the general conclusions drawn from this thesis. We also outline some future research directions arising from this work.

In chapter 3, we have presented and validated a framework based on stochastic geometry to analyze the coexistence of overlaid LTE and IEEE 802.11ax Wi-Fi networks. In particular, three coexistence mechanisms (LTE, LTE-U, and LAA) in addition to the Wi-Fi baseline scenario were evaluated analytically and numerically. Several performance metrics were utilized which are MAP, SINR coverage probability, DST and Shannon throughput. Analysis shows that the effect of the coexistence of LTE is not the same for all traffic types. In addition, in most scenarios, LTE-U and LAA appear as a good neighbor to IEEE 802.11ax when compared to the baseline scenario. Also, we showed that the SR technique provides a boost in performance of IEEE 802.11ax transmissions. Finally, we discussed the performance of different type of MU mode where we showed that the trigger based deterministic access has the best performance. In the future, this work can be extended by considering dynamic channel selection to reduce the interference between LTE and Wi-Fi. In addition, delay analysis can be done by assuming non-full buffer to study further the QoS performance of IEEE 802.11ax with different LTE-coexistence schemes.

In chapter 4, we have presented and validated a framework using stochastic geometry to analyze the effect of different channel access priorities on the performance of four different coexisting LAA networks in the unlicensed band. The coexistence of LAA networks with each other is a major issue on the road toward 5G. Based on this, we adopted 3GPP release 14 specification for LAA downlink. Throughout the analysis, we used several performance metrics such as MAP, SINR coverage probability, and rate coverage probability. Results show that operators may exploit the unlicensed bands using different traffic types but with a trade off between the achieved performance and the number of traffic classes used. We showed that most of the traffic classes may maximize their benefit from the unlicensed channel when a single traffic class is used. However, the diverse impact on the performance of each class starts when increasing the number of

classes being transmitted. Results showed that classes A and B retain an acceptable performance and are better than that of classes C and D when coexisting with one or two other classes having different types. However, when all classes coexist, there is a severe impact on the LAA network in the case of all classes. Also, when analyzing the lower and upper performance bounds, we can see that they are similar in case of classes A, B, and C. Whereas in case of class D, we have an improvement in the rate coverage probability by about 20% in the upper performance bound. In the future, this work can be extended by analyzing the performance of the network considering multiple frequency bands toward large number of channels and by assuming different traffic assumptions like non-full buffer downlink.

On the other hand, we also presented an analytical framework for assessing the performance of an arbitrary number of coexisting LAA operators using load based equipment (LBE) channel access as LBT mechanism and finite user density. This framework allows to analyze individual system throughput per unit area (in Gbps/km^2) of coexisting operators as their number increases, and the trade-off between the number of operators and subscribers per operator. We find that the contention window size, which is determined by the traffic type, plays a major role in the fairness between operators. This highlights the need for regulations to guarantee fairness. We also find that a limit in the number of operators is needed to prevent severe performance degradation. These findings unveil new questions regarding practical aspects for deploying LAA-LTE. Extending this framework to capture more LAA specifications as well as the use of multiple LAA bands, fairness mechanisms, and non-persisting traffic are promising research paths to follow.

In Chapter 5, we presented and validated an analytical framework that uses stochastic geometry to assess the impact of allowing 802.11ax Wi-Fi to coexist in the unlicensed ITS band with DSRC. Throughout the analysis, we used the area system throughput (AST) as a performance metric to evaluate the impact of coexistence. The results showed the impact of the different operation modes of Wi-Fi for both uplink and downlink directions and involving access points and users. Throughout the analysis, we can see that when there is a single DSRC network with no coexisting DSRC or Wi-Fi network, the DSRC network achieves its best AST performance. However when a DSRC network coexists with another DSRC network (baseline scenario) with the same node density there is about 65% decrease in the AST performance. Whereas, when a DSRC network coexists with a Wi-Fi network instead of a DSRC one, there is about 40%-55% decrease in the AST performance which is lower than the effect of another DSRC network for the same node density. In addition, Wi-Fi users showed less impact on the DSRC performance than Wi-Fi APs. On the other hand, trigger-based deterministic access uplink transmissions showed slightly more impact by about 5% on the AST performance of the DSRC network than the tigger-based random access uplink transmissions.

In contrast, the impact of the DSRC transmissions on the AST performance of Wi-Fi DL transmissions is less than that of Wi-Fi UL transmissions on DL transmissions by about 10% for the same node density. Also, the impact of DSRC transmissions on Wi-Fi UL is less than that of Wi-Fi DL transmissions on Wi-Fi UL by about 50% for the same density. Thus, compared to the baseline scenario (two coexisitng DSRC networks), we can see that Wi-Fi can fairly coexist with DSRC. Whereas compared to the performance of a single DSRC network, it is clear that there is a need for extra mechanisms to enable the fair coexistence of DSRC and Wi-Fi. In the future, this work can be extended by assuming non-full buffer DSRC and Wi-Fi traffic and by extending the analysis to a more sophisticated model for the distribution of DSRC nodes, such as the Poisson line process (PLP).

Bibliography

[1] UMTS Forum Mobile Traffic Forecasts 2010-2020.

[2] Huawei white paper: U-LTE: Unlicensed Spectrum Utiliza-tion of LTE, 2014.

[3] E. Dinc, M. Vondra and C. Cavdar, "Seamless Gate-to-Gate Connectivity Concept: Onboard LTE, Wi-Fi and LAA," 2017 IEEE 86th Vehicular Technology Conference (VTC-Fall), Toronto, ON, 2017, pp. 1-7.

[4] CEPT ECC Report 214, 6 Jun. 2014. "Broadband Direct-Air-to-Ground Communications (DA2GC)".

[5] NGMN Alliance, "5G White Paper," Feb. 2015.

[6] Air Transport Action Group, "Aviation: Benefits Beyond Borders", Jul. 2016.

[7] B. R. Elbert, White Paper, "Aeronautical Broadband for Commercial Aviation: Evaluating the 2Ku Solution", Application Technology Strategy, L.L.C., Oct. 2014.

[8] EUROCONTROL Trends in Air Traffic, "Planning for Delay: influence of flight scheduling on airline punctuality", vol. 7, 2010.

[9] Cisco Visual Networking Index: Forecast and Methodology, 2014-2019

[10] http://www.multichannel.com/news/technology/comcast-wifi-net-surpasses-10m-hotspots/392510

[11] http://www.techtimes.com/articles/15438/20140912/wi-fi-in-europe-no-problem-if-you-are-a-comcast-subscriber.htm

[12] "Revision of part 15 of the commissions rules to permit unlicensed national information infrastructure devices in the 5 GHz band", tech. rep., Federal Communications Commission, February 20,2013.

[13] M. S. Afaqui, E. Garcia-Villegas, E. Lopez-Aguilera, "IEEE 802.11ax: Challenges and Requirements for Future High Efficiency WiFi," in *IEEE Wireless Communications*, vol.PP, no.99, pp.2-9, December 2016.

[14] A. M. Cavalcante, E. Almeida, R. D. Vieira, F. Chaves, R. C. Paiva, F. Abinader, S. Choudhury, E. Tuomaala, and K. Doppler, "Performance evaluation of LTE and Wi-Fi coexistence in unlicensed bands," in *IEEE 77th Vehicular Technology Conference (VTC Spring)*, pp. 16, Jun. 2013.

[15] T. Nihtila, V. Tykhomyrov, O. Alanen, M. Uusitalo, A. Sorri, M. Moisio, S. Iraji, R. Ratasuk, N. Mangalvedhe, et al., "System performance of LTE and IEEE 802.11 coexisting on a shared frequency band," in *IEEE Wireless Communications and Networking Conference (WCNC)*, pp. 10381043, Jun. 2013.

[16] Qualcomm, "LTE in unlicensed spectrum: Harmonious coexistence with Wi-Fi," white paper, Jun. 2014.

[17] E. Almeida, A. M. Cavalcante, R. C. Paiva, F. S. Chaves, F. M. Abinader, R. D. Vieira, S. Choudhury, E. Tuomaala, and K. Doppler, "Enabling LTE/WiFi coexistence by LTE blank subframe allocation," in *IEEE International Conference on Communications (ICC)*, pp. 50835088, Jun. 2013.

[18] J. Jeon, H. Niu, Q. C. Li, A. Papathanassiou, and G. Wu, "LTE in the unlicensed spectrum: Evaluating coexistence mechanisms," in *IEEE Globecom Workshops (GC Wkshps)*, pp. 740745, Dec. 2014.

[19] H. Zhang, X. Chu, W. Guo and S. Wang, "Coexistence of Wi-Fi and heterogeneous small cell networks sharing unlicensed spectrum," in IEEE Communications Magazine, vol. 53, no. 3, pp. 158-164, March 2015.

[20] 3GPP TR 36.889, "Study on licensed-assisted access to unlicensed spectrum," 2015.

[21] ETSI EN 301.893 v 1.7.1 "Broadband Radio Access Networks (BRAN); 5 GHz high performance RLAN."

[22] R. Ratasuk, M. Uusitalo, N. Mangalvedhe, A. Sorri, S. Iraji, C. Wijting, and A. Ghosh, "License-exempt LTE deployment in heterogeneous network," in *International Symposium on Wireless Communication Systems (ISWCS)*, pp. 246250, Aug. 2012.

[23] Q. Chen; G. Yu; A. Maaref; G. Li; A. Huang, "Rethinking Mobile Data Offloading for LTE in Unlicensed Spectrum," in IEEE Transactions on Wireless Communications vol. 15, no. 7, pp. 4987-5000, July 2016.

[24] J. Andrews, F. Baccelli, and R. Ganti, "A tractable approach to coverage and rate in cellular networks," *IEEE Transactions on Communications*, vol. 59, pp. 31223134, Nov. 2011.

[25] H. Dhillon, R. Ganti, F. Baccelli, and J. Andrews, "Modeling and analysis of K-tier downlink heterogeneous cellular networks," *IEEE Journal on Selected Areas in Communications*, vol. 30, pp. 550560, Apr. 2012.

[26] H. Dhillon, R. Ganti, and J. Andrews, "Load-aware modeling and analysis of heterogeneous cellular networks," *IEEE Transactions on Wireless Communications*, vol. 12, pp. 16661677, Apr. 2013.

[27] S. Mukherjee, "Distribution of downlink SINR in heterogeneous cellular networks," *IEEE Journal on Selected Areas in Communications*, vol. 30, pp. 575585, Apr. 2012.

[28] R. Heath, M. Kountouris, and T. Bai, "Modeling heterogeneous network interference using Poisson point processes," *IEEE Transactions on Signal Processing*, vol. 61, pp. 41144126, Aug. 2013.

[29] H. Dhillon, M. Kountouris, and J. Andrews, "Downlink MIMO HetNets: modeling, ordering results and performance analysis," *IEEE Transactions on Wireless Communications*, vol. 12, pp. 52085222, Oct. 2013.

[30] X. Lin, J. G. Andrews, and A. Ghosh, "Modeling, analysis and design for carrier aggregation in heterogeneous cellular networks," *IEEE Transactions on Communications*, vol. 61, pp. 40024015, Sept. 2013.

[31] R. Zhang, M. Wang, Z. Zheng, X. S. Shen, and L.-L. Xie, "Stochastic geometric performance analysis for carrier aggregation in LTE-A systems," in *IEEE ICC*, pp. 57775782, Jun. 2014.

[32] H. Nguyen, F. Baccelli, and D. Kofman, "A stochastic geometry analysis of dense IEEE 802.11 networks," in *IEEE INFOCOM 2007*, pp. 11991207, May 2007.

[33] Y. Kim, F. Baccelli, and G. de Veciana, "Spatial reuse and fairness of ad hoc networks with channel-aware CSMA protocols," *IEEE Transactions on Information Theory*, vol. 60, pp. 41394157, Jul. 2014.

[34] T. V. Nguyen and F. Baccelli, "A stochastic geometry model for cognitive radio networks," *The Computer Journal*, vol. 55, pp. 534552, Apr. 2012.

[35] W. Lu and M. Di Renzo, "Stochastic geometry modeling of cellular networks: Analysis, simulation and experimental validation",in *18th ACM International Conference on Modeling, Analysis and Simulation of Wireless and Mobile Systems*, pp. 179-188, 2015.

[36] A. Bhorkar, C. Ibars, and P. Zong, "On the throughput analysis of LTE and WiFi in unlicensed band," in *Asilomar Conference on Signals, Systems and Computers*, pp. 13091313, Nov. 2014.

[37] Yingzhe Li, Francois Baccelli, Jeffrey G. Andrews, Thomas D. Novlan, J. Charlie Zhang, "Modeling and Analyzing the Coexistence of Wi-Fi and LTE in Unlicensed Spectrum", in IEEE Transactions on Wireless Communications, vol. 15, no. 9, pp. 6310-6326, Sept. 2016.

[38] V. Chandrasekhar, J. G. Andrews, and A. Gatherer, "Femtocell networks: a survey," *IEEE Communications Magazine*, vol. 46, pp. 5967, Sept. 2008.

[39] S. N. Chiu, D. Stoyan, W. Kendall, and J. Mecke, Stochastic geometry and its applications. John Wiley & Sons, 2013.

[40] "Final report of dsrc coexistence tiger team." https://mentor.ieee.org/802.11/dcn/15/11-15-0347-00-0reg-final-reportof-dsrc-coexistence-tiger-team-clean.pdf, 2015-03-09.

[41] J. Lansford, J. B. Kenney, and P. Ecclesine, "Coexistence of unlicensed devices with dsrc systems in the 5.9 ghz its band," in Vehicular Networking Conference (VNC), 2013 IEEE, pp. 916, 2013.

[42] Y. Park and H. Kim, "On the coexistence of IEEE 802.11 ac and wave in the 5.9 ghz band," Communications Magazine, IEEE, vol. 52, no. 6, pp. 162168, 2014.

[43] G. Naik, J. Liu, J. M. Park, "Coexistence of Dedicated Short Range Communications (DSRC) and Wi-Fi: Implications to Wi-Fi Performance", INFOCOM, 2017.

[44] J. Liu, G. Naik, J.M. Park,"Coexistence of DSRC and Wi-Fi: Impact on the Performance of Vehicular Safety Applications"J. 2017 *IEEE* International Conference on Communications (ICC), Paris, 2017, pp. 1-6.

[45] K.-H. Chang, "Wireless communications for vehicular safety," Wireless Communications, IEEE, vol. 22, no. 1, pp. 67, 2015.

[46] Keysight Technologies white paper: "5 New Features and Test Challenges on 802.11ax", 2018. https://www.comsoc.org/whitepapers

[47] D. J. Deng, S. Y. Lien, J. Lee and K. C. Chen, "On Quality-of-Service Provisioning in IEEE 802.11ax WLANs," in *IEEE Access*, vol. 4, no., pp. 6086-6104, 2016.

[48] B. Bellalta, "IEEE 802.11ax: High-efficiency WLANS," in *IEEE Wireless Communications*, vol. 23, no. 1, pp. 38-46, February 2016.

[49] 3GPP, 3rd generation partnership project; Technical specification group radio access network; Physical Layer Procedures (Release 14), 3GPP TS 36.213.

[50] Jack L. Burbank, William Kasch, Jon Ward, "An Introduction to Network Modeling and Simulation for the Practicing Engineer", John Wiley & Sons, Aug 4, 2011.

[51] A. Busson, G. Chelius, and J.-M. Gorce, "Interference Modeling in CSMA Multi-Hop Wireless Networks," Research Report RR-6624, INRIA, Feb. 2009.

[52] H. ElSawy, E. Hossain and S. Camorlinga, "Multi-channel design for random CSMA wireless networks: A stochastic geometry approach," *2013 IEEE ICC*, Budapest, 2013, pp. 1656-1660.

[53] 3GPP RP-140808, "Review of regulatory requirements for unlicensed spectrum," June 2014.

[54] R. Zhang, M. Wang, L. X. Cai, Z. Zheng, X. Shen, L. Xie, "LTE Unlicensed: The future of spectrum aggregation for cellular networks," *IEEE Wireless Communications Magazine*, Vol. 22, No.3, pp. 150-159, June 2015.

[55] J. G. Andrews, A. K. Gupta, and H. S. Dhillon, "A Primer on Cellular Network Analysis Using Stochastic Geometry, *arXiv:1604.03183 [cs.IT]*, 2016.

[56] G. Bianchi, I. Tinnirello, and L. Scalia, "Understanding 802.11e contention-based prioritization mechanisms and their coexistence with legacy 802.11 stations", *IEEE Network*, 2005.

[57] G. Bianchi, Performance analysis of the IEEE 802.11 distributed coordination function, in *IEEE Journal on Selected Areas in Communications*, vol. 18, no. 3, May 2000, pp. 535-547.

[58] C. L. Huang and W. Liao, Throughput and delay performance of IEEE 802.11e Enhanced Distributed Channel Access (EDCA) under saturation condition, in *IEEE Transactions on Wireless Communications*, vol. 6, no. 1, Jan. 2007, pp. 136-145.

[59] F. Peng, B. Peng, D. Qian, Performance analysis of IEEE 802.11e enhanced distributed channel access, in *IET Communications*, vol. 4, no. 6, Apr. 2010, pp. 728-738.

[60] M. D. Foegelle, "Coexistence of LTE-U and LAA in a Wi-Fi world," in *10th European Conference on Antennas and Propagation (EuCAP)*, Davos, 2016, pp. 1-5.

[61] A. k. Ajami and H. Artail, "On The Modeling and Analysis of Uplink and Downlink IEEE 802.11ax Wi-Fi with LTE in Unlicensed Spectrum," in *IEEE Transactions on Wireless Communications*, In press, DOI: 10.1109/TWC.2017.2715834.

[62] A. k. Ajami and H. Artail, "LTE Frequency One Re-use Factor: Would It Be An Efficient Solution For The Unlicensed Bands? A Stochastic Geometry Analysis", in *13th International Wireless Communications & Mobile Computing Conference (IWCMC 2017)*, Valencia, Spain, June 2017.

[63] A. k. Ajami and H. Artail,"Fairness in future Licensed Assisted Access (LAA) LTE networks: What happens when operators have different channel access priorities?," *2017 IEEE International Conference on Communications Workshops (ICC Workshops)*, Paris, France, 2017, pp. 67-72.

[64] Dahlman, Erik, Stefan Parkvall, and Johan Skold, "4G, LTE-Advanced Pro and the Road to 5G", 2016.

[65] C. Casetti, "Coexistence of IEEE 802.11n and licensed-assisted access devices using listen-before-talk techniques," *13th IEEE Annual Consumer Communications & Networking Conference (CCNC)*, Las Vegas, NV, 2016, pp. 562-567.

[66] A. Guo and M. Haenggi, "Asymptotic deployment gain: A simple approach to characterize the sinr distribution in general cellular networks," *IEEE Transactions on Communications*, vol. 63, pp. 962976, Mar. 2015.

[67] Huawei, "U-LTE: Unlicensed Spectrum Utilization of LTE", 2014.

[68] H. J. Kwon, J. Jeon, A. Bhorkar et al., "Licensed-Assisted Access to Unlicensed Spectrum in LTE Release 13", *IEEE Commun. Magazine*, vol. 55, no. 2, pp. 201-207, Feb. 2017.

[69] A.k. Ajami and H. Artail, Performance Bounds of Different Channel Access Priority Classes in Future Licensed Assisted Access (LAA) LTE Networks, *Physical Communication*, V. 25, N. 1, pp. 110-127, Oct. 2017.

[70] Y. Chen, M. Ding, D. Lopez-Perez et al., "A Space-Time Analysis of LTE and Wi-Fi Inter-Working", *IEEE J. Sel. Areas in Commun.*, vol. 34, no. 11, pp. 2981-2998, Nov. 2016.

[71] V. V. Chetlur and H. S. Dhillon, "Coverage analysis of a vehicular network modeled as cox process driven by poisson line process," arXiv preprint arXiv:1709.08577, 2017.

[72] S. Eichler, "Performance Evaluation of the IEEE 802.11p WAVE Communication Standard," 2007 IEEE 66th Vehicular Technology Conference, Baltimore, MD, 2007, pp. 2199-2203. doi: 10.1109/VETECF.2007.461

[73] *IEEE* Std 802.11-2012, *IEEE* standard for information technology telecommunications and information exchange between systems local and metropolitan area networks specific requirements part 11: Wireless lan MAC and PHY.